CHALMERS

Transient Overvoltages in Cable Systems

Part 2 – Experiments on fast transients in cable systems

Master of Science Thesis

MAIALEN BOYRA

MSc. in Electric Power Engineering 60p (Degree of Civilingenjörexamen, eq. 180p)
Department of Electric Power Engineering
Division of Energy and Environment
CHALMERS UNIVERSITY OF TECHNOLOGY
Göteborg, Sweden, 2007

Abstract

In this thesis work, transient overvoltages in cable systems are characterized through both simulations in PSCAD and laboratory experiments on a system of limited extension at medium voltage. The system includes a longer and a shorter cable, a vacuum circuit breaker in between and two transformers, on the supply side and load side, respectively. Modeling of the transformer for proper representation of high frequency components is a key point, which is dealt with in detail in the report. For the laboratory setup, which includes two single-phase cables, an extensive analysis of the measurements done is presented. These include open and close operation of the vacuum circuit breaker at no load, with resistive load and inductive load, respectively. The experimental results are also compared with simulations made in the software PSCAD/EMTDC. A number of simulated cases for a similar system including three-phase cables are also presented. It was found that certain conditions must be fulfilled in order for the reignitions to occur. In opening operations, for example, reignitions are more likely to happen if the contact separation starts just before the current zero crossing. However, for the closing operation it has been difficult to determine an instant in which the reignitions are more frequent.

Keywords: cable, vacuum circuit breaker, transformer, fast transient, overvoltage, high frequency modelling.

Preface

For six months I have studied a very particular type of transients: the transients that occur in cable systems due to switchings and faults. Power systems are mostly analyzed under steady state conditions and transients are often seen as unknown events that happen in an extremely short time scale. For this reason, I feel especially lucky for having the opportunity of examining these phenomena in deep and for being surrounded by some of the most skilled people in this field. It has been a real pleasure to work in ABB Corporate Research where the working atmosphere has been fantastic.

In first place I would very much like to thank my supervisors Ambra Saninno and Lars Liljestrand for the good advices and exceptional guidance and to all the people that have helped and supported me throughout the months: Henrik Breder, Franz Svendsen, Josef Medvegy, Leif Hederström, Kenneth Johansson, Dierk Bormann, Lars Gertmar, Magnus Backmann, Majed Ali and a large etcetera. Without them this work would not have been possible.

I would like to thank my supervisor at Chalmers Torbjörn Thiringer for his ready help and counselling and for his always interesting lectures.

I will never forget the “multi-culti” conversations, lunches at Mälardalens Högskola and dinners at our tiny Skalden rooms with the “youngs”: Dan, Oliver, Johan and Veronica, Mila, Michele, Mirko, Georg, Amandine and Mikael.

I would like to thank to my friends in Göteborg, Julio and Olga, Julia and Björn, Masoud, Ben, Heng, Cyril, Kishore, Per, Susana, Tarik, the Zambians, Horacio and all the people that have contribute to make this experience unforgettable.

Finally I would like to thank my boyfriend Cédric and my family for being the best boyfriend and family that one could have.

1. TABLE OF CONTENTS

2. INTRODUCTION

2.1 BACKGROUND

As a consequence of the increasing electric power demand and the limited fossil fuel resources a huge effort is being put design new efficient renewable energy generation methods. After many years of intensive research wind power has become a mature technology and the quantity and size of wind power plants is growing very fast, especially offshore [15]. However, offshore WPs (WPs) are facing new challenges that have not been observed in inland WPs. One of these challenges is related to the design of the sub-sea grid, which interconnects the wind turbines (WTs). Until now the WP layout was designed as a traditional medium voltage (MV) distribution system but this scheme seems not to be the optimum. If the MV rural/urban distribution systems and the offshore WPs are analysed many differences are observed:

- The power flows in opposite directions: offshore WPs generate power while rural/urban distribution systems consume it.
- “Loads” in WPs are rotating machines, with or without power electronics, which connect and disconnect according to the wind. In rural/urban areas rotating loads are a much smaller fraction of the total load.
- The maintenance in offshore WPs can be very complicated and risky due to the harsh weather conditions during periods of the year. Therefore the reliability of these plants must be very high. Rural/urban areas are not as critical although due to the de-regulation of the markets the consumers have become more self-conscious of their rights and have started to demand better quality services.

On the contrary, many analogies have been found with industrial systems:

- The loads in industrial systems are very often rotating machines, which can also include power electronics and drives. These loads are continuously connecting and disconnecting and the switches operate at a heavy work load. This is also valid for WPs at least during the commissioning phase when many CB operations are made to test the equipment.
- Industrial systems must also be very reliable because a stop in the production may cause huge money losses.
- Some industrial systems can have cogeneration systems that supply power to the grid.

This last parallelism can be very useful to predict the problems that may arise in offshore WPs. For example, one of the problems that power engineers have had to deal with in the industrial systems is the appearance of dangerous transient overvoltages that frequently damage the insulation of electrical equipment. Problems such as this have just started to happen in offshore WPs due to the considerable amount of cables and vacuum circuit breakers (VCBs).

During transients electromagnetic waves propagate, reflect and refract through all the system negatively affecting the insulation of electrical apparatus. The apparatus concerned are designed to operate under steady state conditions and the magnitude and rate of rise of the incoming waves stress their insulation. The effect of the travelling waves is more harmful if the system is connected by cables rather than by overhead lines. The reason is that the characteristic impedance of cables (<40 Ω) is lower than the characteristic impedance of overhead lines (300-400 Ω) and, the lower the surge impedance the higher the time derivatives of the voltage generated in the terminals of the equipment. The last statement can easily be understood looking at the time constant of the new wave (see fig. 1). If the load is a transformer at no load and it is modelled as a capacitance in parallel to its magnetizing inductance the time constant is $\tau = Z_o \cdot C_{load}$ (in this case the slower time constant of the inductive part has been neglected). A ten times lower surge impedance will produce approximately a ten times faster voltage wave.

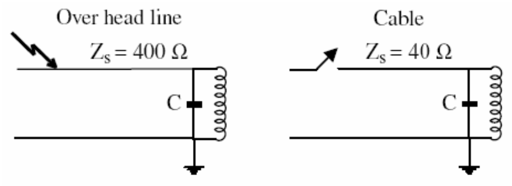

fig. 1. Travelling waves reaching a transformer at no load

2.2 AIM

This thesis work is part of a larger project in which several aspects of WPs are analysed. In particular, the aim of this thesis is to study fast transient phenomena that occur due to the switching of VCBs and due to faults in cable systems. For this purpose a laboratory experiment that resembles a small section of a WP has been set up, see fig. 2.

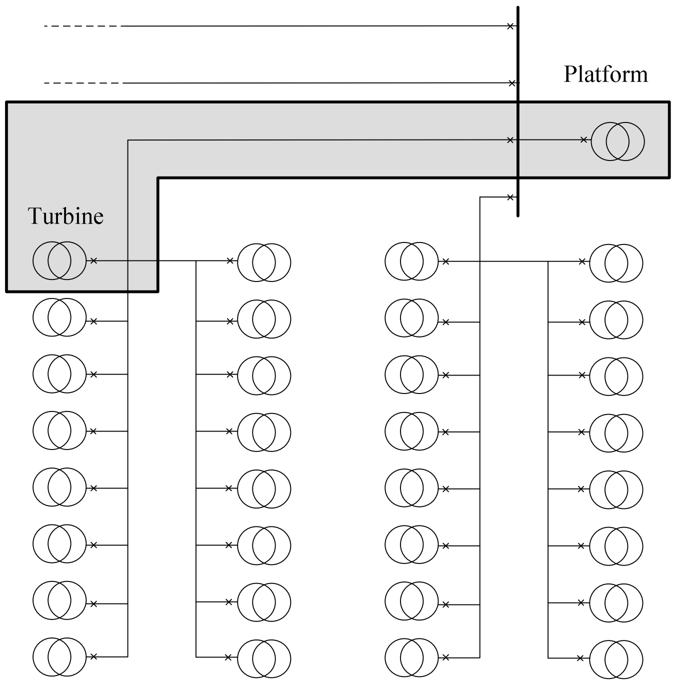

fig. 2. Part of the WP that is going to be analysed

This project has been based on the analysis of the WP branch shown in fig. 3 and the investigation has been carried out by both simulations with PSCAD/EMTDC and experiments.

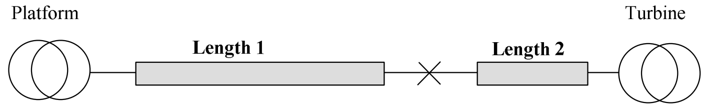

fig. 3. WP branch under analysis

The experimental measurements are used to calibrate the models of the system, whose elements are modelled to be sensitive not only to the power frequency, but also to higher frequencies. A graphical representation of the work in this thesis is given in fig. 4.

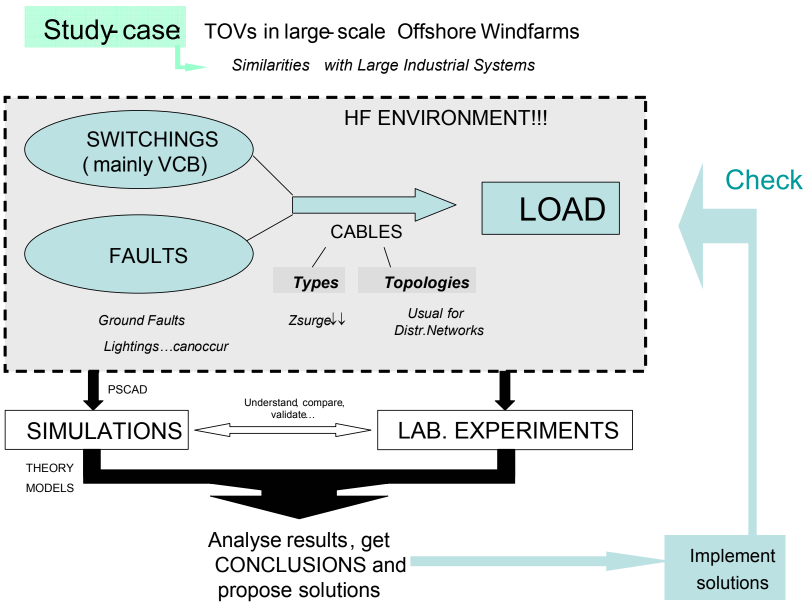

fig. 4. Graphical explanation of the thesis work

2.3 STRUCTURE

This report is divided into four major blocks:

i. *General theory on electromagnetic wave propagation and transients in circuits:*
For a better understanding of different fast transient phenomena the most important concepts have been gathered in this section. The objective is not to give a course on electrical transients but to provide some essential knowledge to facilitate the reading.

ii. *Modelling equipment that is able to represent high frequency behaviour:*
Most of the studies in power systems consider an operating frequency of 50/60Hz and therefore the models of the systems components are designed for power frequencies. If fast transient behaviour is to be analysed the adequacy of the traditional models must be reviewed and new solutions found. The difficulty lays in the fact that fast transients are not confined to a certain frequency. The frequency range is so broad that different models are needed depending on the phenomenon to be investigated.

iii. *Comparison of the laboratory experiment with the simulated results:*
During several years many measurements have been taken in industrial plants but it is difficult to obtain an accurate model of these plants due to the lack of information and uncertainties in the parameters. For large offshore WPs this task is complicated even

more by the fact that very few such systems have been in operation for a relatively short time.
A laboratory experiment gives a better opportunity of calibrating the simulation models because many of the parameters can be obtained or approximately estimated.
As a first step, a relatively simple test circuit has been built including single-phase cables, which were available at the time, three-phase oil-filled transformers and a vacuum circuit breaker. The results are used to verify the models and draw preliminary conclusions on the characteristics of the transient overvoltages to be expected in a WP and their propagation.

iv. Simulations of a three phase cable setup for future laboratory experiments:

A second set of experiments using three-phase cables is planned within the next few months. Simulations have been done in order to forecast. However, this second round of experiment is out of the scope of this report.

3. GENERAL THEORY ON WAVE PROPAGATION ON CABLES AND FAST TRANSIENT PHENOMENA

This chapter provides the essential theory necessary to understand fast transient related phenomena. The chapter starts by a general introduction to electrical transients where the relevance of energy conservation is underlined. It continues explaining different kinds of switching transients, which have been grouped as normal and abnormal switching transients. Wave propagation, focusing on reflection and refraction in line discontinuities, is after described. The chapter ends by two different examples: one analyses the wave shape of the voltages after a closing operation of a breaker; the other one explains the different oscillating modes in a simple circuit.

3.1 INTRODUCTION TO ELECTRICAL TRANSIENTS

“An electrical transient is the outward manifestation of a sudden change in circuit conditions, as when a switch opens and closes or a fault occurs on a system”, [5]. The duration of a transient is generally very short comparing to the time systems operate at steady-state. However, these short periods cannot be ignored because it is in fact often during transients when circuit components are subjected to the most dangerous stresses. In addition, electrical insulation and other sensitive properties of the components are typically designed to optimally work at rated values and are therefore susceptible to deviations from the rated operation.

A transient could be also be defined as the unbalance that occurs when the system passes from one steady-state condition to a new steady-state condition. When there is a sudden change in the system the energy must be redistributed to meet the new conditions such as when a switch is operated, fig. 5. It takes a certain amount of time to redistribute the energy.

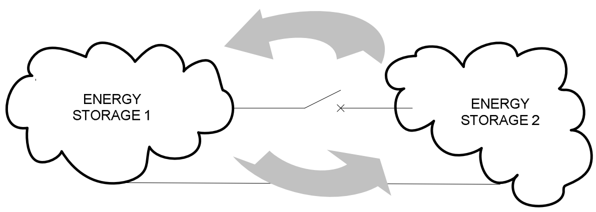

fig. 5. Energy balance across a switch

The energy of an electric circuit is stored in different parts of the system as magnetic or electric energy. Pure inductances (*L*) are characterized by their ability to store energy in their magnetic field while pure capacitors (*C*) store energy in their electric field. Resistors (*R*) dissipate energy converting it into heat. However, the components of an electric system are never purely of one or the other kind and they all own both attributes in different proportions and in distributed quantities, see fig. 6.

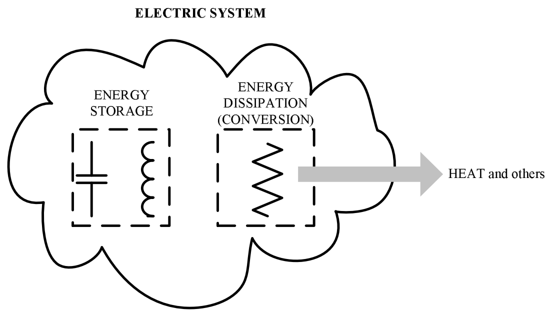

fig. 6. Components of an electric system

In order to understand electrical transients in power systems the following premises must be accounted for:

a) The current through an inductor cannot be subjected to a sudden change
b) The voltage across a capacitor cannot suddenly change
c) Energy conservation must be maintained

The study of electrical transients requires some mathematical background and it is usually more interesting to analyze transients in a time base than in a frequency base. The analysis of the problem, starts by expressing the differential equations that describe the behaviour of the system. The solutions of these differential equations give some useful information as far as circuit behaviour is concerned. The solution of a differential equation is divided into two parts: the *complementary* or *homogeneous* solution and the *particular* solution. The complementary solution describes the change of the system between the initial and the final steady-state conditions while the particular solution represents how the circuit reacts to a stimulus.

The complementary solution provides a very valuable parameter called *time constant (τ)* and it is contained in an exponential expression ($e^{-t/\tau}$) known as thumbprint, see fig. 7. The time constant tells how quickly the system can pass from the initial state to the final state. If the circuits are simple the complementary solution is simple but it is possible to deduce the solutions of complex circuits by means of superposition. It must be mentioned that LC-circuits do not have any time constant because they never reach a steady state value but continue oscillating forever at a frequency called natural frequency (w_n).

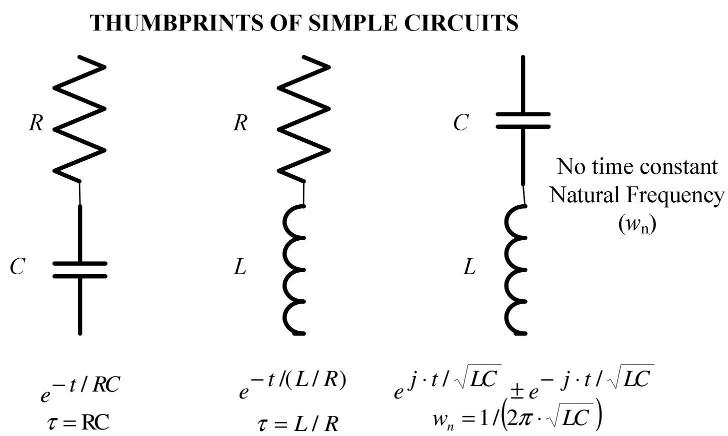

fig. 7. Thumbprints of simple circuit

Tools like Laplace Transform are very useful to deal with differential equations, which then is handled in the frequency domain.

3.2 SIMPLE SWITCHING TRANSIENTS

This thesis deals with fast transients that are caused by switching of VCBs and faults. However, it is important to briefly explain the most important implications of closing a breaker (energizing) and opening it, especially when breaking a fault.

3.2.1 CLOSING A SWITCH

Closing a switch implies connecting two systems together and hence an inherent energy flow. As soon as the switch closes a current starts flowing until an energetic equilibrium is obtained. Depending on the instant in which the switch is closed, the system will start to change from different initial conditions. Some initial states can generate higher transient currents and they should be avoided. There are infinite circuit cases but the basic responses are well defined in the two following examples: closing an inductive load and a capacitor bank.

3.2.1.1 CLOSING AN INDUCTIVE CIRCUIT

The current through a LR-circuit, shown in fig. 8, rises according to the expression

$$\mathrm{I(t)} = \frac{\mathrm{V_m}}{\sqrt{\mathrm{R}^2 + \mathrm{w}^2 \cdot \mathrm{L}^2}} \cdot \left[\sin(wt + \theta - \varphi) - e^{-\alpha t} \cdot \sin(wt + \theta - \varphi)\right] \qquad \textbf{(eq. 1)}$$

where,

$\alpha = R/L$

θ: Initial angle of the voltage

$\varphi = \arctan(wL/R)$ and,

where the complementary and the particular solutions are well differentiated. The first term corresponds to the particular solution and it means that once the steady state is reached the current is sinusoidal. The second term is the transitory term that eventually becomes zero following an exponential pattern.

On the one hand, the best closing moment corresponds to the instant in which $\theta = \varphi$ because then the current starts from zero and is symmetrical, in all other cases the current will be asymmetrical. On the other hand, the worst closing moment corresponds to $\theta - \varphi = \pm\pi/2$ because at that closing time the initial current is twice as big as the steady state current. The resulting current when closing the switch is shown in fig. 9.
Similar asymmetrical currents occur when a fault happens. In that case the switches may also have to interrupt very high initial currents (twice the short circuit current).

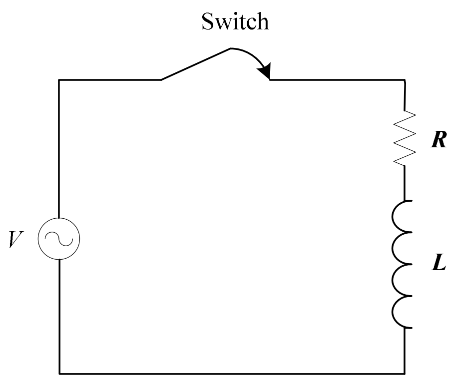

$$R \cdot I + L \cdot \frac{dI}{dt} = V_m \cdot \sin(wt + \theta)$$

fig. 8. RL-circuit

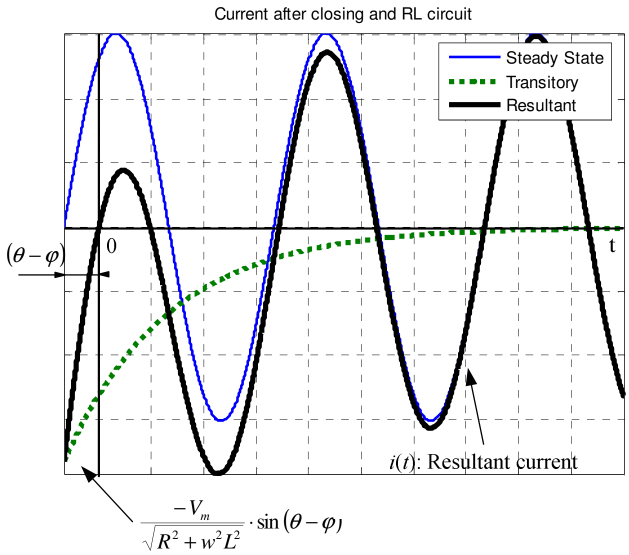

fig. 9. Asymmetrical alternating current (solution)

3.2.1.2 CLOSING A CAPACITIVE BANK

When energizing a capacitive bank, shown in fig. 10, the closing instant must be very carefully chosen to avoid high inrush currents and consequent overvoltages. The capacitor is charged through the source inductance as described in

$$I(t) = V(0) \cdot \sqrt{\frac{C}{L}} \cdot \sin(w_o \cdot t), \textbf{ where } w_0 = \frac{1}{\sqrt{LC}} \qquad \textbf{(eq. 2)}$$

where it can be observed that the current is directly proportional to the voltage at the closing instant. If the switch is closed at the voltage zero crossing then the current will smoothly start to rise from zero at the same pace as the voltage.

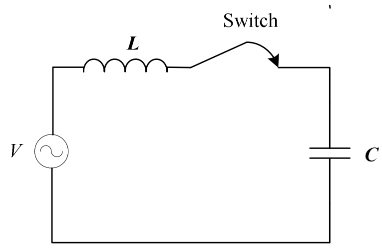

$$V_c + L \cdot \frac{dI}{dt} = V$$

fig. 10. LC circuit

3.2.2 OPENING A SWITCH

When a switch opens a voltage starts to grow across its terminals. The difference between the voltage on the supply side and on the load side is called transient recovery voltage (TRV). The shape of the TRV is dependent on the nature of the circuit being interrupted, whether primarily resistive, capacitive, inductive, or a combination of them. For VCB manufacturers it is very important to know which the contour of a TRV is because the breaking operation will only be successful if the circuit breaker (CB) is able to withstand the TRV and the power frequency recovery voltage, see fig. 11.

Three main types of TRVs (or its combination) can occur: oscillatory, exponential or triangular, see table 1. The most severe *oscillatory* or *exponential* recovery voltages are likely to appear across the first interrupting pole when the voltage is in its peak. Triangular TRVs are related to line faults and the closer the fault is to the CB the steeper the initial rate of rise of the TRV is. On the contrary, if the rate of rise increases the magnitude decreases and they are only noticeable during a short time after the switch opens [16].

table 1. TRV curve types (from [19])

Exponential TRV (a)	Oscillatory TRV (b)	Triangular TRV (c)
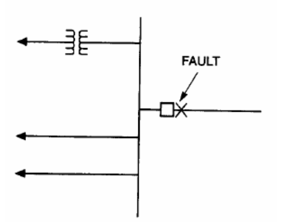	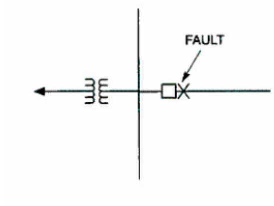	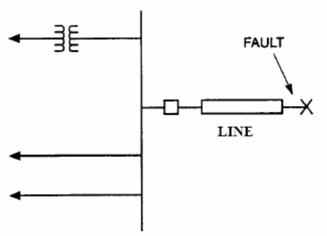
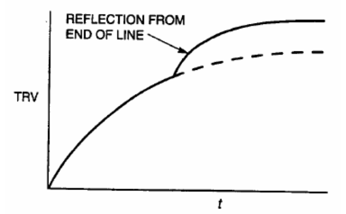	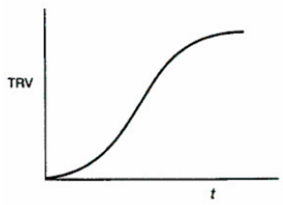	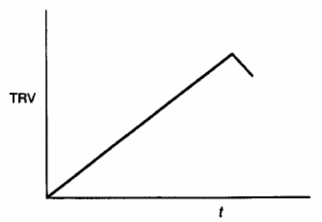

Exponential TRVs occur when at least one transformer and one line exist in the not faulted side of the CB. Oscillatory TRVs take place when there is no line present to provide damping and the only element that can limit the fault is a transformer or reactor. Triangular TRVs are observed in the so called “short-line”-s or “kilometric fault”-s. For further understanding of these phenomena refer to section 9.7 of [5].
During this project it has mostly been dealt with oscillatory TRVs since the circuit under analysis is “isolated” and does not account for other lines.
In order to choose the correct CB the system TRV envelope must be known. The selected CB must be able to withstand the system TRV otherwise another CB must be used or the system must be adapted (i.e. by adding capacitors to the bus).

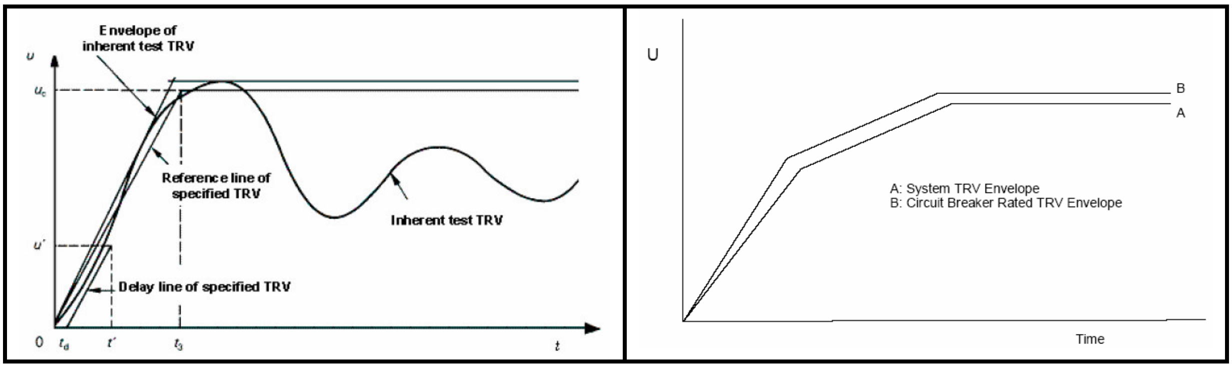

fig. 11. System and CB rated TRV envelopes

3.3 DAMPING

Losses are rarely considered in the first approach of a transient analysis because they add complexity to the problem and they make the analysis more difficult. Logically, the results obtained are not damped and the overvoltages can reach very high values. Once the behaviour of the system has been determined, the affect of losses can be analysed. In reality losses come from the components' inherent resistance, the iron cores and the loads.

On one hand, the damping in fast transients is more difficult to handle because the time that the flux has to penetrate adjacent structures (cores and conductors) is not negligible comparing to the fast transient time scale. One consequence is the *skin effect* which confines the majority of the current in the outer layer of the conductor and reduces the effective cross section. Thus, as the frequency increases the effective cross section decreases and the conductor resistance grows.

On the other hand, the oscillatory behaviour of a circuit is a combination of many different frequency modes. Each mode oscillates at a different frequency and higher frequencies damp out more quickly because their cycles elapse faster.
It can be concluded that modelling the damping of the circuit can become a very complex task.

3.4 ABNORMAL SWITCHING TRANSIENTS

A transient is said to be normal [5] if the transient starts when the circuit is in a quiescent state, this is, it has not extra stored energy. On the contrary, if the system has already some energy stored then the effects of the transient can be stronger and the transient is known as abnormal. It can happen that a normal transient stores energy and the following transient becomes an abnormal transient. In the particular case studied in this report, where it is common to observe multiple reignitions, abnormal switching transients are frequent because transients follow one after the other within a very narrow time period. In the next subsections some of these abnormal switching are explained.

3.4.1 CURRENT SUPPRESSION

When the contacts of a CB start to separate the current does not suddenly vanish. It continues to flow through an arc until it reaches its zero crossing. Sometimes the arc becomes unstable before reaching the current zero and the current suffers a sudden decay called current chopping. The current chopping or current suppression, as it is generically known, generates abnormal overvoltages because there is still some magnetic energy trapped that has to be released. It is usually observed when switching the no load current of a transformer or when a shunt reactor is being disconnected, see fig. 12.

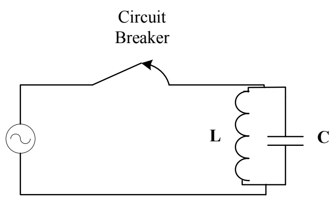

fig. 12. Simple LC circuit representation

At the moment of the chopping, a certain quantity of the current (I_o) is flowing through the switch. This current is associated to a magnetic energy that resides in the inductance

$$W_{\text{magn.}} = \frac{1}{2} L I_0^2 \qquad \textbf{(eq. 3)}$$

Since the current does not have a path through the switch, the magnetic energy stored in the inductance is converted into electric energy that is diverted into the capacitor. The energy stored in the capacitor increases together with the voltage across its terminals according to

$$\frac{1}{2} C V^2 = \frac{1}{2} L I_0^2 \text{ and} \qquad \textbf{(eq. 4)}$$

$$V = I_0 \sqrt{\frac{L}{C}}\,. \qquad \textbf{(eq. 5)}$$

This states that the peak voltage reached across the capacitor is given by the instantaneous chopped current and the surge impedance of the load. If the current in fig. 13 is examined, the phenomena of current chopping can be observed from t=-1ms to t=0ms. When the current reaches a value around 3A, the gap becomes unstable and the current starts oscillating. Then it is suddenly chopped.

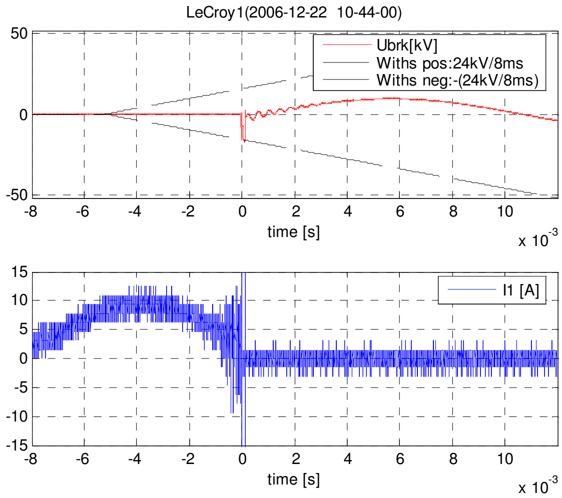

fig. 13. Current chopping in a VCB

3.4.2 CAPACITIVE SWITCHING

Disconnection of capacitor banks and dropping of unloaded overhead lines and cables, which also have a highly capacitive behaviour, can lead to some dangerous overvoltages. The most hazardous situations are presented when the breaker does not break at once and a reignition or restrike takes place, fig. 14.

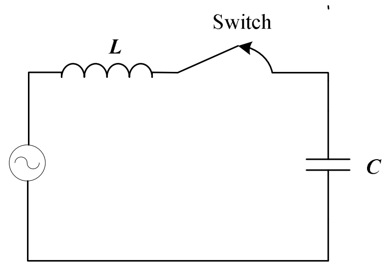

fig. 14. Capacitive breaking

If the current extinguishes at the system voltage peak (V_p), as it is illustrated in fig. 15, the voltage across the capacitor is maintained constant and the voltage across the switch will start to oscillate between zero and twice the value of the system voltage peak.

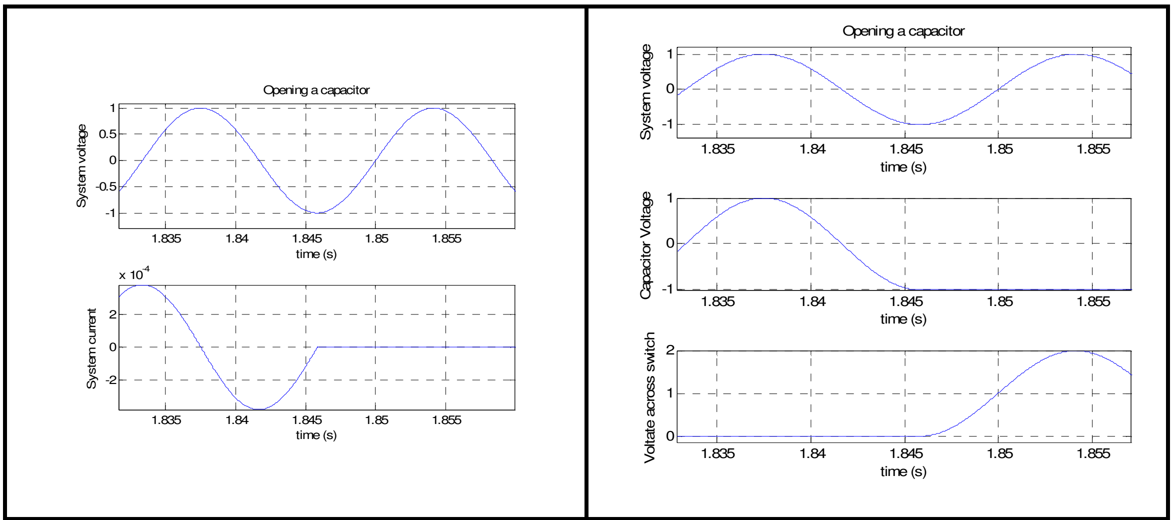

fig. 15. Voltages and currents in capacitive breaking

However, if the CB reignites when the voltage across the breaker is at its maximum ($2V_p$) the circuit will start to oscillate at its natural frequency:

$$f_0 = \frac{w_0}{2\pi} = \frac{1}{2\pi\sqrt{LC}} \qquad \textbf{(eq. 6)}$$

Accordingly to (eq. 2) current is given by

$$I = (2V_p)\cdot\sqrt{\frac{C}{L}}\cdot\sin(w_0 t)$$

The capacitor voltage is charged at a 1p.u value and at the instant in which the CB reignites this voltage is added to the system voltage. The result is a voltage excursion of $3V_p$ across the capacitor ($1V_p$ of its own charge$+2V_p$ of the system voltage). The capacitor voltage is eventually damped and it settles to the system voltage (fig. 16).

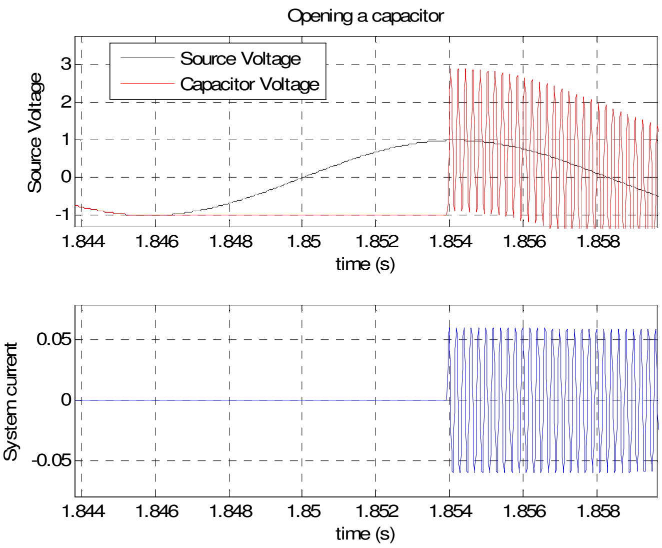

fig. 16. Capacitor switching with a restrike at peak voltage

3.4.3 OTHER RESTRIKING PHENOMENA

Generally reignitions do not come alone, it is usual to observe a series of reignitions and restrikes. A brief explanation of the phenomenon is hereby given.
When the CB opens, the load side inductance and capacitance start to resonate at the frequency

$$f_{01} = \frac{w_{01}}{2\pi} = \frac{1}{2\pi\sqrt{L_2 C}} . \qquad \textbf{(eq. 7)}$$

If the CB starts its separation procedure near the current zero crossing, the gap does not have enough time to build a sufficient distance, and according a sufficient strong withstand voltage, and the result is that it reignites, see fig. 17.

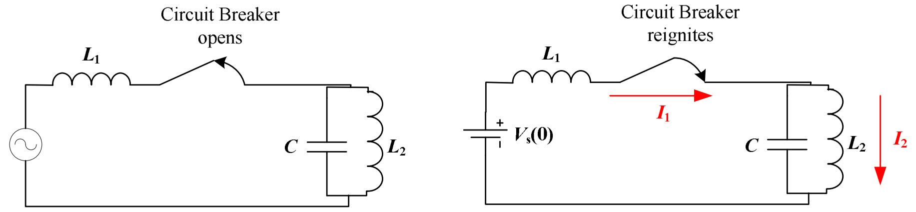

fig. 17. Breaking and subsequent reignition

Without very complex calculations it is possible to deduct that the current that will flow through the CB contacts has two components: a linear ramp and an oscillatory component (see section 5.4 of [5]), plotted in fig. 18. The CB current passes through zero when the ramp current and the oscillatory current are equal in value but opposite in sign. At that instant the switch breaks again. However, even if current I_1 is zero at that moment, current I_2 is not zero (I_0) and it is stored as magnetic energy in L_2. This is similar to chopping a current at I_0 that generates a TRV of $I_0(L_2/C)^{1/2}$.

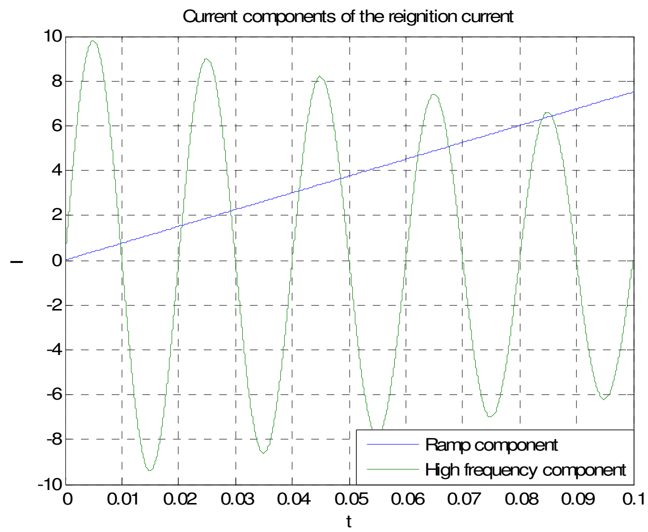

fig. 18. Components of the reignition current

It is probable that the contact gap cannot hold this new TRV and that it reignites again. The second time that it reignites the breakdown voltage is higher, the current is therefore higher and the process repeats again and again trapping more and more energy each time. The successive interruptions and energy trapping lead to a phenomenon called voltage escalation, which is illustrated in fig. 19.
An arcing ground is also another source of sequential reignitions but it only occurs in ungrounded systems.

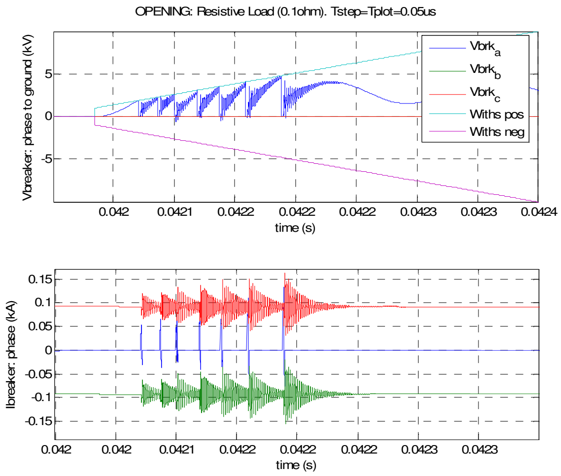

fig. 19. Voltage scalation

3.4.4 TRANSFORMER INRUSH CURRENTS

Transformer inrush currents are not frequently observed and they are a special case of closing an RL-circuit (see section 3.2.1.1) where the inductance is not linear. Nevertheless, since one of the objectives of this report is to study the energizing of transformers, this phenomenon is shortly explained.

Under normal conditions the magnetizing current of a transformer varies between 0.5-2% of the rated current. The magnetizing current represents the required current to magnetize the iron core but, due to the nonlinear properties of the ferromagnetic materials, it is not sinusoidal. Hence, the magnetizing current follows an hysteresis loop oscillating between $\pm I_m$ while the flux varies sinusoidally, see fig. 20.

When the transformer is disconnected there is still a significant amount of flux in the iron core that is called remanent flux (Φ_R). In reality the flux trapped in the core is less than the remanent flux because just after disconnection some current flows through the transformer winding discharging the flux (Φ_1).

When the transformer is connected again the initial polarity of the flux can be either increasing or decreasing. Before the voltage peak is reached the flux will increase in Φ_m, and this will draw a current from the supply that can be several times the rated current.

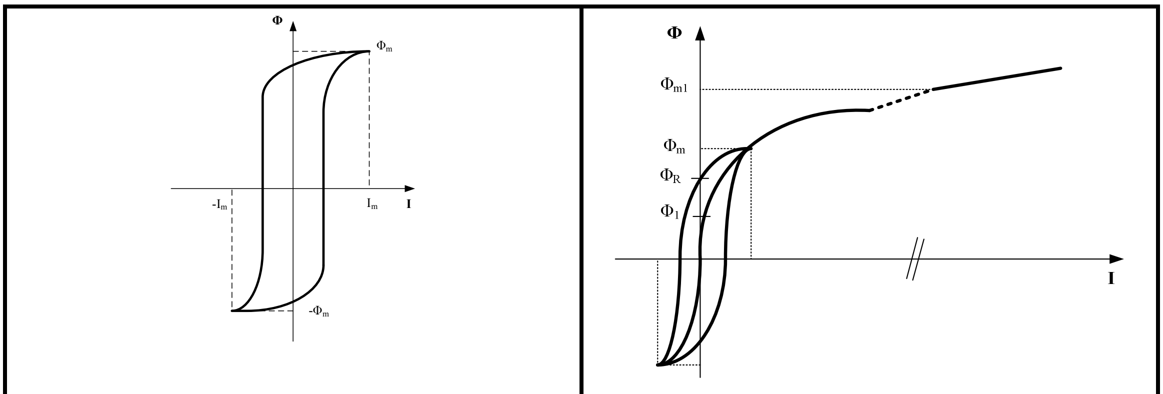

fig. 20. Magnetization curves of a transformer: normal (left) and illustrating the cause of inrush currents

3.4.5 FERRORESONANCE

Ferroresonance is a special case of series LC resonance where the inductance involved is nonlinear and it is usually related to equipment with iron cores. A typical case of ferroresonance is found in transformer energizing, mainly in delta-wye connections, when only one of the poles of the switch is closed, as shown in fig. 21. Ideally no current should flow until the three switches are closed but due to the stray capacitances the current finds a path to ground and the systems starts to resonate. The resonance can impress severe overvoltages across the transformer windings, the cables and the unenergized phases.

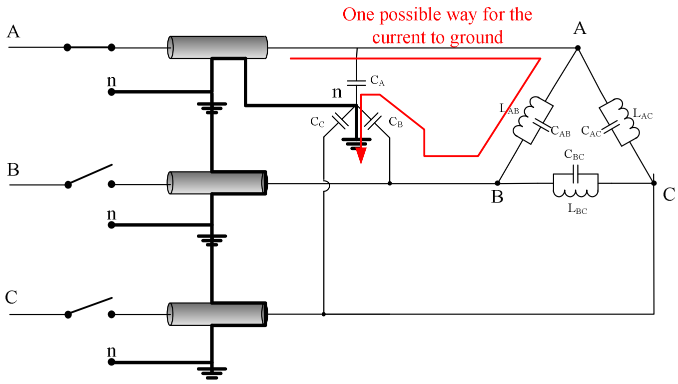

fig. 21. Energizing of a Dy transformer: first pole closed

3.5 ELECTROMAGNETIC WAVE PROPAGATION

Electricity and magnetism are very closely related and Maxwell's equations describe the electric and magnetic fields when charges and currents are present [21]:

I. Gauss' law for electric fields

$$\oiint \vec{E} \cdot d\vec{A} = \frac{Q}{\varepsilon_o} \quad \textbf{(eq. 8)}$$

II. Gauss' law for magnetic fields

$$\oiint \vec{B} \cdot d\vec{A} = 0 \quad \textbf{(eq. 9)}$$

III. General Ampère's law

$$\oint \vec{B} \cdot d\vec{s} = \mu_o \cdot \vec{I} + \mu_o \cdot \varepsilon_o \cdot \frac{d}{dt} \iint_s \vec{E} \cdot d\vec{A} \quad \textbf{(eq. 10)}$$

IV. Faraday's law

$$\oint \vec{E} \cdot d\vec{s} = -\frac{d}{dt} \iint_s \vec{B} \cdot d\vec{A} \quad \textbf{(eq. 11)}$$

According to Maxwell's equations the electric and magnetic fields are coupled when they are time dependent. Together they can transport energy during longer distances. The coupling between electric and magnetic fields produce travelling waves called *electromagnetic waves*. Maxwell's equations describe the behaviour of the electromagnetic waves in vacuum and when they travel through a material the equations must be slightly modified in accordance with the environment.

$$v = \sqrt{\frac{1}{\mu \cdot \varepsilon}} \equiv \frac{c}{n} \quad \textbf{(eq. 12)}$$

where,

v: propagating speed of the electromagnetic wave

n: speed reduction factor
μ, μ_o: permeability, permeability in vacuum, respectively
ε, ε_o: permittivity ,permittivity in vacuum, respectively
k: dielectric constant
χ_m: susceptivity of a material.

The dielectric constant and the susceptivity are a property of each material and they modify the value of permittivity and permeability in vacuum as

$$\varepsilon = k \cdot \varepsilon_0 \quad \textbf{(eq. 13)}$$

$$\mu = (1 + \chi_m) \cdot \mu_0 \quad \textbf{(eq. 14)}$$

3.5.1 LINE DISCONTINUITY

The previous introduction explains how the propagating speed of electromagnetic waves change according to the environment they are travelling in. In the case of cables the electromagnetic waves are confined between the conductor and the shield and their speed depends on the insulating material. In addition, current waves travelling through transmission lines are always proportional to voltage waves by a proportionality factor (Z_o) called characteristic impedance of the transmission line [5]. The characteristic impedance of a cable also depends on the properties of the insulating layer and it varies from cable to cable. If a travelling wave finds a discontinuity in the line, it is very probable that the characteristic impedance at each side of the junction is different. In that case current and voltage values must be readjusted in order to match the impedance requirement. In order to fulfil the condition of proportionality two new wave pairs are generated: a refracted wave pair, which penetrates the discontinuity point, and a reflected wave pair, which travels in the opposite direction to the incident wave and is superimposed to this. The energy conservation is automatically satisfied, see fig. 22.

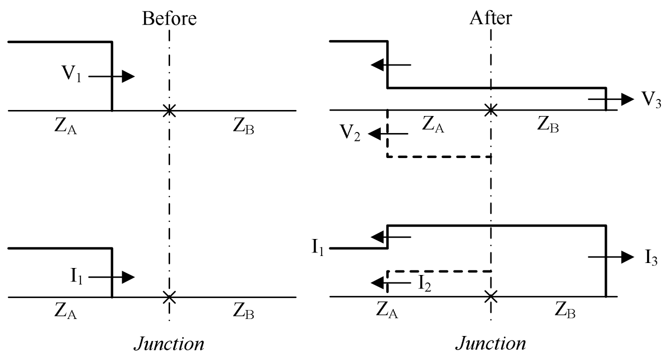

fig. 22. Voltage and Current waves in a line junction

The amplitude of the new formed waves can be easily deduced from

$$I_1 = \frac{V_1}{Z_A} \quad \textbf{(eq. 15)}$$

$$I_2 = -\frac{V_2}{Z_A} \quad \textbf{(eq. 16)}$$

$$I_3 = \frac{V_3}{Z_B} \quad \textbf{(eq. 17)}$$

where the subscript **1** stands for the incident wave, **2** for the reflected wave and **3** for the refracted wave. Z_A and Z_B are the characteristic impedances of the two lines and the positive direction of *x* is the direction of the incident wave by definition.

At the junction voltage and current must be continuous:

$$V_1 + V_2 = V_3 \quad \textbf{(eq. 18)}$$

$$I_1 + I_2 = I_3 \quad \textbf{(eq. 19)}$$

Substituting (eq. 15), (eq. 16) and (eq. 17) yields (eq. 19)]:

$$\frac{V_1}{Z_A} - \frac{V_2}{Z_A} = \frac{V_3}{Z_A} \quad \textbf{(eq. 20)}$$

It is possible to relate the reflected or refracted wave in terms of the incident wave rewriting (eq. 20) as

$$V_2 = \left(\frac{Z_A - Z_B}{Z_A + Z_B}\right) \cdot V_1 = a \cdot V_1 \quad \textbf{(eq. 21)}$$

$$V_3 = \left(\frac{2 \cdot Z_B}{Z_A + Z_B}\right) \cdot V_1 = b \cdot V_1 \quad \textbf{(eq. 22)}$$

The reflection coefficient, a, and the refraction coefficient, b, are defined as follows:

$$a = \left(\frac{Z_A - Z_B}{Z_A + Z_B}\right) \text{, where } [-1 \le a \le 1] \quad \textbf{(eq. 23)}$$

$$b = \left(\frac{2 \cdot Z_B}{Z_A + Z_B}\right) \text{, where } [0 \le b \le 2] \quad \textbf{(eq. 24)}$$

Observe that both coefficients can be complex values and that at a junction the value of the incident wave could be either doubled or become zero.
If the junction is divided into more than one line, as shown in fig. 23, the same procedure is used to determine the reflected and refracted waves: voltage and current continuity in the joint must be regarded.

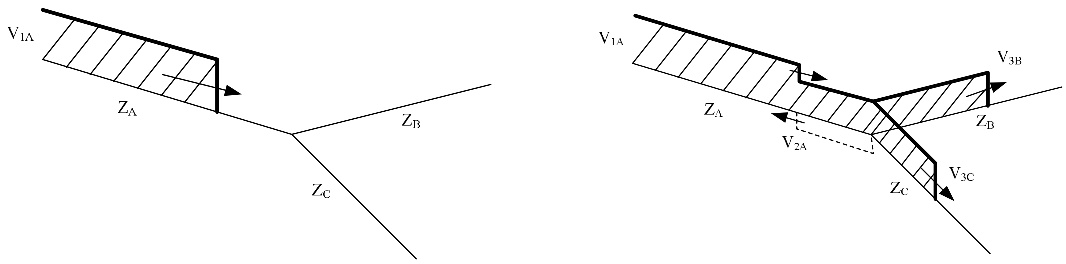

fig. 23. Behaviour of voltage wave in a bifurcation

With the symbols in fig. 26 we obtain the refracted current waves

$$I_{3B} = \frac{V_{3B}}{Z_B}, I_{3C} = \frac{V_{3C}}{Z_C} \ldots I_{3N} = \frac{V_{3N}}{Z_N} \text{, where N: number of bifurcated lines} \quad \textbf{(eq. 25)}$$

and the reflected current wave:

$$I_2 = -\frac{V_{2A}}{Z_A} \quad \textbf{(eq. 26)}$$

Equations that express the continuity of voltage and current in the junction:

$$V_{1A} + V_{2A} = V_{3B} = V_{3C} = \ldots = V_{3N} \quad \textbf{(eq. 27)}$$

$$I_{1A} + I_{2A} = I_{3B} = I_{3C} = ... = I_{3N} \quad \textbf{(eq. 28)}$$

3.5.2 LINE TERMINATION

A line termination could be seen as a particular case of line discontinuity where there is no transmission line after the junction, a finishing end is placed instead. A line termination can be of a very diverse nature but the most extreme cases are the short circuit and the open circuit.

3.5.2.1 SHORT CIRCUIT

If two points of a circuit are at the same voltage level, i.e. if there is no voltage difference between them, it is said that those two points are in short circuit. The incident voltage wave coming into a short circuit must be cancelled by the reflected voltage in order to fulfil this requirement. There will not be any refracted waves, see fig. 24.

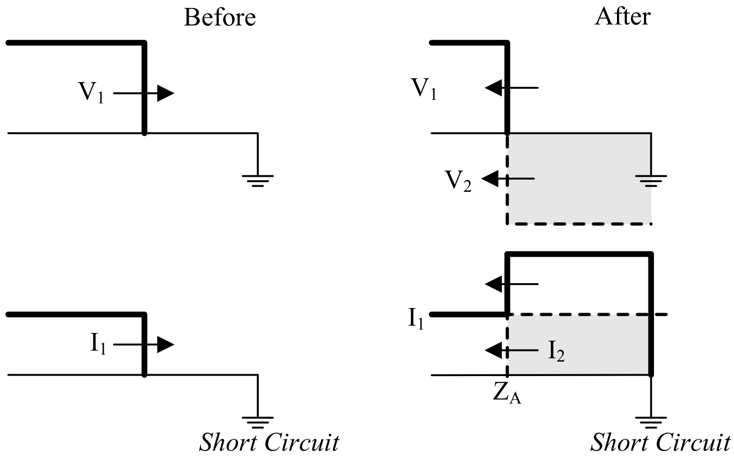

fig. 24. Wave behaviour when encountering a short circuit

The reflected voltage wave will have the same magnitude of the incident voltage wave but negative sign while the reflected current wave will return with the same magnitude and sign as the incident current wave. The voltage at the short circuit point is zero whereas the current is doubled.

The doubling of the current can be understood from an energy point of view. The total energy of a travelling wave is equally contained in the magnetic and the electric field. When the travelling wave encounters a short circuit the voltage is annihilated and all the energy that resides in the electric field is discharged. In a lossless system the released electric energy cannot be dissipated so it transforms into magnetic energy. In the short circuit point all the energy contained in the wave is magnetic: the energy of the incident wave plus the energy of the reflected wave. This is obtained by doubling the current, which turns into a four times larger magnetic field.

If a short circuit is applied to a transmission line fed by a constant voltage source (V) with no source impedance the short circuit current can be expected to indefinitely increase at a rate of V/Z_0. However, the short circuit current does not rise instantaneously due to travelling wave phenomena. The current increases in steps of $2V/Z_0$ at intervals of 2τ as it is shown in fig. 25, where τ stands for the travelling time of the wave from the source to the short circuit and vice versa.

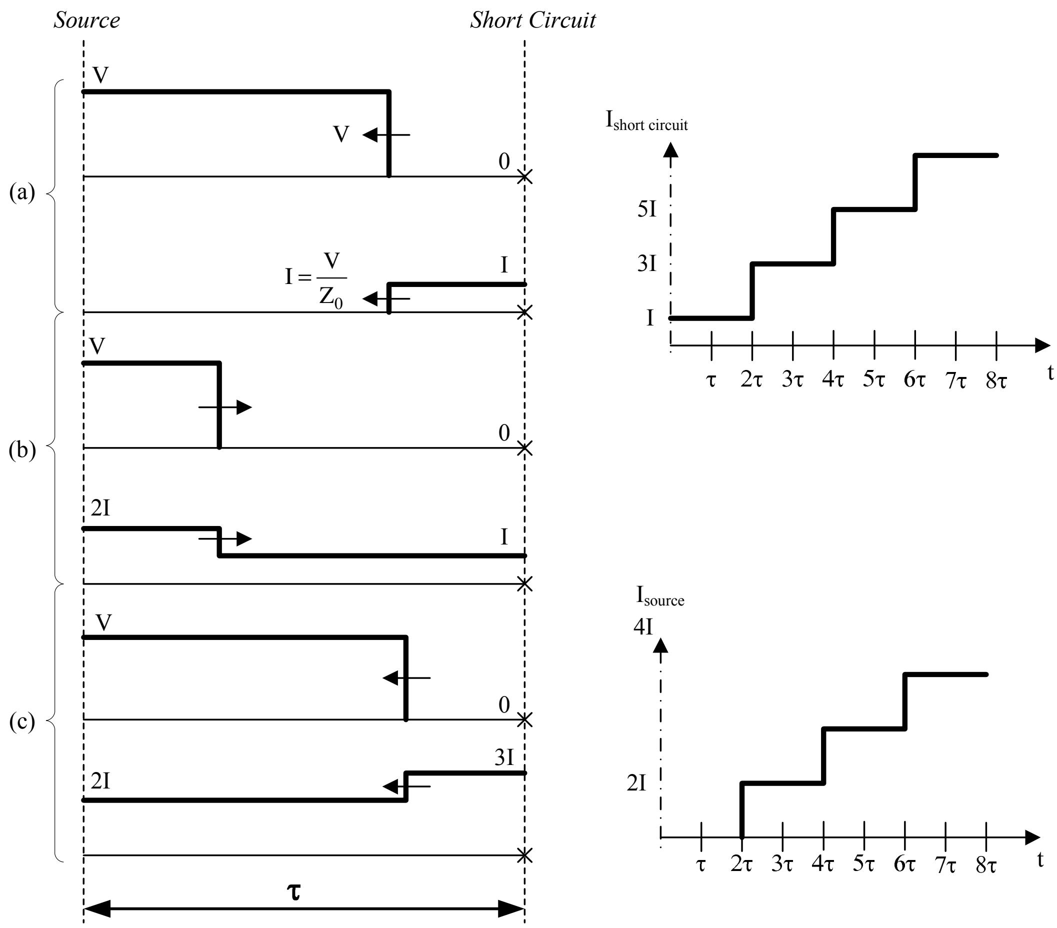

fig. 25. Travelling waves generated in a short circuit

The difference between an AC and a DC circuit is that the source voltage varies with time.

3.5.2.2 OPEN CIRCUIT

The open circuit case is just the opposite case to the short circuit where the current is zero at the open circuit. The energy stored in the magnetic field is transferred to the electric field and the voltage is consequently doubled. In order to maintain the current to zero the reflected current wave must be negative and of the same magnitude as the incident wave. At the same time, the reflected voltage wave will acquire the opposite sign to the reflected current. The sum of incident and reflected voltage waves will produce a double magnitude wave at the open circuit terminals.

Due to this voltage doubling effect open circuits can be very harmful for the system equipment when the lines are energized, see fig. 26.

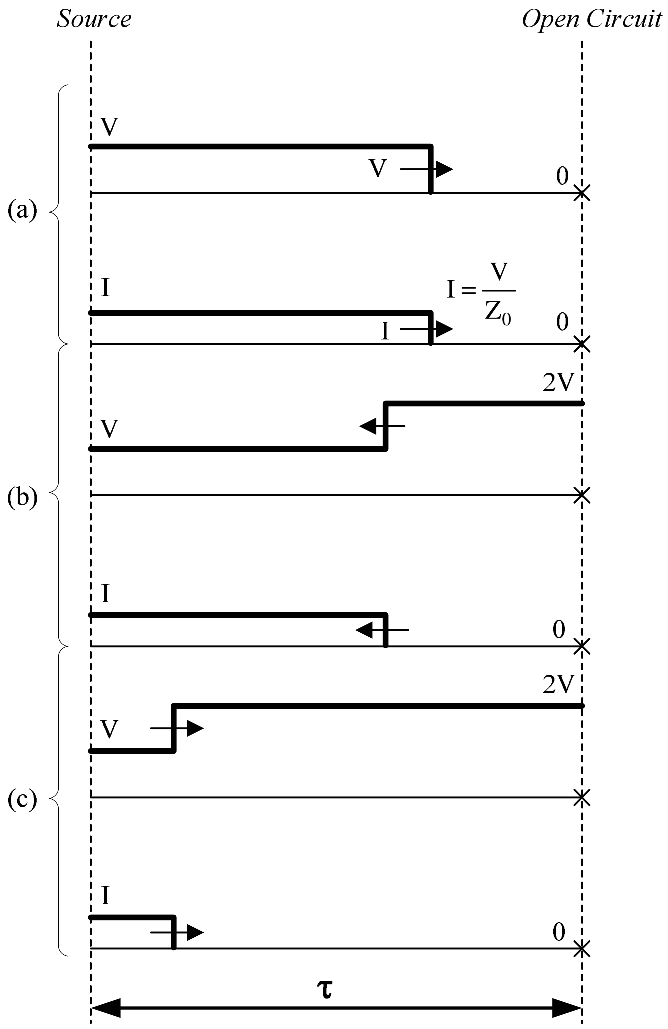

fig. 26. Travelling waves created by energizing an open circuit

3.5.2.3 CHARACTERISTIC IMPEDANCE TERMINATION: IMPEDANCE MATCHING

There is a special case in which the line is terminated in a resistance of the same value as the characteristic impedance of the line. In this case all the energy contained in the wave is absorbed by the resistor and no reflected or refracted waves are created.

3.5.2.4 CAPACITIVE TERMINATION

If the line ends in a capacitor, when the incident wave reaches the capacitor for the first time it sees a short circuit. The reflected voltage wave cancels the incident voltage wave, the voltage wave becomes zero and starts travelling backwards (negative sense of x). On the contrary, once the capacitor is completely charged, the current becomes zero and the termination behaves as an open circuit: the voltage at the line termination is doubled. The transient voltage at the line end will build up from zero to double the source voltage following a familiar exponential function, see fig. 27.

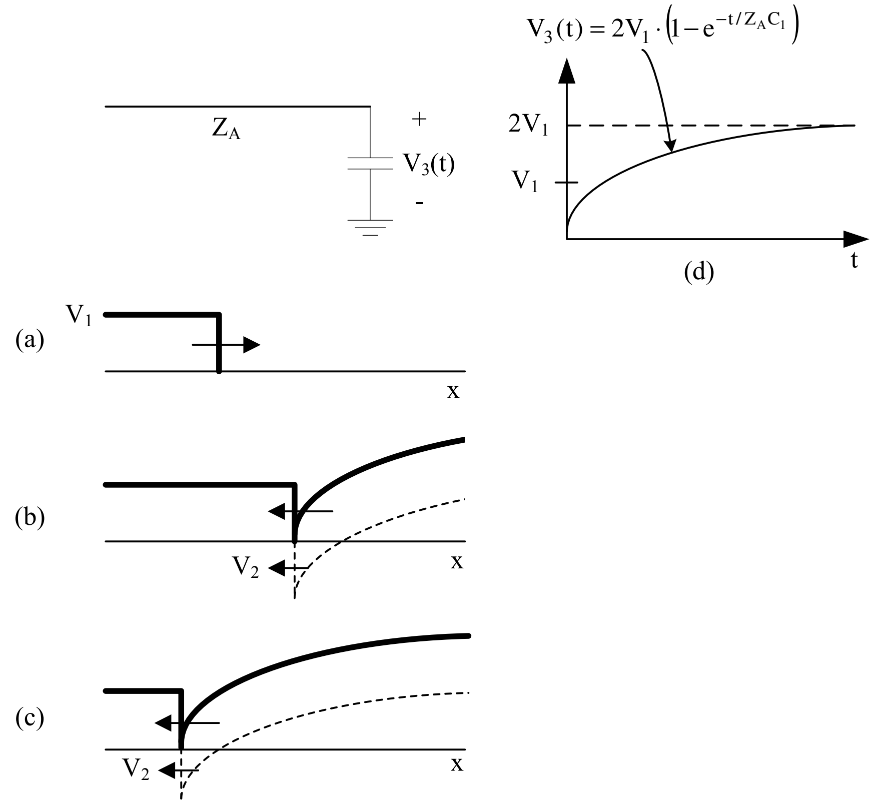

fig. 27. Travelling wave with a pure capacitive termination

3.5.2.5 INDUCTIVE TERMINATION

If the line finishes in an inductance the inverse happens. The current cannot penetrate instantly through the inductance and the wave sees the line termination as an open circuit, the voltage is therefore doubled. Ultimately the inductance behaves as a short circuit and the voltage at the terminals is annulled. In this case the transient voltage will also take an exponential shape, see fig. 28.

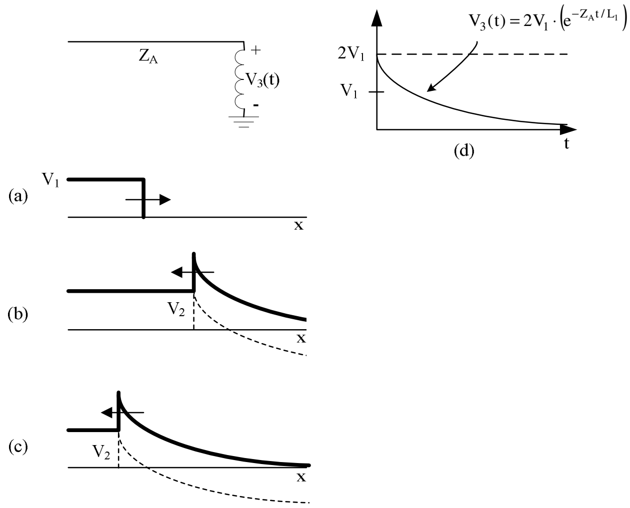

fig. 28. Travelling wave with a pure inductive termination

The exponential shape of the voltage across the circuit terminals can be easily deduced using the reflection and refraction coefficients using either the domain analysis or the *laplace transform*.

Reflection Coefficient: $a = \left(\dfrac{Z_A - Z_B}{Z_A + Z_B} \right)$ and,

Refraction Coefficient: $b = \left(\dfrac{2 \cdot Z_B}{Z_A + Z_B} \right)$

$v_2(s) = a \cdot v_1(s)$ **, where v2(s): reflected wave and v1(s): incident wave** **(eq. 29)**

$v_3(s) = b \cdot v_1(s)$ **, where v3(s): refracted wave** **(eq. 30)**

If the incident wave is a step function of amplitude V_1, then $v_1(s) = V_1/s$. After operating the equation systems, the following results are obtained:

CAPACITIVE TERMINATION

$$v_2(t) = V_1 \cdot \left(1 - 2e^{-\alpha t}\right)$$
$$v_3(t) = 2 \cdot V_1 \cdot \left(1 - e^{-\alpha t}\right)$$
$$\alpha = \frac{1}{C_1 \cdot Z_\mathrm{A}} = \frac{1}{\text{time constant}}$$

INDUCTIVE TERMINATION

$$v_2(t) = -V_1 \cdot \left(1 - 2e^{-\chi t}\right)$$
$$v_3(t) = 2 \cdot V_1 \cdot e^{-\chi t}$$
$$\beta = \frac{Z_\mathrm{A}}{L_1} = \frac{1}{\text{time constant}}$$

The refracted wave at the line termination can also be calculated using the Thévenin Theorem, see fig. 29. According to this theorem the voltage across two terminals can be obtained from an equivalent circuit which is reduced to an equivalent voltage source and impedance in series. The equivalent *Thévenin source* is the voltage measured at the open terminals and the equivalent *Thévenin impedance* is obtained by short circuiting all the voltage sources of the system and getting the total impedance seen from the open terminals.

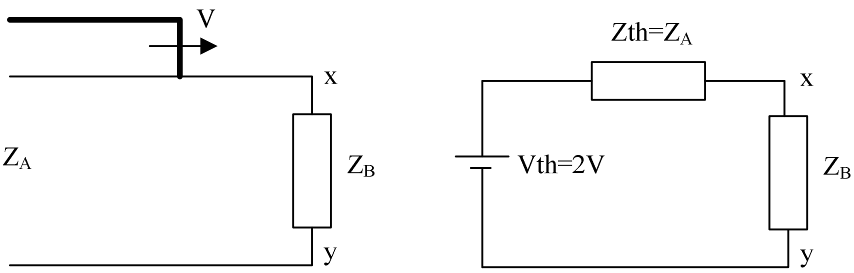

fig. 29. Thévenin equivalent circuit (right) for calculation of reflected and refracted waves

The voltage across the terminals, which represents the refracted wave, can be obtained without difficulty looking at fig. 29. It is checked that the voltage across the terminals is the incident wave multiplied by the refraction coefficient.

$$V_\mathrm{xy} = V_3 = \frac{2 \cdot V \cdot Z_\mathrm{B}}{Z_\mathrm{A} + Z_\mathrm{B}} \qquad \textbf{(eq. 31)}$$

3.6 PRACTICAL EXAMPLE EXTRACTED FROM A SIMULATION

This chapter explains how the voltage and current waveshapes build up during the first microseconds after a transformer energization (at no load). A point by point explanation is given which helps understanding the wave reflection and refraction mechanisms. For this purpose the three-phase circuit that is shown in fig. 30 has been used.

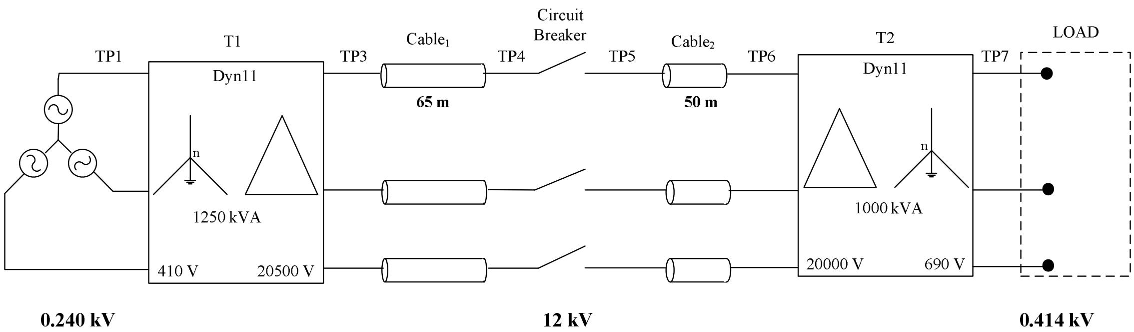

fig. 30. Three phase circuit used to explain the voltage reflections

Energizing the transformers is a sensitive action as far as fast transient overvoltages are concerned. When the CB is closed there is a sudden energy transfer from the supply side of the circuit to the load side. The energy propagates through the cables and reflects back and forth due to the impedance mismatch in different parts of the circuit causing steep voltage wave fronts. Fig. 31 and fig. 32 explain how the travelling waves are formed.

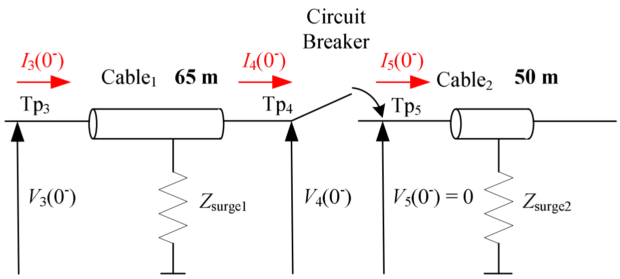

fig. 31. CB an instant before closing

An instant before the CB is closed the supply voltage is found at nodes 3 and 4 while there is no voltage at node 5. When the CB closes the voltage difference between nodes 4 and 5 becomes zero and a part of the initial voltage in node 4 is transferred to the load side. The delivered energy travels to the load side as a positive voltage step and a negative voltage step travels towards the supply in order to obtain the same voltage at the breaker.

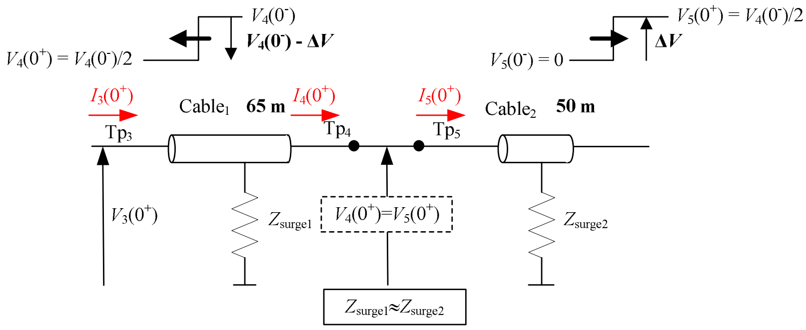

fig. 32. CB an instant after closing

If both cables have the same surge impedance the voltage at nodes 4 and 5 will be halved as soon as the breaker closes. However, the general expression is provided:

$$V_4(0^+) = V_5(0^+) = \frac{Z_{surge2}}{Z_{surge1} + Z_{surge2}} \cdot V_4(0^-) = \Delta V$$

In this simulation the transformer saturation has not been enabled. The reason for not enabling saturation in the transformers is to see a more “pure” shape of the reflected and refracted waves (saturation makes the magnetizing characteristic of the transformer not linear and the analysis becomes more complicated). Graphs fig. 33, fig. 41 and fig. 42 show the very beginning of the energizing process where the shape of the waves can be understood by means of a basic electromagnetic wave theory.

NO-LOAD ENERGIZING. SATURATION NOT ENABLED. Tstep=Tplot=0.05µs

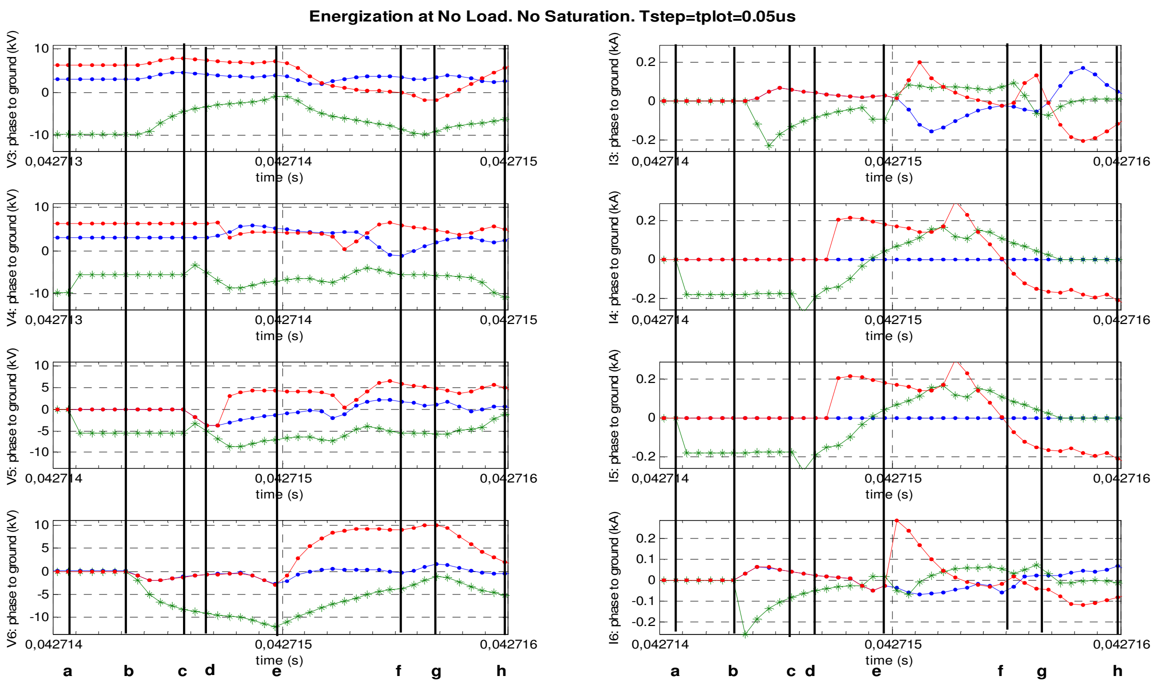

fig. 33. Voltage and Current wave shapes the first microseconds after energizing

Phase a: blue, Phase b: red, Phase c: green

Top to bottom: voltages and currents at point 3, 4, 5 and 6

Left: Voltages

Right: Currents

In order to explain how the waves are generated a time window of 2µs is zoomed. If the load side of the circuit is analyzed during this first 2µs eight main points are observed:

POINT a

At this point the voltage in phase c (test point 4) is higher than the voltage withstand capability of the breaker. The CB cannot withstand such a high voltage across it, it reignites and the first arc appears. The voltage between the two terminals becomes almost zero and a current starts flowing through phase c.

When the voltage in phase c (point 4) reaches the withstand curve it has a value of -9.664 kV. After the arc is ignited the voltage at point 4 and point 5 (the two terminals of the breaker c) must be equal. The characteristic impedance of both cables is very similar so this initial voltage is approximately halved to -5.452 kV. If we take the positive x in the direction of the load and the negative x in the direction of the supply, we will be able to observe two travelling waves. One will move towards the load with a magnitude of (-5.452 kV) and the other one will travel towards the supply with a positive magnitude of [(-5.452 kV)-(-9.664 kV)] = 4.212 kV. See fig. 34.

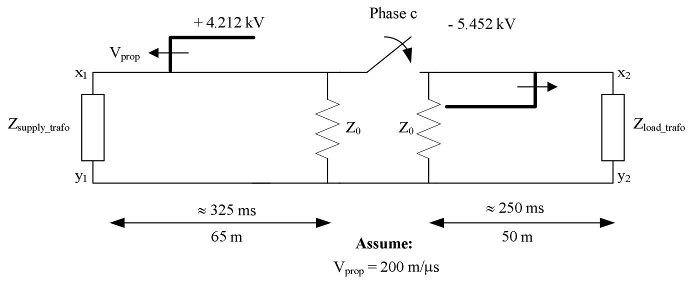

fig. 34. Thévenin equivalent circuit (right) for calculation of reflected and refracted waves

In the very first moment, the voltage wave only "sees" the characteristic impedances because it needs a certain time to reach the end. The formed current step will be proportional to the actual voltage level at point 4 and 5 (-0.1816 kA). This means that the characteristic impedance is in the order of (-5.452 kV) / (-0.1816 kA) ≈ 30 Ω, a value that can be obtained from the distributed inductance and capacitance of the cable. If the distributed resistance and conductance of the cable are negligible in comparison to the inductance and capacitance, then the characteristic impedance is calculated as in (eq. 32):

$$Z_0 = \sqrt{\frac{L_{\text{distributed}}}{C_{\text{distributed}}}} \qquad \textbf{(eq. 32)}$$

For example, for the 50m cable:

$$Z_{0\_50\text{m}} = \sqrt{\frac{L_{\text{distributed}}}{C_{\text{distributed}}}} = \sqrt{\frac{150\text{nH/m}}{169.52\text{pF/m}}} = 29.75\Omega$$

For the 65m cable:

$$Z_{0\_65m} = \sqrt{\frac{L_{\text{distributed}}}{C_{\text{distributed}}}} = \sqrt{\frac{116\text{nH/m}}{220.28\text{pF/m}}} = 22.95\Omega$$

It can also be observed that for the 65 m cable the estimated impedance is not so close. This can be due to a poor approximation of the distributed parameters (mostly the inductance).

POINT b

The wave travelling towards the load needs about 250 ms to reach the load (point b). Until this moment the voltage and current values are maintained constant in all the points of the circuit. When the wave hits the load, the magnitude of the voltage at point

6 in phase c starts to grow (observe that it is negative because the incident voltage step is also negative).

However, this voltage increase does not only affect phase c. Phases a and b are also coupled by the ground capacitances and stray capacitances of the transformer windings. Figures fig. 35 through fig. 37 explain how to deduce an equivalent circuit to represent how the voltage changes in the other phases when a voltage step is introduced in one of them.

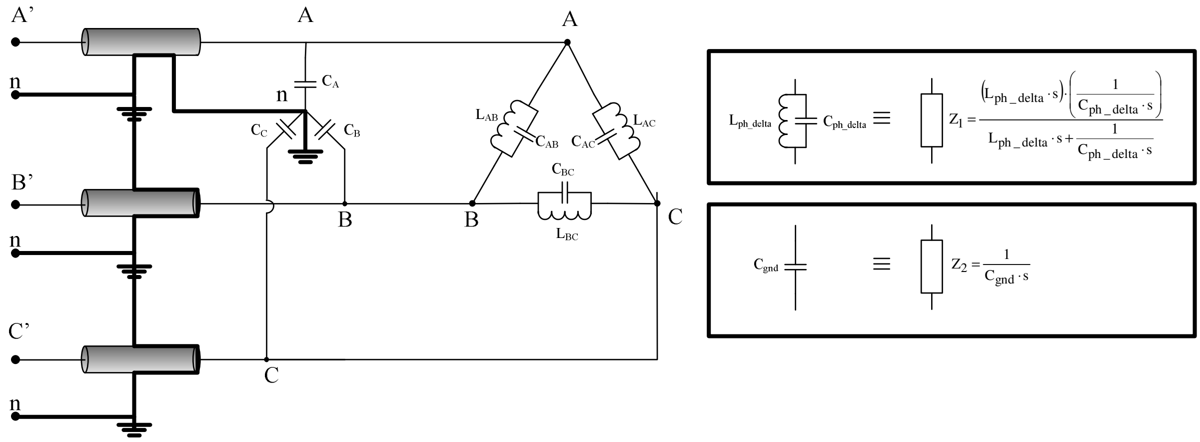

fig. 35. Load side of the CB

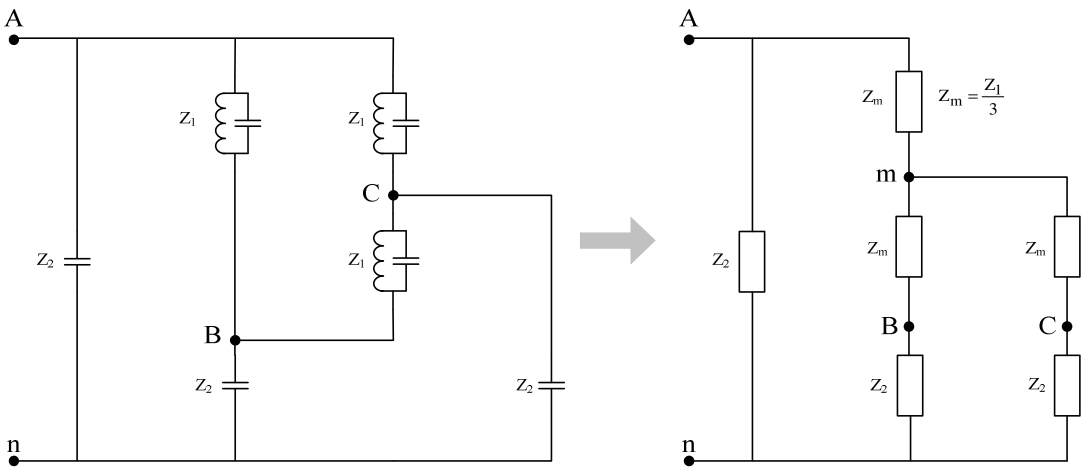

fig. 36. Simplification of the load side of the CB

The final equivalent circuit is represented in fig. 37. When a CB is opened the step source is short circuited and the incident wave only sees the characteristic impedance. The step voltages and the times in which they are applied vary dynamically with time. For this reason it can get quite complicated to simulate the system for long periods (*long* here means more than twice or three times the propagation time).

During a pre-strike o restrike sequence the three phases of the CB do not “open” and “close” (opening and closing refers to the existence of an arc: open, no arc; close, arc) at the same time so the input to the equivalent circuit shown in fig. 37 is continuously varying.

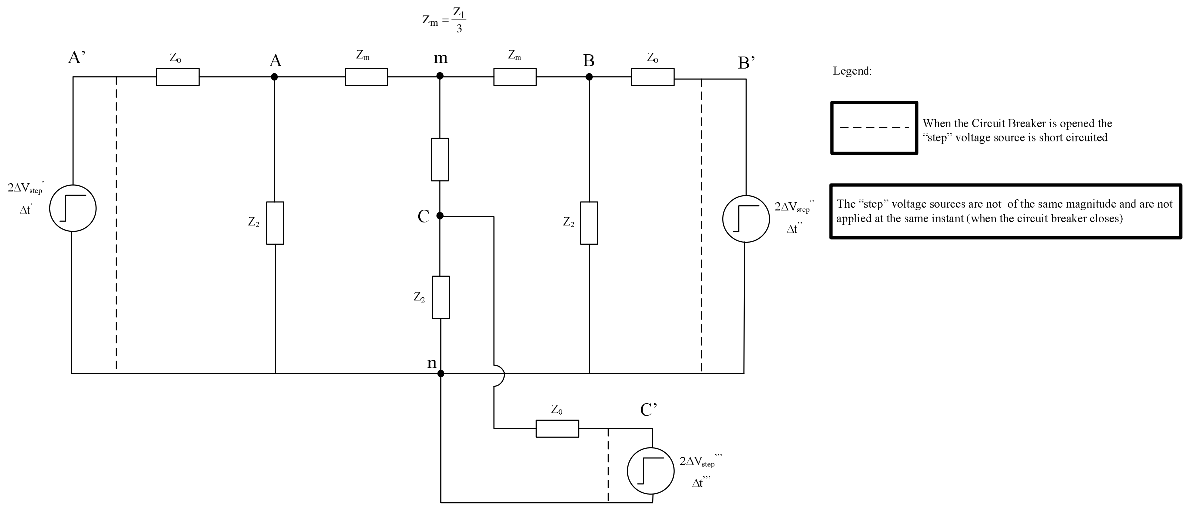

fig. 37. Circuit for estimating refracted waves

This circuit has been checked by simulations in PSCAD, see circuit in fig. 38.

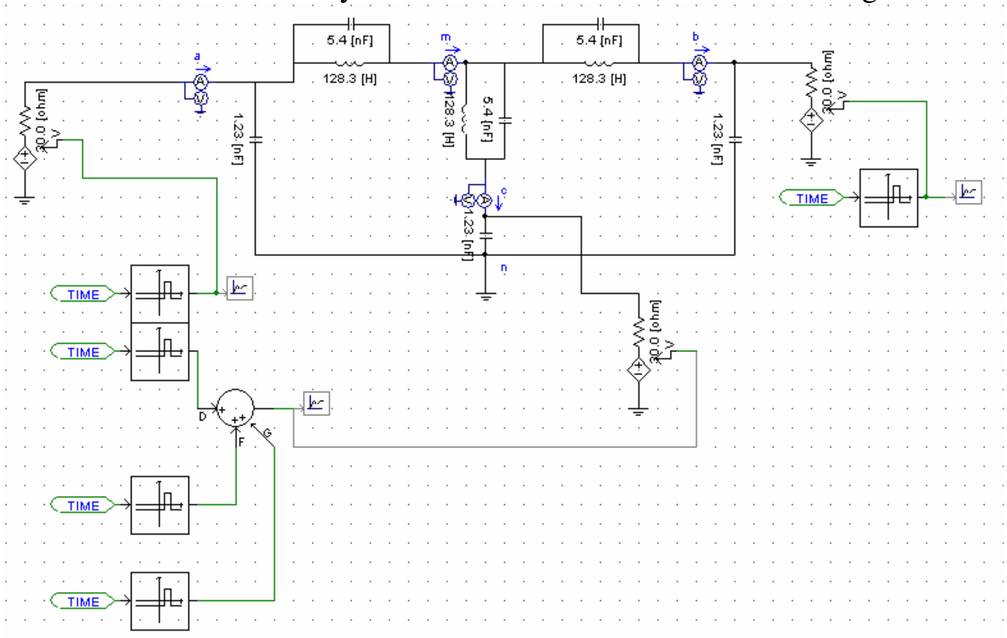

fig. 38. Pscad circuit used to understand the shape of the refracted waves

The wave shapes obtained from the equivalent circuit built in PSCAD and the shapes observed at the test point 6 are not exactly the same because the input voltage steps and times must be more adequately adjusted but they are enough to validate the equivalent circuit, see fig. 39and fig. 40.

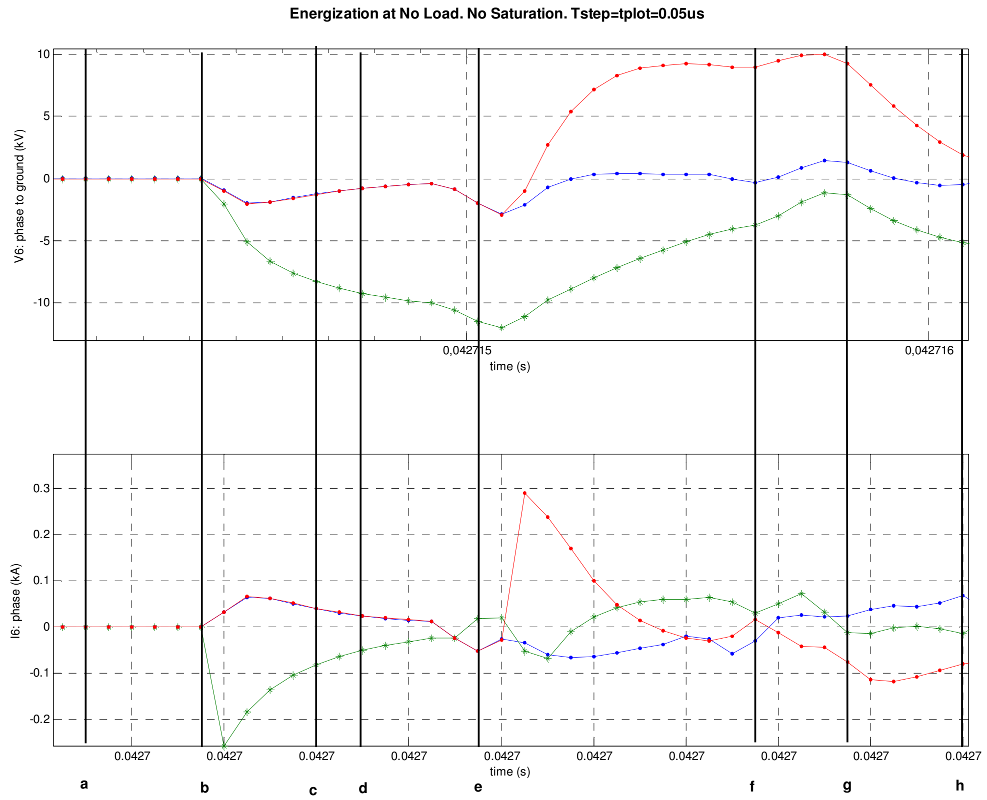

fig. 39. Voltage and Current at point 6

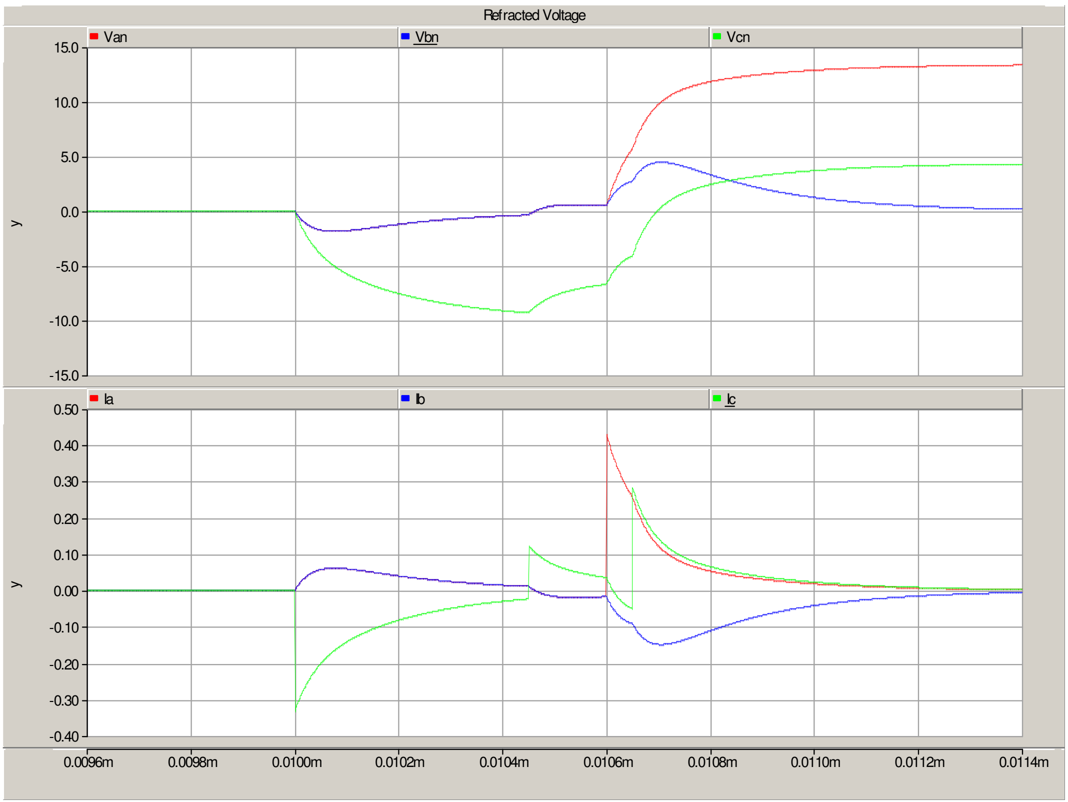

fig. 40. Voltage and Current obtained from equivalent PSCAD circuit

At point b a wave travelling in direction of the CB is created. This wave varies its magnitude in time.

POINT c

The travelling wave generated at the load returns to the CB and finds a discontinuity. If both cables are exactly the same the wave should not find any difference in the characteristic impedance. Nevertheless, in this particular case the cables are different and once again a reflected wave (going to the load) and a refracted wave (penetrating the junction) is created. Observe that phase c finds a discontinuity (because the phase c CB is ignited) and its voltage values is approximately halved, while phase a and b double their voltages at point 5 (the wave sees an open circuit) but keep constant at point 4. Due to the increase of the voltage in phase a and b the voltage across the breaker will also rise and phase a voltage will exceed the voltage withstand capability of the breaker.

VOLTATE AND CURRENT ACROSS THE CB

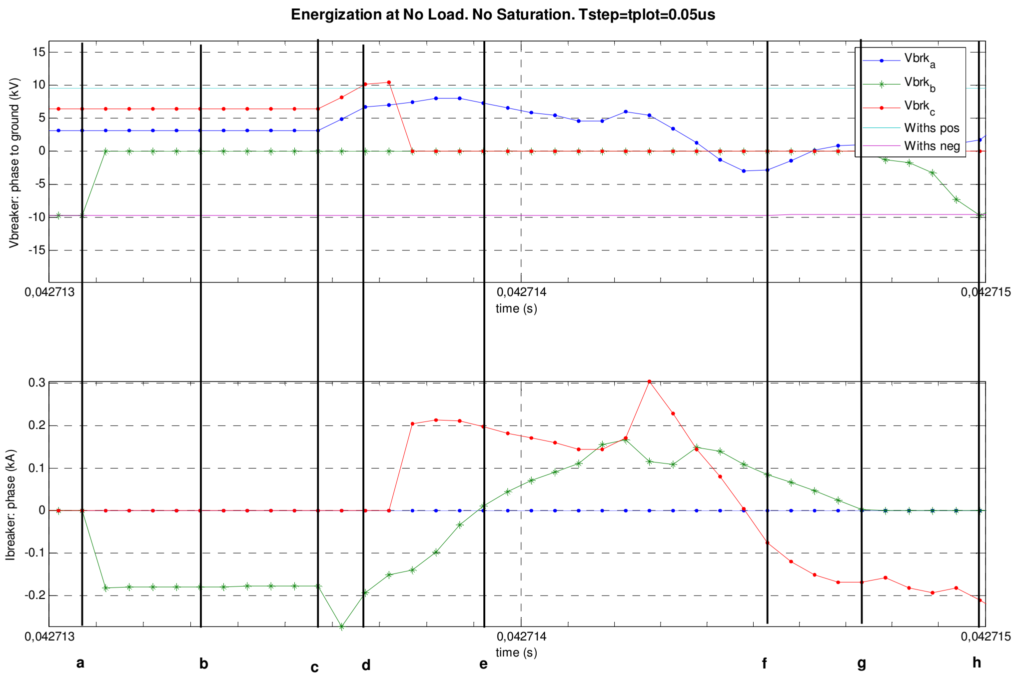

fig. 41. Voltage and Current across the CB the first µs-s after energizing

POINT d

At point d the voltage at phase a has already exceeded the voltage withstand capability of the breaker and will provoke the breaker to ignite. At this moment there are two phases igniting at the same time.

On the other hand, the wave that was produced in the delta side of the supply transformer finds the junction (the CB) but in the opposite direction: from the supply side to the load. From this moment on, the wave coming from both ends will be superimposed and the analysis will become harder.

POINT e

At point e the current flowing through phase c passes the zero crossing but, unexpectedly, the breaker c does not open. The voltage wave created from the closing of breaker a reaches the load and the voltages at point 6 starts to increase (all phase voltage increase: phase c and a in the same rate and phase b, which is not closed yet, at a lower rate).

At the supply side transformer (point 3), the voltage wave that had been generated due to the wave coming from the load side hitting the junction arrives.

POINT f

At point f the current through phase a is made zero but the breaker does not open (this might be due to a large simulation step) so it continues flowing with a negative sign.

POINT g

At point g the current through phase c becomes zero and breaker c opens. Two other travelling waves will be created.

After point g all the waves will travel in every direction producing reflected and refracted waves in each discontinuity point found. Since all the waves are superimposed it gets more and more complicated to follow the trajectory of each of them. Furthermore, the three breakers open and close uninterruptedly (until the contacts are physically touching) becoming an incessant source of new waves.

VOLTAGE AND CURRENT IN THE DELTA SIDE OF THE LOAD TRANSFORMER

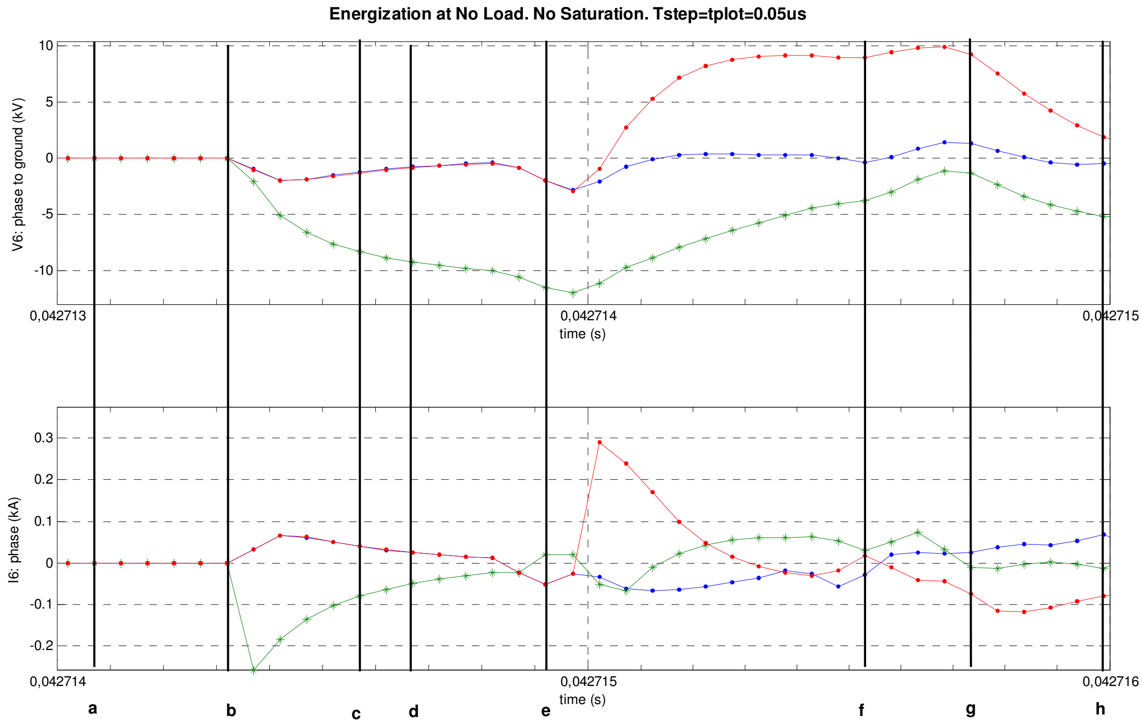

fig. 42. Voltage and Current in the delta side of the load transformer the first µs-s after energizing

3.7 OSCILLATIONS IN A SIMPLE CIRCUIT

In this section the main oscillation modes of a very simple circuit are presented. The objective is to explain how the different parts of the circuit resonate. In fact, almost every inductance resonates with every capacitance but some of the combinations resonate at such high frequencies that they are damped instantaneously. Moreover, if two inductances are in series and their values are in different order of magnitudes (one much larger than the other) then the biggest inductance is the dominant one. If two capacitors are in series, the smallest prevails. In the particular circuit shown in fig. 43 it has been considered that the busbar capacitor is much bigger than the load and cable capacitor and that the stray inductance of the gap is much smaller than the cable inductance.

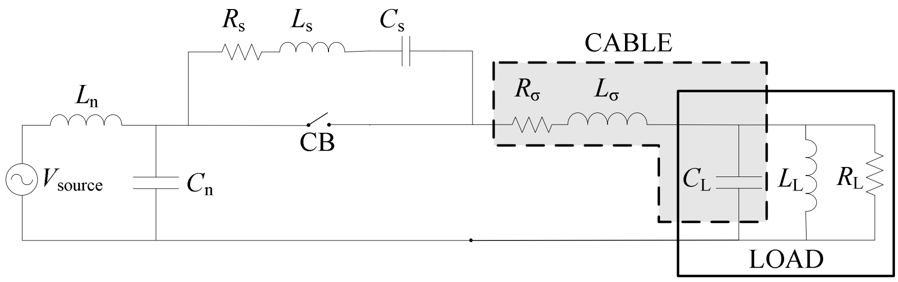

fig. 43. Simple circuit to explain oscillatory behaviour

This simple circuit represents a load connected to a voltage supply by means of a CB and a cable. The source has been modelled with an AC voltage source (V_{source}), a source inductance, including busbar inductance (L_n), and stray capacitance of the busbars (C_n) and connecting equipment. The elements named in fig. 43 with a suffix "s" are the parasitic parameters of the vacuum gap. The model of the cable has been simplified so much that it only contains a series resistance (R_σ) and an inductance (L_σ) and a parallel capacitance in the load side (with has been drawn already added to the load capacitance C_L). In order to represent the cable with a pi-link the cable capacitance should have been split into two halves and connected at both ends of the series RL. For simplicity the pi link has not been modelled.

The data introduced in the model, which has been reported in table 2, has been picked from [18] and the circuit has been simulated and frequency scanned in PSCAD.

table 2. Data of the circuit of fig. 43

	Capacitance (nF)	Inductance(μH)	Resistance (kΩ)
Source and busbars (n)	C_n=100	L_n=5·10^3	
Gap (s)	C_s=0.1	L_s=0.050	
Cable (σ)	C_L=10	L_σ=40	
Load (L)		L_L=120·10^3	R_L=100

The frequency plots are a very useful tool to analyse and understand the oscillatory behaviour of a circuit. However, for fast transient analysis it is more important to determine when these resonances happen, which is the damping and how relevant are they in the frequency spectrum.

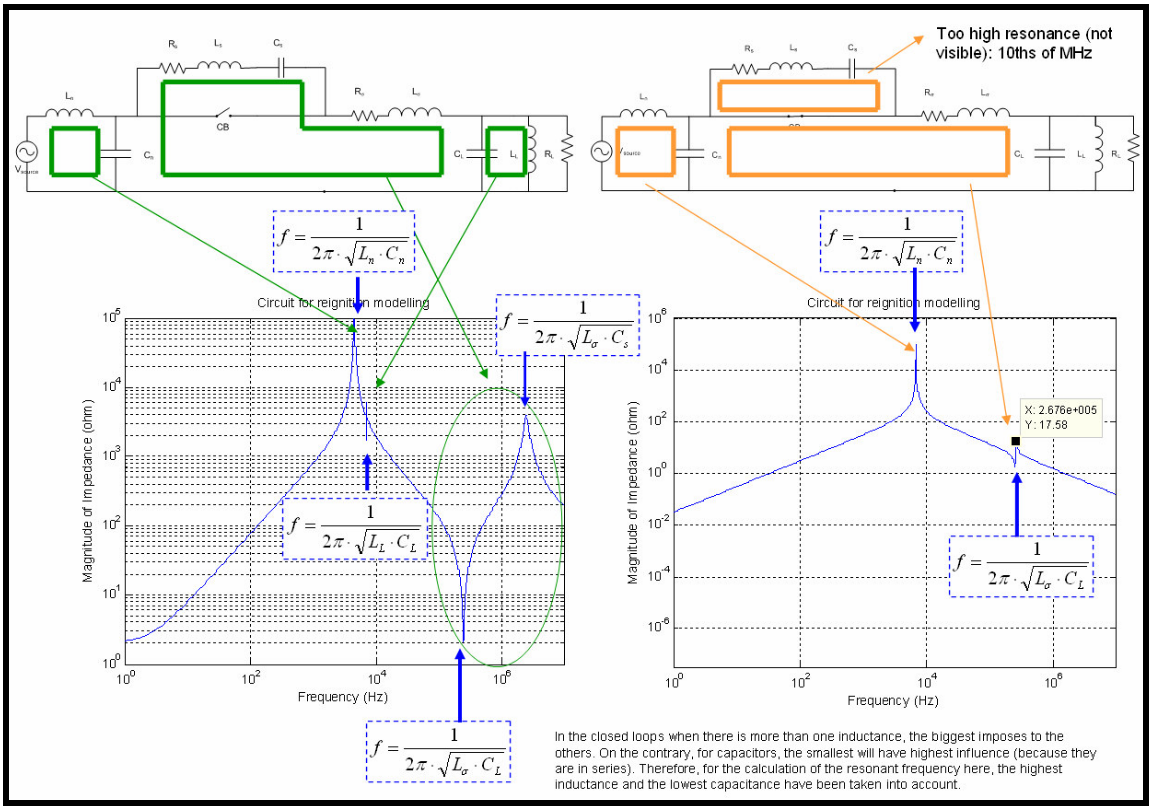

fig. 44. Main resonace frequencies of a simple circuit when opened and when closed

By examining fig. 44, the following conclusions can be extracted:

i. The busbar inductance and capacitance always resonates. This means that this oscillation is always present independently of the switch position. It is usually noticeable some time after opening the switch.

ii. As soon as the current extinguishes, three other main oscillations are observed.

   a. The "self" oscillation of the load (in which the cable capacitance is also embedded) at the frequency

$$f_{\text{load}} = \frac{1}{2\pi\sqrt{L_{\text{L}} C_{\text{L}}}} \quad \textbf{(eq. 33)}$$

   This is the lowest oscillating frequency (apart from the source oscillation). It is in the order of a few kHz (depending on the circuit) and it corresponds to the natural oscillation frequency of the load.

   b. The cable inductance resonates in series with the load capacitance, the gap stray capacitance and the busbar capacitance but since the busbar capacitance is much larger than the others its effect is neglected.

      - The resonance of the cable inductance with the load capacitance is at the frequency

$$f_{\text{cable\_load}} = \frac{1}{2\pi\sqrt{L_\sigma C_{\text{L}}}} \quad \textbf{(eq. 34)}$$

      which is around hundreds of kHz.

      - The resonance of the cable inductance with the stray capacitance of the load is at the frequency

$$f_{\mathrm{cable\_gap}} = \frac{1}{2\pi\sqrt{L_\sigma C_\mathrm{S}}} \qquad \textbf{(eq. 35)}$$

which has a value of around a few MHz.

iii. When the vacuum circuit reignites two oscillatory behaviours are observed:

a. The resonance of the cable inductance with the stray capacitance of the load, which is the same as in (eq. 34).

$$f_{cable\_load} = \frac{1}{2\pi\sqrt{L_\sigma C_S}} \qquad \textbf{(eq. 36)}$$

This frequency is around a few hundreds of kHz.

b. The gap stray inductance and capacitance oscillation:

$$f_{gap} = \frac{1}{2\pi\sqrt{L_S C_S}} \qquad \textbf{(eq. 37)}$$

This resonance cannot be seen in the frequency plot because the time step used for simulating the circuit is too large. This frequency is in the order of tens of MHz and it usually appears as a high frequency component of the reignition current.

3.8 CONCLUSIONS

- A transient is the change in the steady-state conditions of a system. The majority of the transients analysed in this work are caused by the interconnection and/or disconnection of two systems and they are called switching transients.
- In literature [5] switching transients have been grouped in two categories: simple switching transients and abnormal switching transients. The main difference between them is that an abnormal switching transient does not start from a quiescent energy state. Some of the most typical switching operations have been explained in this chapter.
- Wave propagation is also an interesting phenomenon because the higher wave travelling speeds in cables generate a fast response of the system to switching transients. Moreover, waves reflect and refract in the discontinuity points.
- Two simple examples have been examined in this chapter. One of the examples describes a methodology for obtaining an equivalent circuit to predict the shape of the reflected waves in a no-load transformer energization case. The other example explains the oscillations modes of a simple circuit.

4. MODELS FOR FAST TRANSIENT ANALYSIS

A power system is formed by many different kinds of components and equipments. The purpose of the present chapter is to describe a general modelling methodology for the components of the system under study, see fig. 45. For this reason, the components that will be analysed correspond to a particular setup formed by a supply grid, transformers, cables, a VCB and other secondary equipment.

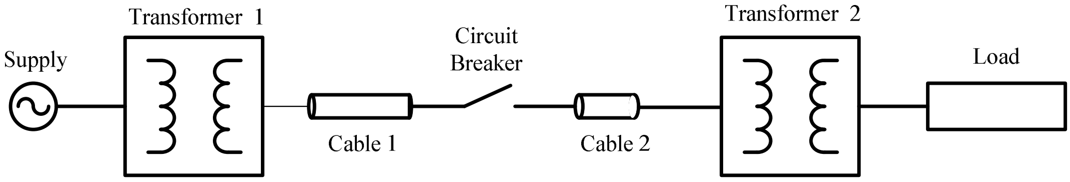

fig. 45. Schematic view of the three-phase setup

4.1 INTRODUCTION TO HIGH FREQUENCY MODELLING

The most typical models used in power systems are optimized to operate at the power frequency of 50 or 60 Hz. However, it is not possible to focus on a single fixed frequency when talking about fast transients. In a multiple restrike case, for example, a broad range of frequencies are excited, see fig. 46, starting from a few kHz to tens of MHz. According to [20] four different oscillatory behaviours are distinguished:

1. **Voltage Oscillation (1-1.5 kHz)**: when the switch is totally opened, and after the series of multiple reignitions (if there are) the load oscillates at its natural frequency.
2. **Re-strikes (20-100 kHz)**: the multiple reignitions are responsible of exciting this frequency range.
3. **Breakdown (≈ 1.5 MHz):** this high frequency corresponds to the breakdown oscillation that occurs when the voltage across the switch exceeds the dielectric withstand of the gap and an arc is initiated.
4. **Cable reflection (tens of MHz):** the reflection frequency depends on the speed of propagation of the electromagnetic waves on a particular cable and the length of the cable. A typical value for the propagation speed of waves on cables is 200 m/µs but this value varies from cable to cable.

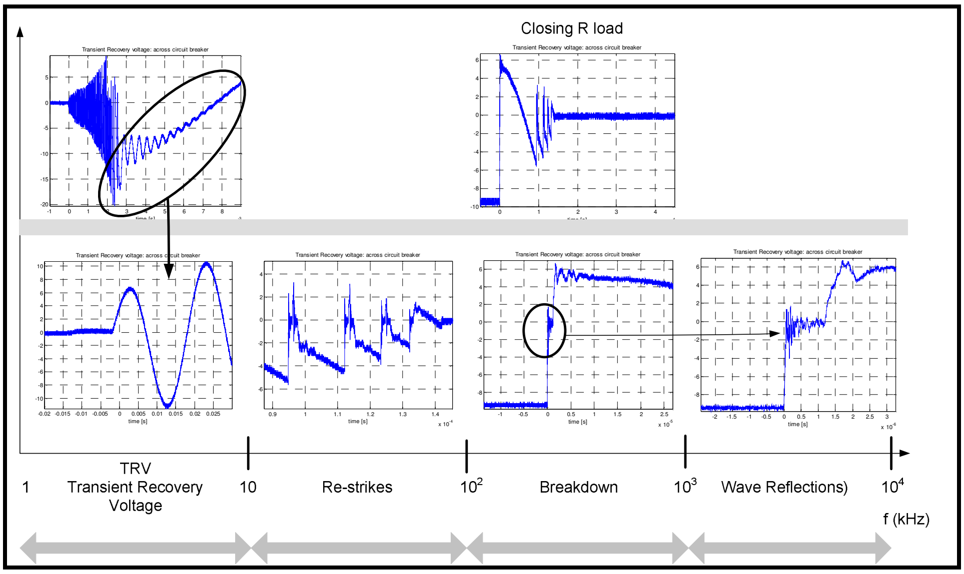

fig. 46. Frequency spectrum of restrikes.

Modelling the fast transient behaviour of a system component is not an easy task. Two main problems are observed:

- Fast transients do not happen at a single, fixed frequency. They happen at a wide range of frequencies. Every piece of equipment is frequency dependent in a higher or lower manner and thus, the parameters take different values according to the frequency that they are being exited at that instant.
- Each fast transient phenomenon that are to be studied must be determined and a model built accordingly. It is not possible to build a unique model that is valid to represent all kinds of fast transient phenomena.

The simulations have been performed using the power systems simulation tool called PSCAD-EMTDC which is a worldwide recognized program among power system engineers. Indeed, one of the main reasons for using PSCAD and not any other in-house simulation package is that the results can be verified by any member of the research community. PSCAD has many interesting features for modelling power systems but it is certainly incomplete in this particular case where fast transient phenomena are to be studied.

Solutions are needed for the modelling of the following equipment, where standard PSCAD models are insufficient:

- High frequency transformer modelling
- Three phase cables: surrounding armour
- Detailed VCB model

4.2 SUPPLY GRID

The most common way of modelling a supply grid is by an AC voltage source and a series source inductance, see fig. 47. If the system under analysis is being fed by a strong grid the source inductance can be neglected but if the source is not strong, then some other considerations must be made:

- **Source reactance**:

A reflection must be made about which value of the reactance of the generator to use: the synchronous reactance, the sub-synchronous reactance or another high-frequency dependent reactance. Few researchers have considered the last option but it is evident that at very high frequencies the sub-synchronous reactance representation it is not valid anymore.

- **Inductance of the connecting cables:**

Usually the source is connected to the transmission lines and other equipment by means of busbars or other conducting equipment. This connecting equipment has some inductance, which must be calculated in order to determine whether it is negligible or not.

- **Busbar capacitances**:

It must be evaluated if the busbar stray capacitances have a significant value comparing to the neighbouring equipment.

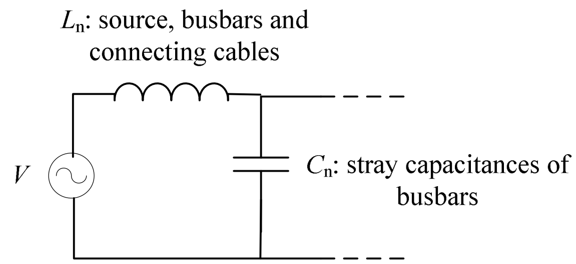

fig. 47. Modelling of supply grid

4.3 TRANSFORMERS

4.3.1 General theory on high frequency transformer modelling

Even though transformers are some of the most common components of the power system, their modelling can become a complex issue, especially at high frequencies. To model the transient behaviour of a transformer, both its non-linear behaviour and its frequency-dependent effects must be considered.
Article [3] summarizes the two main transformer high frequency modelling techniques:

1) **Detailed internal winding models**. This type of model consists of large networks of capacitances and coupled inductances obtained from the discretization of distributed self and mutual winding inductances and capacitances. The calculation of these parameters involves the solution of complex field problems and requires information on the physical layout and construction details of the transformer. This information is not available and it is generally considered as property of transformer manufacturers. These models have the advantage of allowing access to internal points along the winding, making it possible to assess internal winding stresses. In general, internal winding models can predict transformer resonances but cannot reproduce the associated damping. This makes this class of models suitable for the calculation of initial voltage distribution along a winding due to impulse excitation, but unsuitable for the calculation of transients involving the interaction between system and transformer. Moreover, the size of the matrices involved makes this kind of representation impractical for EMTP system studies (for example PSCAD studies).

2) **Terminal Models**. Models belonging to this type are based on simulation of the frequency and/or time domain characteristics at the terminals of the transformer by means of complex equivalent circuits or other closed-form representations. These "terminal" models have had varying degrees of success in reproducing the

frequency behaviour of single-phase transformers accurately. The main drawback of the methods proposed to date appears to be that they are not sufficiently general to be applicable to three phase transformers.

It seems obvious that the most adequate transformer model is a terminal model, since the interest lays on analysing the interaction of the transformer with the system. For the moment, there is not so much concern about knowing which the response of a particular winding is to an external stimulus.

A good analysis of modelling needs is found in [4] :

Operation of VCBs causes switching surges that generate electromagnetic transients in a wide range of frequencies. Therefore, the transformer model must be able to represent the behaviour of the system not only at power frequency but also at high frequencies. Extensive research has been carried out by CIGRE WG 13.02 on switching of small inductive currents but the transformer models used were often simplified by considering the transformer hysteresis or saturation and the total transformer capacitance. The main disadvantage of these kinds of models is that the total transformer capacitance does not adequately characterize every frequency component. However, the transformer model used in this work considers only the stray capacitances of the transformer and is able to represent frequencies of up to 100 kHz. The stray capacitances comprise the phase to ground capacitances and the lumped winding capacitances.

Before building any transformer model, the working frequency range must be determined. Two separate cases can be distinguished:

If no reignitions occur, then the electromagnetic transients remain in the low frequency domain and an unloaded transformer behaves as a non-linear reactor. The non-linearity is caused by magnetic saturation and the hysteresis of the transformer core. Also because of the non-linear transformer core, inrush currents flow when a transformer is energized. Depending on the rate of saturation, the inrush currents can reach values a few times larger than the rated transformer current. Switching off such inrush currents can lead to virtual current chopping in the surrounding network that can cause severe overvoltages. In order to calculate the electromagnetic transients accurately, the residual flux should be considered.

If the VCB reignites a high frequency modelling of the transformer is needed. At high frequencies, fast flux variations take place and the saturation and hysteresis of the transformer core do not play a significant role and can therefore be neglected. Due to the flux penetration at a relatively higher frequency range, the performance of an iron core winding tends to be linear. However, below 100 kHz, where switching transients are likely to be present, the linear assumption is not obvious.
The terminal impedance characteristic gives sufficient information about the wide frequency range performance but it is different depending of the load. If the transformer is not loaded the magnetizing inductance takes more weight than the leakage inductance for frequencies below 100 kHz and as a consequence the magnitude of the impedance rises and the resonance frequencies shift (the value of the magnetizing inductance is much higher than the leakage inductance). On the contrary, if the transformer is short circuited the main flux in the core is partially cancelled by the secondary ampere turns and the effect of the iron core is negligible (the leakage inductance is dominant).
Depending on the frequency, the behaviour of the transformer is different. This implies that we can accurately calculate switching overvoltages if a different model is used for each different transient condition. However, this is not possible since there is not a general transformer model that can describe the response at all operating conditions.

The following table (fig. 48) taken from [4] can serve as a good guideline to choose the suitable transformer model for each case. In this table the transformers are classified according to two criteria: the frequency range in which they operate most efficiently and their ability for surge transfer. Modelling surge transfer is useful if there is an interest of knowing what happens at the secondary side.

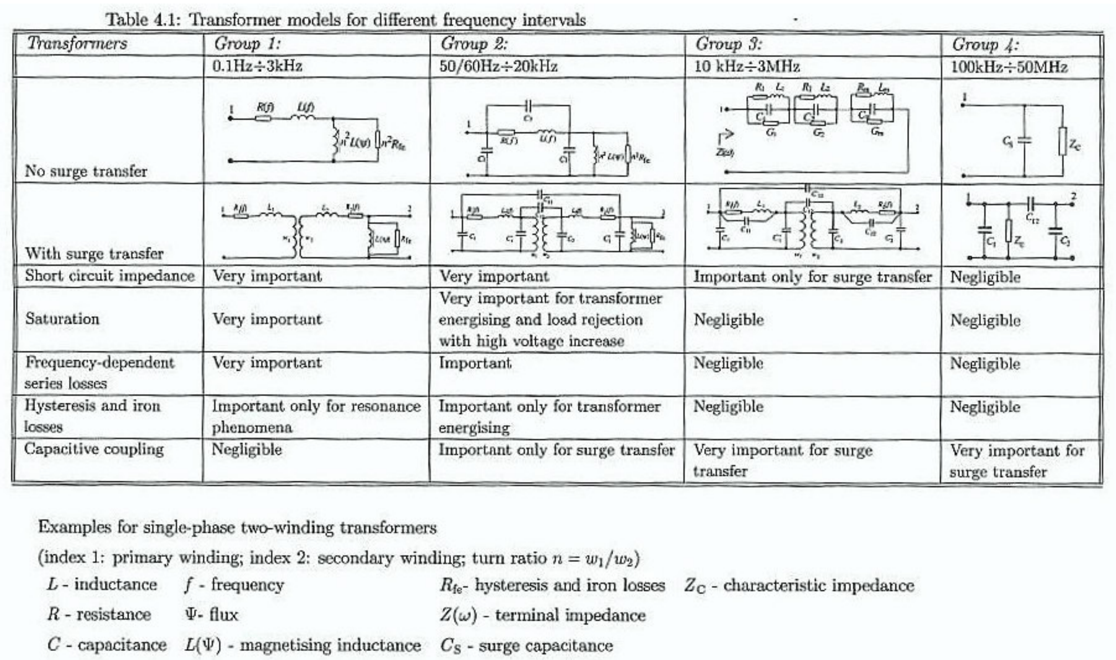

Table 4.1: Transformer models for different frequency intervals

Transformers	*Group 1:*	*Group 2:*	*Group 3:*	*Group 4:*
	0.1Hz÷3kHz	50/60Hz÷20kHz	10 kHz÷3MHz	100kHz÷50MHz
No surge transfer				
With surge transfer				
Short circuit impedance	Very important	Very important	Important only for surge transfer	Negligible
Saturation	Very important	Very important for transformer energising and load rejection with high voltage increase	Negligible	Negligible
Frequency-dependent series losses	Very important	Important	Negligible	Negligible
Hysteresis and iron losses	Important only for resonance phenomena	Important only for transformer energising	Negligible	Negligible
Capacitive coupling	Negligible	Important only for surge transfer	Very important for surge transfer	Very important for surge transfer

Examples for single-phase two-winding transformers
(index 1: primary winding; index 2: secondary winding; turn ratio $n = w_1/w_2$)
L - inductance f - frequency R_{fe}- hysteresis and iron losses Z_C - characteristic impedance
R - resistance Ψ- flux $Z(\omega)$ - terminal impedance
C - capacitance $L(\Psi)$ - magnetising inductance C_S - surge capacitance

fig. 48. Transformer models for different frequency intervals. From [4]

4.3.2 Description and parameter estimation of the chosen transformer model

For the moment, the analysis of the voltage at the secondary winding of the transformer is not of interest in this work and therefore there is no need for modelling surge transfer. In this work a transformer model belonging to Group 2 (see fig. 48) has been chosen. The model is basically a typical power frequency transformer model (shown in fig. 49) to which the winding lumped stray capacitances and the phase to ground capacitances have been attached (fig. 50). The proposed model is reasonably accurate for frequencies below 100 kHz but for higher frequencies another more complex model must be used.

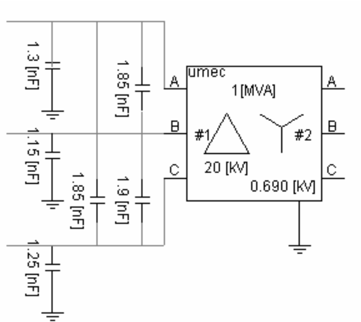

fig. 49. Transformer model for PSCAD

The transformer parameters are obtained from the nameplates of the transformers (refer to appendix I) and the capacitance values have been measured by means of a low voltage frequency scan. The frequency scan also provides information about the short circuit and open circuit inductances but the values obtained are very different from the rated values because the frequency scan is done at a very low voltage level (1V). At this voltage the magnetizing curve of the transformer does not follow a linear characteristic (fig. 51).

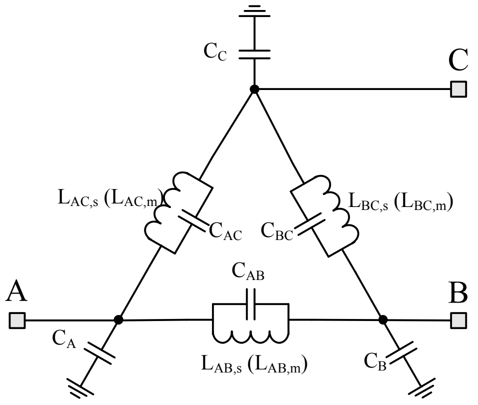

fig. 50. Transformer model for frequencies below 100 kHz

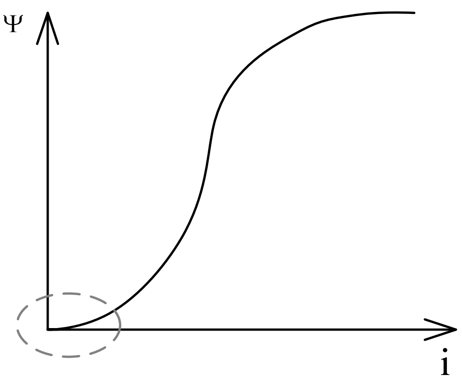

fig. 51. Magnetization curve of the transformer

The stray and ground capacitances of the model have been obtained from the actual transformers used in the experiments. In order to get the values of the capacitances and inductances 14 measurements have been done at each transformer: 7 with the low voltage terminals short circuited and 7 with the low voltage terminals in open circuit, as described in fig. 53.

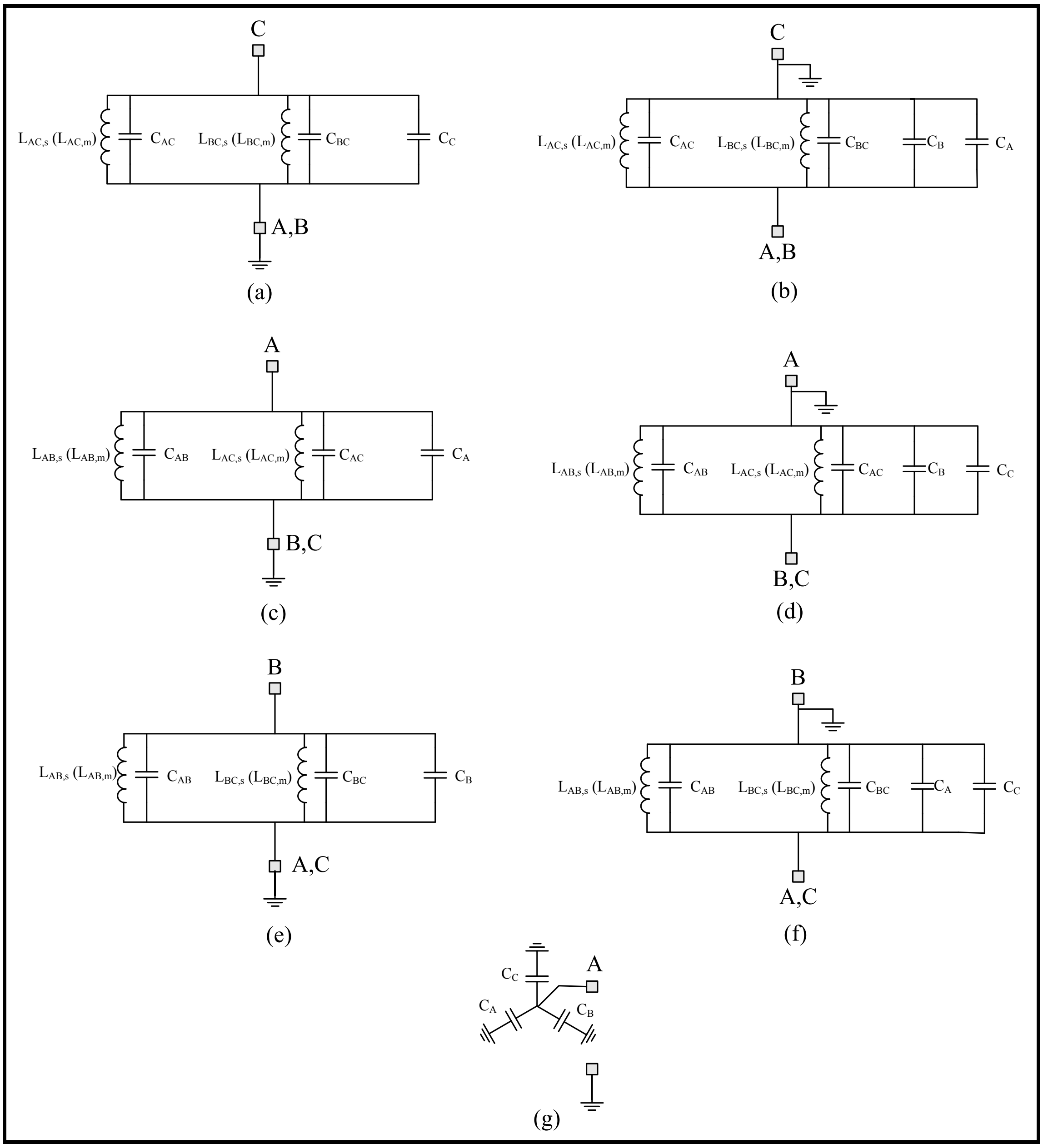

fig. 52. Measurements performed to obtain the transformer data

The results, shown in table 3, are obtained after solving the system of equations.

table 3. Capacitance and inductance values obtained from the LV frequency scan

TX1 (1250 kVA)		TX2 (1000 kVA)	
$\begin{pmatrix} C_A \\ C_B \\ C_C \\ C_{AB} \\ C_{AC} \\ C_{BC} \end{pmatrix} = \begin{pmatrix} 1.75nF \\ 1.6nF \\ 1.75nF \\ 2.8nF \\ 2.45nF \\ 2.8nF \end{pmatrix}$	$\begin{pmatrix} L_{s,ab} \\ L_{s,ac} \\ L_{s,bc} \\ L_{m,ab} \\ L_{m,ac} \\ L_{m,bc} \end{pmatrix} = \begin{pmatrix} 172mH \\ 172mH \\ 172mH \\ 56.2801H \\ 64.2464H \\ 182.2305H \end{pmatrix}$	$\begin{pmatrix} C_A \\ C_B \\ C_C \\ C_{AB} \\ C_{AC} \\ C_{BC} \end{pmatrix} = \begin{pmatrix} 1.3nF \\ 1.15nF \\ 1.25nF \\ 1.85nF \\ 1.65nF \\ 1.9nF \end{pmatrix}$	$\begin{pmatrix} L_{s,ab} \\ L_{s,ac} \\ L_{s,bc} \\ L_{m,ab} \\ L_{m,ac} \\ L_{m,bc} \end{pmatrix} = \begin{pmatrix} 192mH \\ 192mH \\ 196mH \\ 35.2939H \\ 36.7349H \\ 179.7004H \end{pmatrix}$

4.4 CABLES

The cable has been modelled using the cable model available in PSCAD because is the best possible model that has been found so far. During literature search it was found that the model in PSCAD is based on the world's leading researchers' publications ([6], [7], [8] and [9]).

There are three types of distributed transmission models that may be selected in PSCAD [10] to represent the transmission cable: the *Bergeron model*, the *Frequency-Dependent (Mode) model*, and the *Frequency-Dependent (Phase) model*.

The ***Bergeron model*** represents the L and C elements of a PI section in a distributed manner (not using lumped parameters like PI sections). It is accurate only at a specified frequency and is suitable for studies where the specified frequency load-flow is most important (e.g. relay studies).

The ***Frequency-Dependent (Mode) model*** represents the frequency dependence of all parameters (not just at the specified frequency as in the Bergeron model). This model uses modal techniques to solve the line constants and assumes a constant transformation. It is therefore only accurate for systems of ideally transposed conductors (or 2 conductor horizontal configurations) or single conductors.

The ***Frequency-Dependent (Phase) model*** also represents the frequency dependence of all parameters as in the 'Mode' model above. However, the Frequency Dependent (Phase) model circumvents the constant transformation problem by direct formulation in the phase domain. It is based on the theory originally proposed in [11], and its actual implementation into EMTDC is outlined in more detail in [12]. It is therefore accurate for all transmission configurations, including unbalanced line geometry. PSCAD help [10] recommends choosing this option unless a specific reason exists to select another one and it assures that "it is the most advanced and accurate time domain line model in the world!"

For more information on the Frequency-Dependent (Phase) model please refer to [19].
The next step after choosing the PSCAD cable model, is to select the correct parameters to fill in. For this purpose a detailed description of the real cable is needed: number of phases, geometrical layout (distance to ground, separation between phases…), diameter and material properties of cable layers, cable length…In addition, it is also valuable to know the working frequency range so the cable model is accurate enough at the interest range of interest.

The PSCAD cable model is based on a curve fitting algorithm which calculates the poles and the zeros of the cable transfer function according to a known frequency response. PSCAD gives the possibility of changing some parameters of the curve fitting algorithm to adapt the model to some specific requirements (fig. 53). It is possible to decide on an operating frequency range, the number of frequency increments, maximum number of poles, fitting error and weighting factor (certain frequency sub-ranges might need to be calculated more accurately).

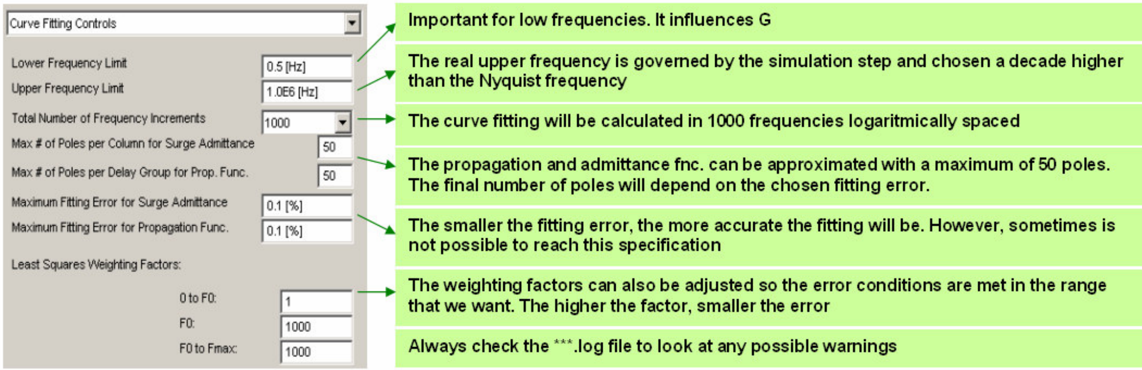

fig. 53. Curve fitting controls of the PSCAD cable

Moreover, it must be taken into account that very demanding requirements might slow down the simulations and generate error warnings.

When it comes to the geometrical layout and internal structure of the cables it is not easy to find the exact dimensions and material properties because manufacturers keep them fort themselves. In this work most of the required information has been extracted from [22], see fig. 55. Different cables are shown in fig. 54.

fig. 54. XLPE cables. Extracted from [22].

For instance, it is known that the two cables used in the experiments have a cross section of 95 mm^2, they are designed to operate at a rated voltage of 24 kV and they are single phase. Thus, in this case table number 24 must be chosen, reported in fig. 61.

Cross-section of conductor	Diameter of conductor	Insulation thickness	Diameter over insulation	Cross-section of screen	Outer diameter of cable	Cable weight (Al-conductor)	Cable weight (Cu-conductor)	Capacitance	Charging current per phase at 50 Hz	Inductance (trefoil)	Inductance (flat)	Surge impedance
mm²	mm	mm	mm	mm²	mm	kg/m	kg/m	µF/km	A/km	mH/km	mH/km	Ω
Table 24												
Single-core cables, nominal voltage 20 kV (U_m = 24 kV)												
50	8	5.5	20.6	16	29.0	0.8	1.1	0.18	0.7	0.45	0.74	32.4
70	9.6	5.5	22.2	16	30.0	0.9	1.4	0.20	0.7	0.42	0.70	29.0
95	11.2	5.5	23.8	25	32.0	1.1	1.7	0.22	0.8	0.40	0.68	26.2
120	12.6	5.5	25.2	25	34.0	1.2	2.0	0.24	0.9	0.39	0.65	24.0
150	14.2	5.5	26.8	35	35.0	1.5	2.4	0.26	1.0	0.37	0.63	22.1
185	15.8	5.5	28.4	35	37.0	1.6	2.8	0.28	1.0	0.36	0.62	20.5
240	18.1	5.5	30.7	35	40.0	1.9	3.4	0.31	1.1	0.35	0.60	18.5
300	20.4	5.5	33.0	35	42.0	2.1	4.0	0.34	1.2	0.33	0.57	16.8
400	23.2	5.5	35.8	35	45.0	2.5	5.0	0.38	1.4	0.32	0.56	15.1
500	26.2	5.5	39.4	35	49.0	2.9	6.0	0.42	1.5	0.31	0.54	13.9
630	29.8	5.5	43.0	35	53.0	3.4	7.3	0.47	1.7	0.30	0.52	12.5
800	33.7	5.5	46.9	35	58.0	4.0	9.0	0.52	1.9	0.30	0.50	11.3
1000	37.9	5.5	51.1	35	62.0	4.8	11.0	0.57	2.1	0.29	0.48	10.2
1200	44	5.5	59.0	35	68.0	5.5	13.0	0.67	2.4	0.28	0.46	9.4
1400	49	5.5	64.0	35	76.0	6.5	15.2	0.74	2.7	0.28	0.45	8.5
1600	52	5.5	67.0	35	79.0	7.2	17.1	0.77	2.8	0.27	0.45	8.1
2000	56	5.5	71.0	35	83.0	8.4	20.8	0.83	3.0	0.27	0.44	7.6

fig. 55. Single-core cables, nominal voltage 20kV (U_m=24kV)

Starting from the values obtained in table 24 the radius of each layer can easily be deducted as shown in Fig. 56 (both cables of the experiment have the same cross-section, thus the same thickness). Nevertheless, PSCAD model does not account for semiconducting layers, subsequent conductors or subsequent insulators: a conductor layer is followed by an insulator and an insulator by a conductor and so on. This means that some layers must be grouped and the material properties analyzed in order to choose the right value for the permittivity, permeability and resistivity.

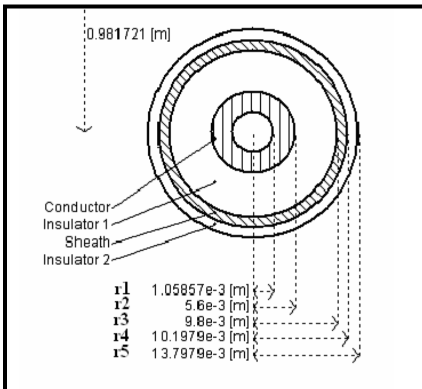

$$r_2 = \frac{11.2}{2} = 5.6\text{mm}$$

$$r_1 = \sqrt{r_2^2 - \frac{95\text{mm}^2}{\pi}} = 1.05858\text{mm}$$

$$r_3 = \frac{19.6}{2} = 9.8\text{mm}$$

$$r_4 \approx \sqrt{\frac{25\text{mm}^2}{\pi} + (9.8\text{mm})^2} \approx 10.1979\text{mm}$$

$$r_5 \approx r_4 + 3.6\text{mm} \approx 13.7979\text{mm}$$

Fig. 56. Estimation of layers' thickness

The models require not only the layer thickness but also the main properties of the layer material. Some approximate values are given in table 4 although different types of the same material can have significant variations.

table 4. Some properties of some cable materials

Cable material properties		
Resistivity [Ω·m]	**Copper**	**$2.2 \cdot 10^{-7}$**
	Aluminium	**$2.82 \cdot 10^{-8}$**
	Lead	**$1.72 \cdot 10^{-8}$**
Relative Permittivity	**XLPE**	**2.3**
Permittivity [F/m]	**Vacuum**	**$8.8541878176 \times 10^{-12}$**

The most used insulating material is the Cross Linked Polyethylene (XLPE) and is, in fact the insulating material used for the experiments. If the thickness and the material of the main insulating layer is the same for the two cables, the per-unit length capacitance and inductance is also equal.

The per-unit length capacitance and inductance of the cables can be calculated as follows:

$$C_{per\_unit} = \frac{2\pi\varepsilon_o\varepsilon_r}{\ln\left(\frac{R_{outer\_insulation}}{R_{inner\_insulation}}\right)} = \frac{2\pi \cdot 8.8541878176 \cdot 10^{-12} \cdot 2.3}{\ln\left(\frac{9.8}{5.6}\right)} = 228.65\text{pF/m} \qquad \textbf{(eq. 38)}$$

$$L_{per\_unit} = \frac{1}{2\pi}\mu_o\mu_r \cdot \ln\left(\frac{R_{outer\_insulation}}{R_{inner\_insulation}}\right) + \underbrace{\frac{1}{8}\mu_o\mu_r}_{\text{Self inductance: Negligible at High Frequencies}} =$$

$$L_{per\_unit} = \frac{1}{2\pi} \cdot 4\pi \cdot 10^{-7} \cdot 1 \cdot \ln\left(\frac{9.8}{5.6}\right) + \frac{1}{8} \cdot 4\pi \cdot 10^{-7} \cdot 1 = 111.92\text{nH/m} + 50\text{nH/m}$$

$$L_{per\_unit}\,(\text{at high frequencies}) \approx 111.92\text{nH/m} \qquad \textbf{(eq. 39)}$$

$$Z_o = \sqrt{\frac{L}{C}} = \sqrt{\frac{111.92\text{nH/m}}{228.65\text{pF/m}}} = 22.124\Omega \qquad \textbf{(eq. 40)}$$

$$v(\text{wave travelling speed}) = \frac{1}{\sqrt{LC}} = \frac{1}{\sqrt{111.92\text{nH/m} \cdot 228.65\text{pF/m}}} = 197.679\text{m/s} \qquad \textbf{(eq. 41)}$$

The expression that describes the inductance in (eq. 39) is divided into two parts: one that describes the mutual inductance between conductor and shield and another one that expresses the self inductance of the conductor. It is interesting to point out that at high frequencies the self inductance term is negligible because the skin effect confines the current to the external surface of the conductor. At high frequencies the inductance has a lower value which is translated into a lower characteristic impedance and a higher speed of propagation. An increase in the speed of propagation originates faster transients.

4.5 VCB

Even though vacuum interrupter technology begun in the early 1960's, it is still considered a rather new technology, perhaps due to the intensive arc research carried out during this time. VCBs have become very popular and it has become difficult for the SF_6 gas technology interrupters to compete with them. There are three main reasons: a) longer lifetime, b) environment friendliness and c) overall superior performance [13]. However, their performance is so outstanding that it can even become a disadvantage in some aspects. VCBs show excellent interruption and dielectric recovery characteristics after current zero, also for high frequency currents that may be superimposed to the power frequency current. At certain switching operations (especially when the currents are inductive) this quenching ability can produce unwanted transients: multiple reignitions and virtual current chopping.

Of course, a CB cannot pass from a close state to an open state instantly. When the CB receives the opening command its contact start to separate but the current cannot automatically cease so an electric arc begins to burn. The arc-voltage is usually of about several tens of volts. Under ideal conditions the arc extinguishes at the moment of current zero, and the transient recovery voltage (TRV) appears across the gap.

The cold withstand capability of the CB increases together with the separation between the CB contacts. If the contacts start to separate just before the power frequency current zero, the gap does not have enough time to build a strong withstand voltage and a high rate of rise of the TRV can cause a reignition.

A reignition causes a high frequency current that a VCB will break in the next zero crossing creating a cascade of multiple reignitions over a few milliseconds (fig. 57). The frequency of this current is given by the combination of inductances and capacitances of the circuit: cables, load, supply etc.

When smaller currents are switched, the arc tends to be instable before zero (in modern CBs this current level is around 3A) leading to a sudden drop of the current [14] that is called current chopping. When current chopping happens some energy gets trapped in the load side of the CB and generates a faster and therefore, higher peak of the TRV. Current chopping is definitively a potential cause of reignitions but it is only observed at power frequencies.

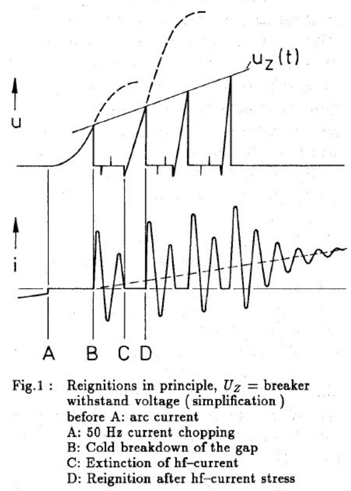

fig. 57. Multiple reignitions. From [14]

A VCB can be modelled in many different ways depending on what effects are to be observed. In the case of analysing fast transient overvoltages the model must include at least three properties:

- High frequency current quenching capability
- Chopping current
- Cold withstand characteristic between breaker contacts

Some authors model the **high frequency current quenching capability** according to the slope of the high frequency current. The model used in this work offers the possibility of quenching the current at the first zero crossing or after a specified number of zero crossings. It does not account for the slope of the current.

The **current chopping level** can as well be defined and it is usually set to a 3A value. However, the current chopping does not exactly work as it should because it should only work before the first power frequency zero crossing but it works every time, even at high frequencies. This creates faster TRVs at high frequencies and therefore a higher density of multiple reignitions. The solution to this problem has been left for future work.

The **cold withstand curve** is not given by VCB manufacturers but it can be estimated from experimental results, see fig. 58. If measurements are available, then the envelope curve of the voltage across the breaker contacts can be estimated. The cold withstand is a function of the contact distance the speed of contact separation. The researchers that have experimentally investigated the withstand capability have found that the data varies following a statistical distribution. Some researchers represent it following an exponential curve while others believe that a linear characterization is enough [17]. This model gives the possibility of specifying an envelope curve with two points other than the origin (the coordinates have to be deduced from the experimental data). Another very interesting phenomenon derived from multiple reignitions is that the gap does not have time to recover from reignition to reignition and its withstand decreases. The reason is that when an arc is extinguished conducting particles precedent from the CB contacts are still floating in the gap and they reduce the withstand capability of the gap. The decreased withstand is known as **hot withstand capability** and is not modelled in this work.

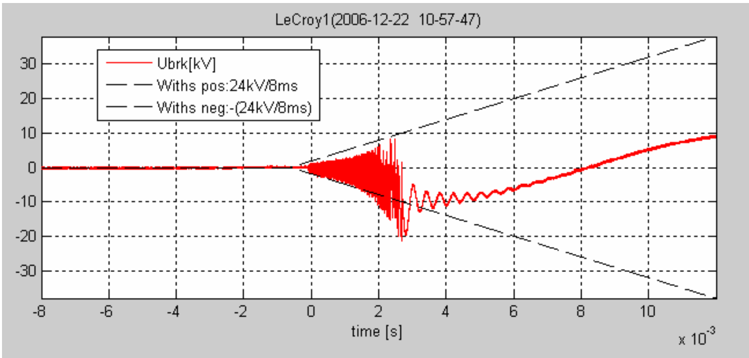

fig. 58. Example of cold-withstand estimated curve

4.6 MEASUREMENT EQUIPMENT

If the measuring equipment was ideal no model would be needed. However, the measuring equipment is not ideal but it can still be chosen to be good enough. The voltage measuring devices used in the experiments are damped capacitive dividers, with the main drawback that they cannot measure DC voltages, see fig. 59.
When the experiments were performed it was observed that the used voltage dividers do not have the same characteristics and that they did not provide the same exact result. In order to obtain a better match between simulations and measurements a damped capacitive voltage divider model has been proposed. The values have been directly obtained from the manufacturer.

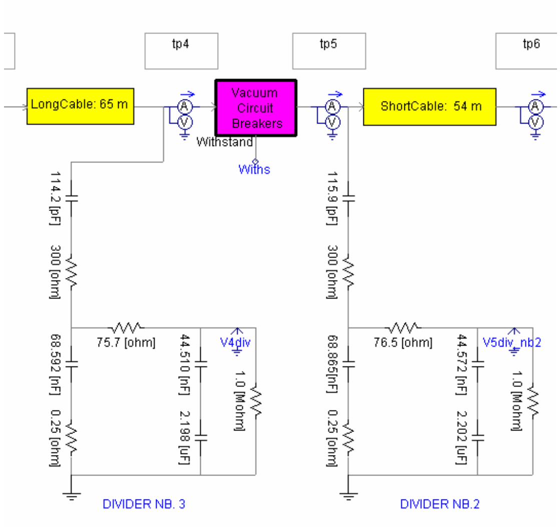

fig. 59. Model of the damped capacitive dividers

Although some simulations that include the models of the damped capacitive dividers have been run, the analysis is done without considering these devices. The reason for not including the measuring equipment in the simulation file is that there is a high probability that the simulation results do not match the experimental records and the comparison is easier if these elements do not disturb the simulation results. Afterwards, when a good matching simulation model is found, a more complex model can be built.

4.7 PROTECTIVE EQUIPMENT

The goal of this work is not to study the surge protection techniques. In spite of that, some sort of protection is needed in order to preserve the laboratory equipment. It must be taken into account that some experiments might damage the insulation of the transformers.

The protection device selected is an 11 kV arrester which detailed description can be obtained in section 5.1.10.

4.8 CONCLUSIONS

- High frequency modelling of equipment is more complex than power frequency modelling. The reason is that fast transients occur at different frequency ranges and hence the models change from range to range. In addition, fast transients can be produced by several reasons and each model is different depending on the phenomenon to observe.
- In this work the supply grid is going to be modelled as a strong grid where the source reactance has been neglected.
- There are two main trends to model transformers. One is based on building a detailed internal winding model and the other is a terminal model that is useful to study the relation of the transformer with the system. For this reason, a terminal model has been chosen in this project.
- Three cable models are available in the PSCAD library. The Frequency-Dependent (Mode) Model is the most appropriate because it represents the frequency dependence of all parameters and it is based on world wide recognized publications.
- The VCB model of PSCAD is not valid to analyze fast transient phenomena. Some features, such as cold withstand characteristic, high frequency quenching capability and current chopping, have been added.

5. LABORATORY EXPERIMENTS AND MODEL CALIBRATION

Fast transients have been a source of problems for a long time in industrial systems and many measures have been taken so far. However, industrial systems are often complex and some of the parameters are difficult to determine. For this reason there is an uncertainty in how well the models resemble reality.

In order to calibrate the models and have a better understanding of the fast transient phenomena that occur when switches interact with cables, it was decided to build a rather simple laboratory experiment. This laboratory experiment would allow trying several arrangements and operating conditions.

5.1 LABORATORY SETUP

The preliminary lab experiment, which is shown in fig. 60, differs from the expected laboratory setup planned in the very beginning of this work. Since some of the required components were not likely to arrive in a relatively short term, it was decided to build a similar setup with the equipment available at the moment.

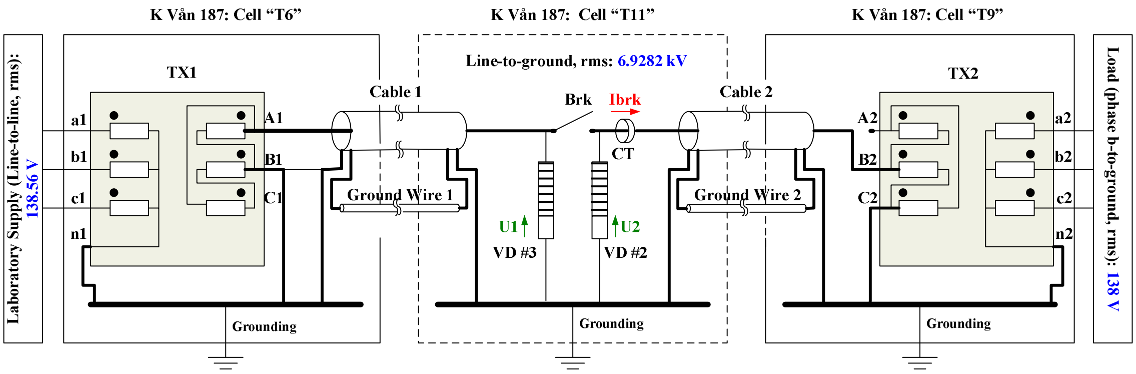

fig. 60. Simplified illustration of the lab experiment

The first arrangement was supposed to be conformed by two 36 kV three phase cables (600m and 80m long), a 36 kV VCB and two 2 MVA nacelle-type transformers.
The new arrangement, on the contrary, is formed by two similar transformers of 1.25 MVA and 1.0 MVA, two similar single phase 24 kV cables (65m and 54m) and a rated 12 kV VCB. connection The laboratory setup is shown in fig. 61 and the characteristics of each component is described next.

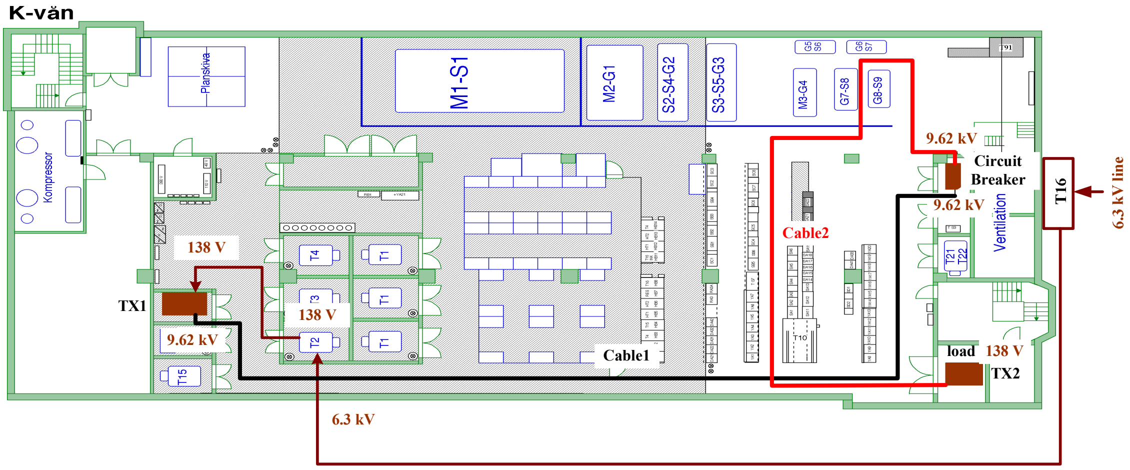

fig. 61. Top view of the laboratory setup

5.1.1 Voltage supply

The existing VCB is rated 12 kV, which means that the voltage should not exceed this operating point. A 6.9282 kV voltage has been chosen because this is the phase-to-ground voltage that corresponds to 12 kV. The laboratory is equipped with a set of transformers that are connected in different configurations to provide the right voltage as it is illustrated in fig. 62. Thus, for this experiment transformer T16 and T2 (fig. 63) adjust the voltage taken from the 6.35 kV external line.

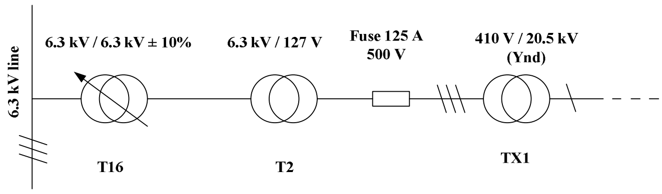

fig. 62. Connection of the laboratory built-in equipment for supplying the experiment

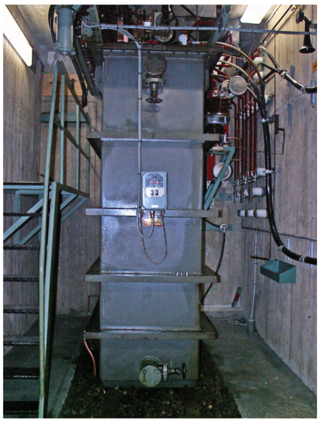

fig. 63. Photo of transformer T2

fig. 64. Photo of transformer TX1

5.1.2 Supply side transformer: TX1

Transformer TX1 (fig. 64) is used to step-up the voltage provided by the in-built laboratory transformer T2, which gives 138.56 V. It transforms this low voltage into 6.928 kV.

This experiment is special because only a single phase is used. This means that only two terminals of the high voltage side (delta configuration) of the transformer have been connected: one to the conductor of the cable and the other one to the shield of the cable and to the system ground. The low voltage side has been connected as a regular three phase connection. The nameplate data of TX1 is reported in table 5.

table 5. Nameplate data of transformer TX1

1250 kVA	**Dyn11**	**50 Hz**
20500 ± 2×2.5 % V	**35.2 A**	
410 V	**1760 A**	
U 125AC50/AC8 kV	**ONAN**	
Zk 5.4 %	**2885 kg**	
Pk 11971 W	**605 kg**	
Po 1455 W		

5.1.3 Cable 1

Cable1, which length is 65m, is meant to be the longest. However, the difference between both cable lengths is very small (Cable2 is 54m long). The properties of Cable1 are shown in table 6.

table 6. Data of Cable1

Rated voltage [kV]	**24**
Cross section of the conductor [mm^2]	**95**
Conductor material	**Al**
Cu shield	
Extra screen consisting of a coated Cu braid shield	

5.1.4 GroundWire1 and GroundWire2

It is a known fact that the sum of currents in a three phase balanced system is zero. The shield of three phase cables is designed to be thinner than single phase cables where the current return is through the shield. This is the reason why a return ground wire was added in parallel to Cable1 and Cable2 (to a distance of around 10cm as it is seen in fig. 65). This ground wire is made of bare copper and has a $25mm^2$ cross section.

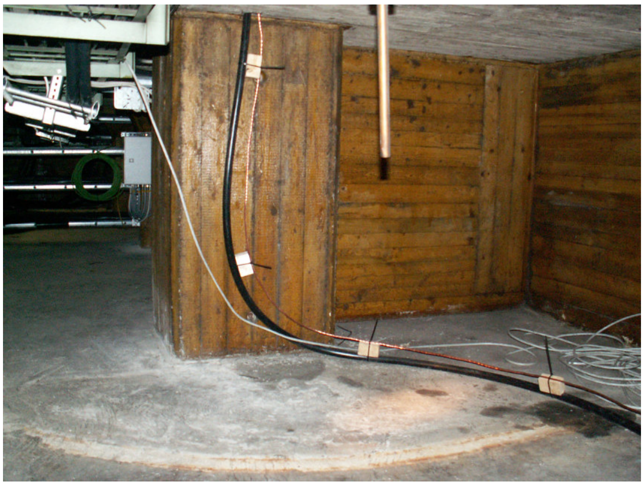

fig. 65. Photo of Cable1 in parallel to GroundWire1

5.1.5 VCB

The VCB has a rated voltage value of 12 kV. The most important technical data is gathered in table 7, table 8 and table 9.

table 7. Technical data of the VCB

Rated voltage	kV	12
Rated frequency	Hz	50/60
Rated lightning impulse withstand voltage	kV	75
Rated power frequency withstand voltage	kV	28
Rated rise of transient recovery voltage	kV/μs	0.35
Peak transient recovery voltage	kV	20.6

table 8. Guideline values for function times of the VCB

Guideline values for function times	
Closing time	approx. 45…60 ms
Opening time	approx. 35…50 ms
Arcing time (at 50 Hz)	≤15 ms
Break time	≤60 ms
Minimum command time on closing	20 ms
Minimum command time on opening	20 ms

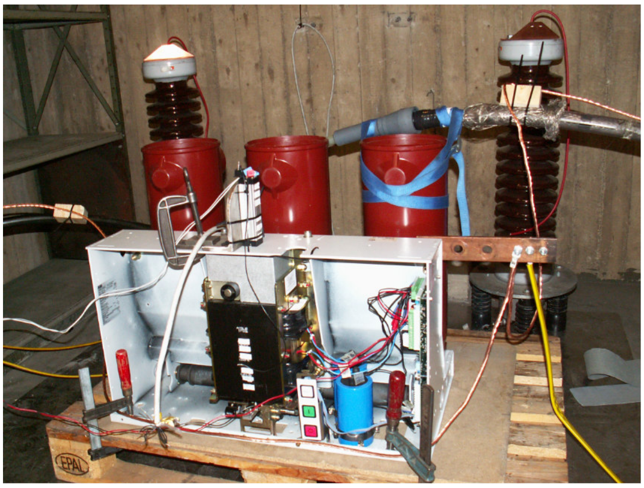

fig. 66. Photo of VCB: BA 504/02 E

The IEC 56 STANDARD specifies the TRV envelope that a CB must follow, see fig. 67 and the data of table 9 and table 10. It is important to note that this withstand characteristic represents the operation when the gap is hot, it is therefore a **hot withstand** curve. The **cold withstand**, which is needed for simulation purposes, must be deduced by other means (i.e. estimating the envelope of a measured breaking/closing operation).

table 9. Definitions of IEC 56 Standar

Name	Condition Description
TD1	10% of measured short-circuit current with less than 20% of DC component
TD2	30% of measured short-circuit current with less than 20% of DC component
TD3	60% of measured short-circuit current with less than 20% of DC component
TD4	100% of measured short-circuit current with less than 20% of DC component
TD5	10% of measured short-circuit current with maximum DC component where opening time is >10ms (50 Hz)

table 10. IEC 56 Standar for 12 kV system voltage

12 kV System Voltage				
First pole to clear: 1,5				
u_c	kV	TD1-2	TD3	TD4-5
t_3	Ms	22	22	60
t_d	Ms	13	26	60
u'	kV	3	5	9
t'	Ms	7.3	7.3	6.9
u_c/t_3	(kV/ µs)	1.7	0.85	0.34

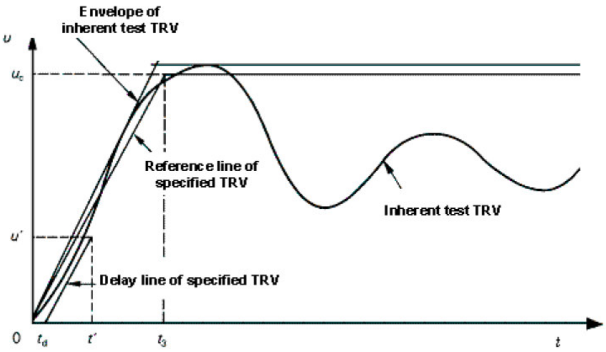

fig. 67. Example of inherent test TRV with two-parameter envelope that satisfies the conditions to be met during type test

5.1.6 Cable 2

Cable2 has a length of 54m and its data is reported in table 11:

table 11. Data of Cable2

Rated voltage [kV]	24
Cross section of the conductor [mm^2]	95
Conductor material	Al
Insulation Thickness [mm]	5.5
Insulation material	XLPE
Inner/outer semiconductor thickness [mm]	0.8/0.7
Lead sheath	
PE jacket	

5.1.7 Load Side Transformer: TX2

The load side transformer (TX2, see fig. 68) steps down the voltage from 6.928 kV to 138 V. The windings of this transformer, as well as transformer TX1, are Dyn11 connected. The conductor of Cable2 is connected to terminal “B2” of the high voltage side and the shield of Cable2 (which is grounded) is connected to terminal “C2”. When the experiment is loaded the load is connected between terminal “b2” and ground in the low voltage side. The nameplate data of TX2 is reported in table 12.

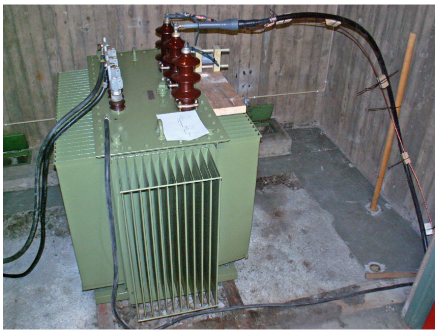

fig. 68. Photo of Transformer TX2

table 12. Nameplate data of transformer TX2

No. 5210667	1997	
CTMU 24 HM 1000	IEC 76	
1000 kVA	Dyn11	50 Hz
20000 ± 2x2.5 % V	28.87 A	
690 V	836.7 A	
U 125AC50/AC8 kV	ONAN	
Zk 5.1 %	2670 kg	
Pk 10260 W	505 kg	
Po 1223 W		

5.1.8 Load

The first experiments have been performed at no-load. The second set of experiments considers a resistive load of 0.5 Ω connected to the low voltage side of the transformer TX2, see fig. 69. It must be observed that the load cannot be connected at any of the three phases. If the cable is attached to terminals “B2” and “C2” in the high voltage side, the load must be joined to terminal “b2” in the low voltage side.

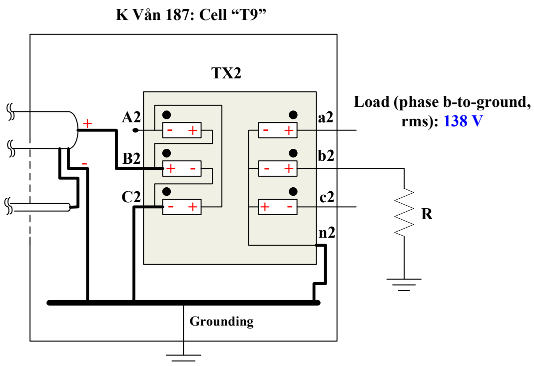

fig. 69. Connections in TX2 transformer: cable and load

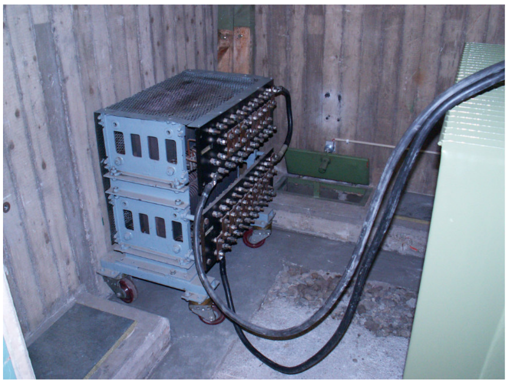

fig. 70. Photo of Resistive load (R=0.5 Ω)

5.1.9 Measuring Equipment

Knowing the characteristics of the measuring equipment is very important because it tells about the precision of the measurements. The recording equipment is fixed to a floating ground by means of a UPS (Uninterruptible Power Supply) to avoid high frequencies coming from the system grounding. The floating ground is a thin copper sheet that can be seen in fig. 71.

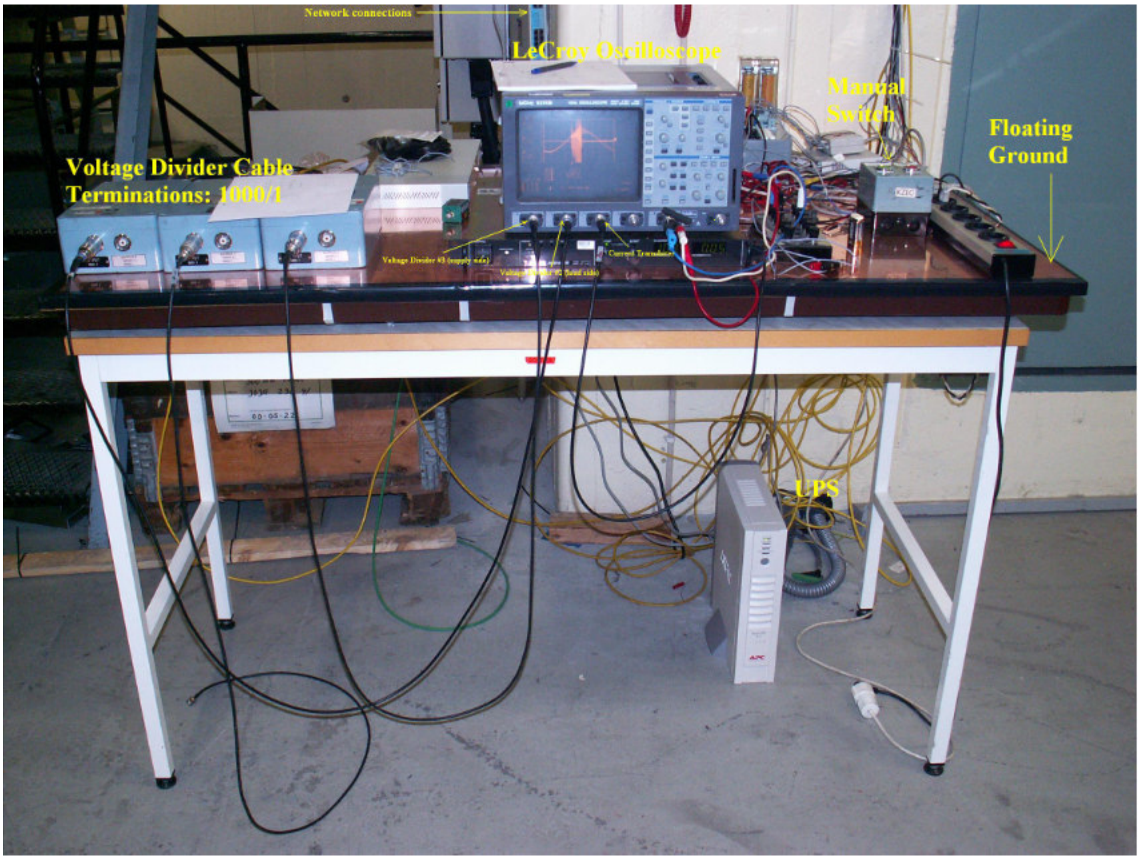

fig. 71. Recording equipment in a floating ground plane

The current measurements showed that the current was distorted by the high frequency components. After consulting experienced measurement specialists, some additional changes have been made in order to improve the rejection of high frequency noise (using a better shielded cable from the current transducer to the oscilloscope, connecting several ferrites to the cable, effectively grounding the incoming channel of the oscilloscope and connecting a net filter). A more detailed diagram of the wiring is shown in fig. 72.

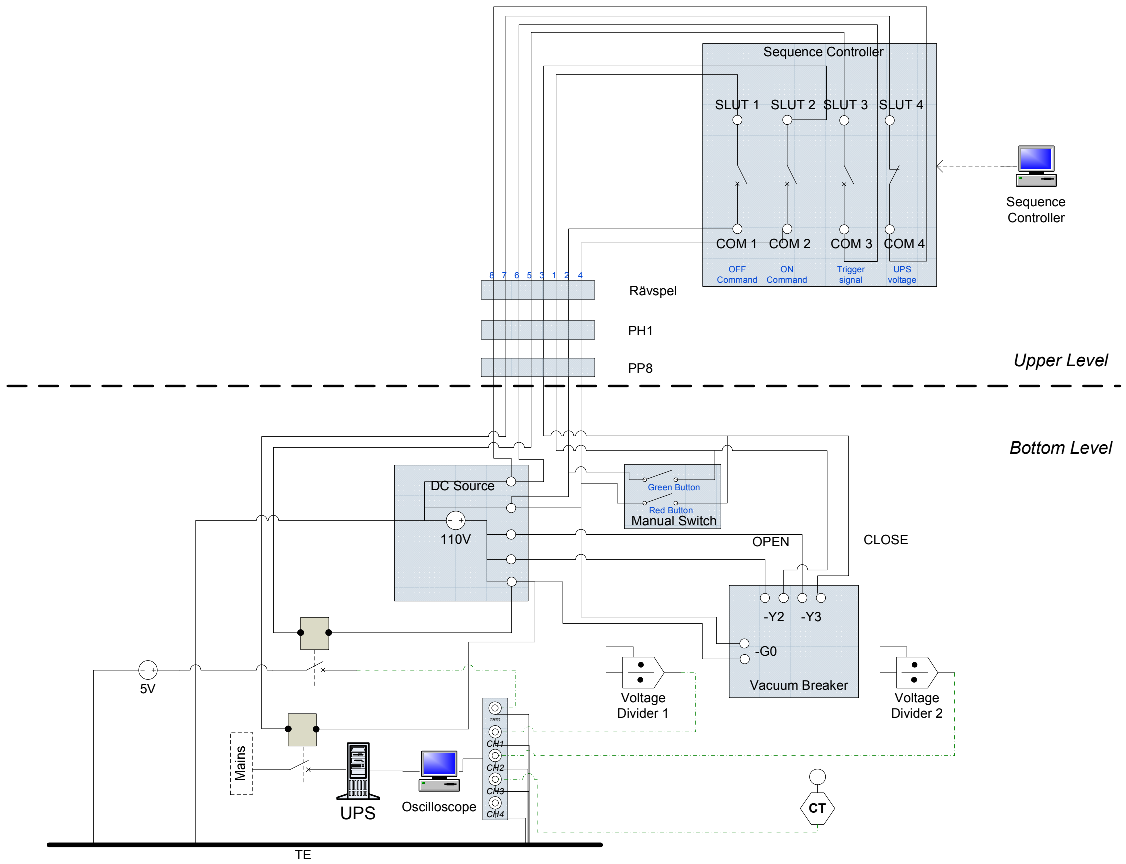

fig. 72. Schematic view of the cabling for operating the CB and recording the measurements

The sequence controller is the device that controls the opening and closing times of the CB and other auxiliary equipment required to run the tests (i.e. other switches to connect the external supply). Usually, the staff conducting experiments stand in the upper floor of the Power Laboratory, where the sequence controller is. However, a manual switch gives the possibility of operating the CB directly from the cellar.
The oscilloscope sends the recordings to a PC also standing at the upper floor by the LAN network.

The UPS connection signal and the oscilloscope trigger signal must be activated by means of a relay or contactor (UPS) to ensure a total isolation from the system ground.
The CB requires an external supply to enable the opening/breaking signals. A 110V DC source delivers the required voltage to activate the breaker signals and the UPS connecting contactor. The oscilloscope is triggered by a relay supplied with a 5V DC battery.

5.1.9.1 Capacitive Voltage Dividers

For the voltage measurement a set of three Haefely voltage dividers has been used. These voltage dividers are damped capacitive voltage dividers designed to measure lightning impulse voltages, switching impulse voltages and alternating voltages. They are not intended to measure DC voltages which could be a drawback. The technical information on the damped capacitive dividers has been gathered in table 12

table 13. Technical characteristics of Haefely Damped Capacitive Dividers

Technical Characteristics of Haefely Damped Capacitive Dividers	
Primary part:	
Primary Capacitance (C1.1)	**115 pF**
Primary Resistance (R1.11)	**300 Ω**
Secondary part:	
Secondary Capacitance (C2)	**0.066 µF**
Burch Total Capacitance ($C_B$tot)	**0.045 µF**
Secondary Resistance (R21)	**0.25 Ω**
Terminal Resistor of the measuring cable (R_K)	**75 Ω**
Transformation ratio:	
Transformation ratio (n_1)	**1000:1**
Rated voltage of the primary part:	
Lightning impulse 1.2/0.5 µs	**375 kV**
Switching impulse 250/2500 µs	**300 kV**
Alternating voltage 50 resp. 60 Hz	**75 kV**
Rated voltage of the secondary part:	
Lightning impulse 1.2/0.5 µs	**0.375/0.0075 kV**
Alternating voltage 50 resp. 60 Hz	**0.375/0.0015 kV**
Transmission characteristics of the complete divider:	
Length of the high voltage lead	**1.5 m**
Response time	**>30 ns**
Rise time	**>30 ns**

The drawing in (fig. 73) represents a simplified model of the damped capacitive voltage divider. Care must be taken regarding the measurement instruments connected through the coaxial cable, particularly when the cables are long. In that case, the capacitance of the coaxial cable cannot be ignored and the “burch” type termination gives the most optimal transmission characteristics. Thereby resistor R3.11 corresponds to the wave impedance value.

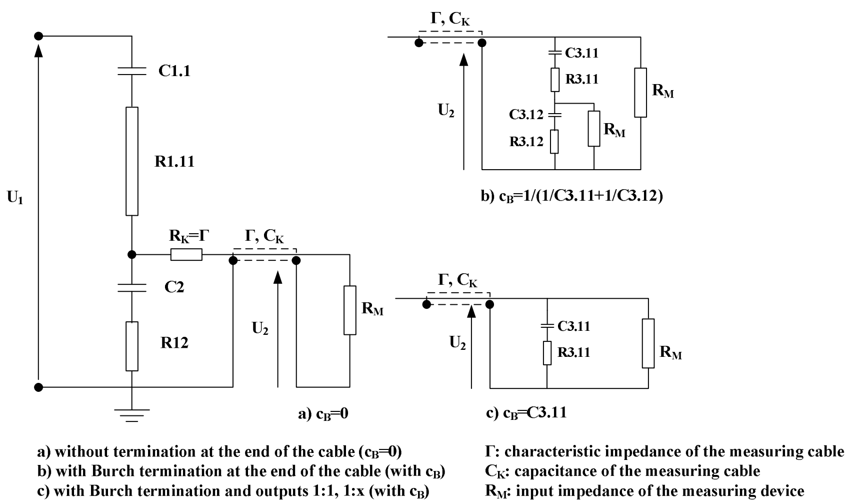

fig. 73. Basic design of damped capacitive voltage divider

The schema illustrated in fig. 73 is very useful to make a model of the dividers.

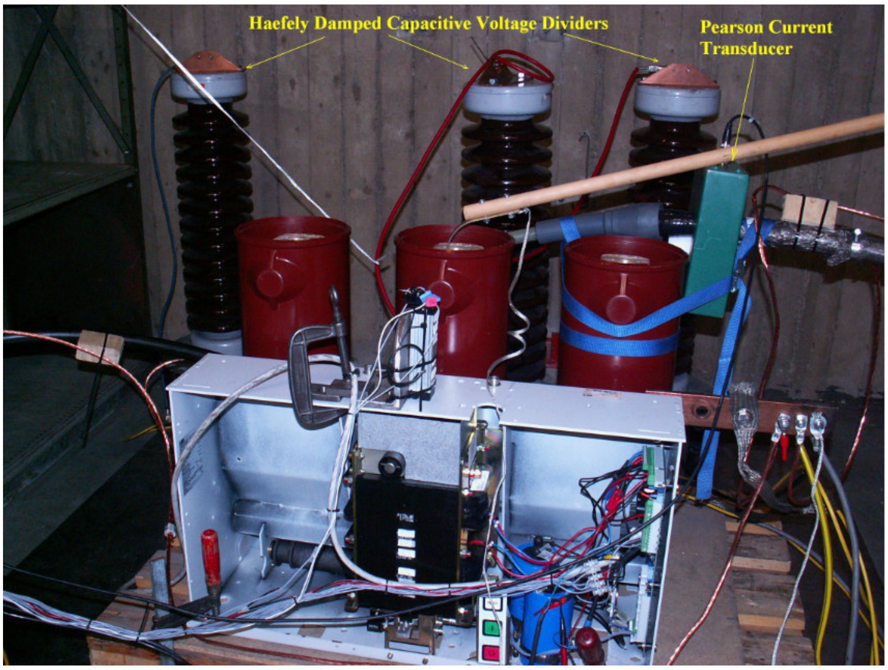

fig. 74. Photo of Damped Capacitive Voltage Dividers and Pearson Current Transducer

5.1.9.2 Current Transducer

The current transducer is a Pearson Electronics 301X with the following characteristics:

table 14. Technical data of the current transducer

General		Time Domain Parameters		Frequency Domain Parameters	
Model Nb.	**301X**	**I max. peak [A]**	**50000**	**Irms max.**	**400**
Output [V/A]	**0.01**	**Droop [%/µs]**	**0.003**	**Appox. 3dB pt.:**	
Hole Diam. [inches]	**3.5**	**Useable rise time [ns]**	**200**	**Low [Hz]**	**5**
		IT max [A·s]	**22**	**High [Mhz]**	**2**

5.1.9.3 Oscilloscope

The oscilloscope is a 4 channel Lecroy type recorder which main features are the summarized below:

<u>LeCroy 9374M:</u>

- Up to 8M Point record length
- 8-bit vertical resolution, 11 with ERES option
- Four Channels
- Portable Hard Disk (PCMCIA III), Memory Card and DOS Compatible Floppy Disk options
- Innovative Peak Detect
- Glitch, Pattern, Qualified, Interval, Dropout and TV Triggers
- Fully programmable via GPIB and RS-232-C
- Internal Graphics Printer Option
- Automatic PASS/FAIL testing
- Advanced Signal Processing
- 1 GHZ BANDWIDTH
- Single channel: 2GS/s. Four channels: 500MS/s

5.1.10 Protective Equipment: ZnO Arrester

The arrester used is a zink oxide arrester formed by two stacks in series.

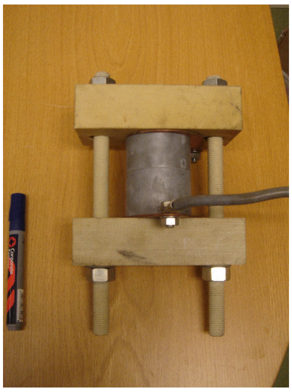

fig. 75. Photo of ZnO Arrester

table 15. Arrester nameplate data and characteristics

	Arrester Stack 1			Arrester Stack 2		
Series nb.	**141QL**	**1407**		**105QL**	**1407**	
	C1101	**859**	**144RL**	**B2451**	**639**	**106RL**
VI characteristics	**14.07 kV@10 kA**			**14.47 kV@10 kA**		
	8.59@1mA			**6.39@1mA**		
Impulse type	**8/20us**			**8/20us**		
	COV=8.59/1.2			**COV=8.59/1.2**		

5.2 SIMULATION MODEL

The simulation model used to represent the laboratory experiment is rather straightforward, fig. 76. The components have been modelled according to the modelling procedures explained in Chapter 4 and using the data presented in the previous sections.

The effects of the measuring and protective equipment have been omitted because they add complexity to the simulation results and it is more difficult to differentiate whether they are influencing the results or not. Nevertheless, simulations have been done in which the damped capacitive dividers and the zink oxide arrester have been present.

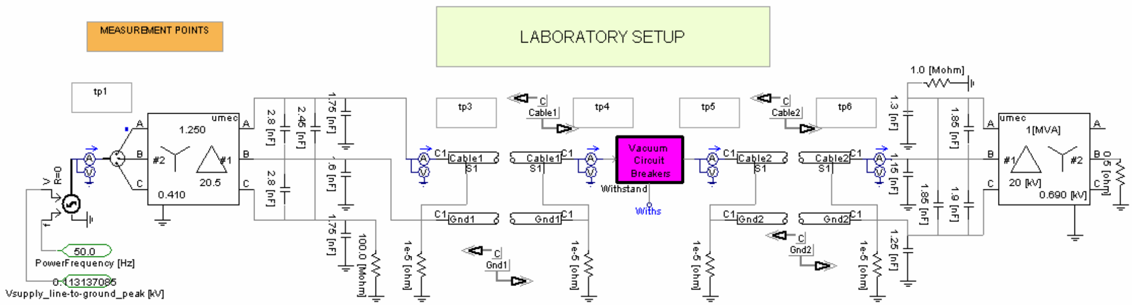

fig. 76. PSCAD simulation diagram

Each modelled element is explained in the following sections.

5.2.1 Supply Grid

The supply grid is modelled as a strong grid (zero source impedance) which provides 138.56 V rms line-to-line. This is the voltage level required to produce 12 kV rms line-to-line in the breaker side. Thus, the CB is supplied with a 6.928 kV rms phase-to-ground.

5.2.2 Transformers: TX1 and TX2

The transformer model used is a terminal transformer model explained in section 4.3.2. This model is built adding measured phase-to-phase and phase-to-ground stray capacitances to the default PSCAD (UMEC) model. Although this PSCAD model is only valid for power frequencies, it takes into account important properties such as the non-linearity of the iron core (the magnetizing curve can be introduced), the no-load losses and the short circuit impedance. In appendix I detailed information is given on how to choose the parameter input to PSCAD and it is also described how PSCAD models a three phase transformer.

After running a simulation, it is sometimes useful to have a single-phase equivalent model of the transformer which provides a single lumped capacitance and inductance value to check if the oscillations observed in the simulations are reasonable. The equivalent termination of the transformer is shown in fig. 77. The equivalent capacitance and inductance values have been calculated in the following equations ((eq. 42) and (eq. 43)) and fig. 78 illustrates a simplified model of the system that is very useful to study the oscillation frequencies of transients.

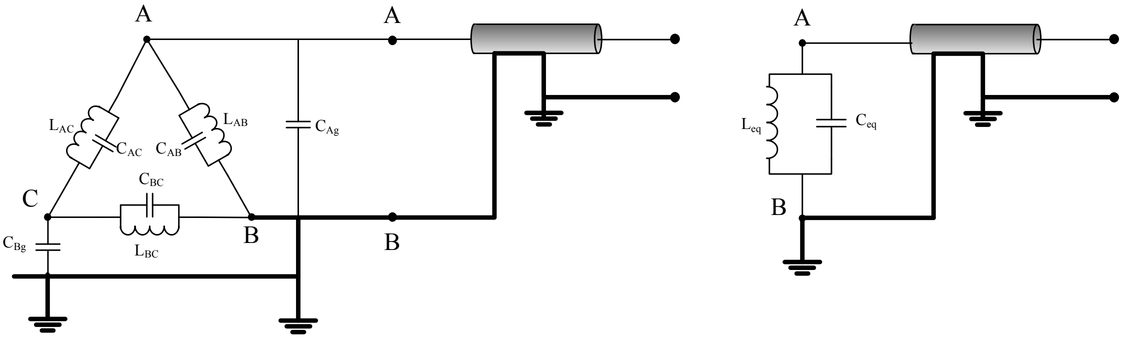

fig. 77. Transformer end and its equivalent circuit

$C_{\text{eq}} = C_{\text{Ag}} + C_{\text{AB}} + \dfrac{C_{AC} \cdot (C_{\text{Cg}} + C_{\text{BC}})}{C_{\text{AC}} + C_{\text{BC}} + C_{\text{Cg}}}$	**(eq. 42)**
$L_{\text{eq}} = \dfrac{L_{AB} \cdot (L_{\text{AC}} + L_{\text{BC}})}{L_{\text{AC}} + L_{\text{BC}} + L_{\text{AB}}}$	**(eq. 43)**

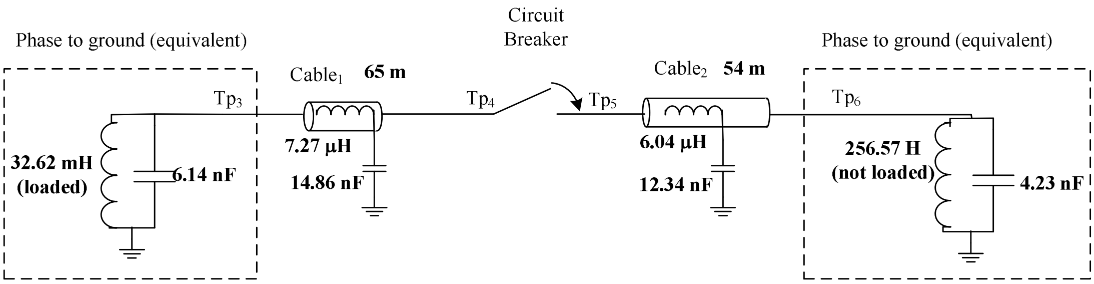

fig. 78. Equivalent capacitances and inductances of the system

5.2.3 Cable1 and Cable2

The two cables have been modelled according to the instructions given in section 0 using the input values of section 5.1.3 and 5.1.6.

5.2.4 GroundWire1 and GroundWire2

The ground wires are bare copper conductors formed by various self-twisted copper strands. They have been laid in parallel to the main conductive cables at a distance of around 10 cm from the cable. Efforts were made to keep the distance constant using little wooden blocks of the same size every meter (fig. 65). Therefore, their length is the same as the cables they are in parallel with. The cross section of these copper conductors is of $25mm^2$.

5.2.5 VCB

The vacuum circuit model has been explained in section 4.5 but a summary of the most important features is given next:

- Current chopping capability: this model gives the possibility of enabling or disabling the current chopping (a 3A value has been chosen). The main disadvantage of this model is that if the current chopping is enabled the current is also chopped at high frequencies.
- Cold withstand curve: in this curve a two point linear withstand curve can be defined but the hot withstand is not modelled. The cold withstand rate of rise have been deduced from measurements (3 kV/ms).
- High frequency quenching capability: this model opens at the high frequency zero crossings independently of the slope of the current. The number of zero crossings before breaking can be chosen.

5.2.6 Load

The load has been modelled using the available items from PSCAD (resistor, inductance…) and has been connected from phase-b to ground (see explanation in 5.1.8)

5.3 EXPERIMENTS

The following experiments have been performed:

i. Opening at no load
ii. Closing at no load
iii. Opening a resistive load (R=0.5Ω)
iv. Closing a resistive load (R=0.5Ω)

All simulations have been done with a ZnO arrester connected in the HV side of TX2 first. Afterwards all the experiments have been repeated without arrester and it has been proven that the protection device does not affect the results.

The description of the plotted curves is given below:

U1 (blue): voltage at the supply side of the VCB.
U2 (green): voltage at the voltage side of the VCB.
Ubrk or **Ubreaker** (red): voltage across the contacts of the VCB.
I1 (blue): current flowing through the VCB.

5.3.1 OPENING AT NO LOAD

The function of the ZnO arrestor is to limit the magnitude of the voltage at the high voltage terminals of the load transformer (alias TX2). In order to verify whether this safety device influences the results or not, two tests were carried on (with and without arrester). Both measurements happened to be almost identical (fig. 79 and fig. 80). Observe that the opening times are not exactly the same ones.

MEASUREMENTS

With ZnO:

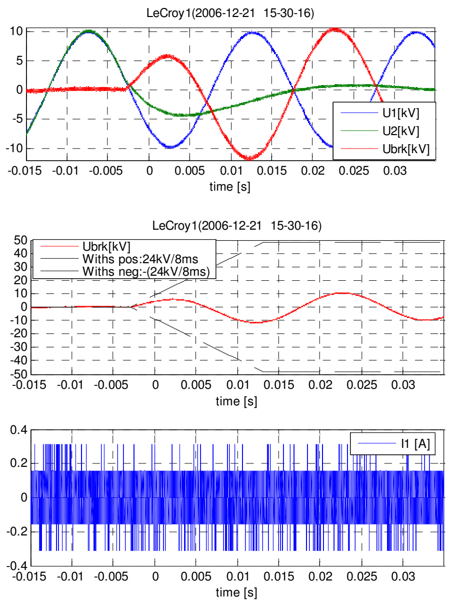

fig. 79. Test: Opening at no load with 11kV ZnO. 10 MS/s

Without ZnO:

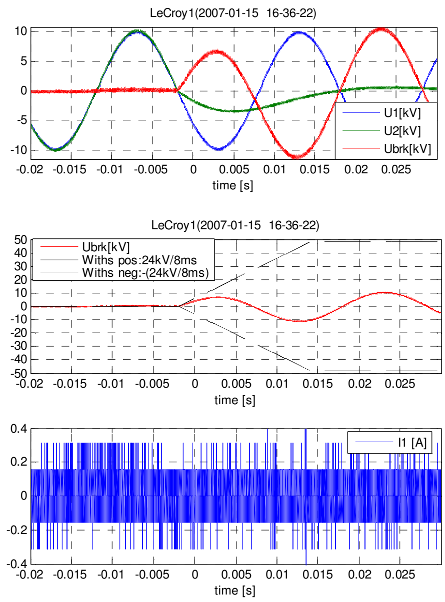

fig. 80. Test: Opening at no load without 11kV ZnO. 10 MS/s

PSCAD simulations also give the same results with and without arrester.

PSCAD SIMULATIONS

With ZnO:

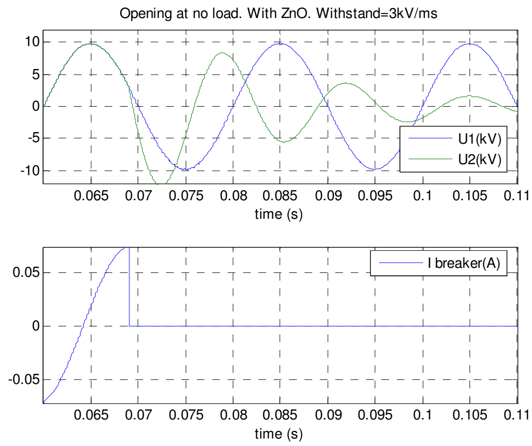

fig. 81. PSCAD: Opening at no load with 11kV ZnO. Tstep=0.05 µs

Without ZnO:

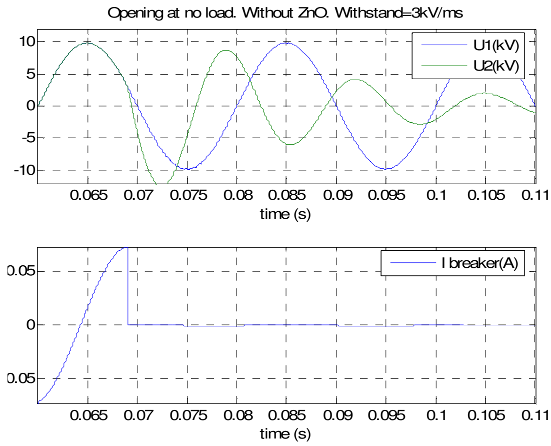

fig. 82. PSCAD: Opening at no load without 11kV ZnO. Tstep=0.05 µs

With ZnO:

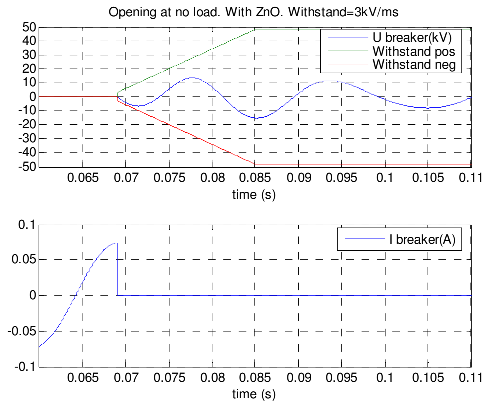

fig. 83. PSCAD: Opening at no load with 11kV ZnO. Tstep=0.05 µs

Without ZnO:

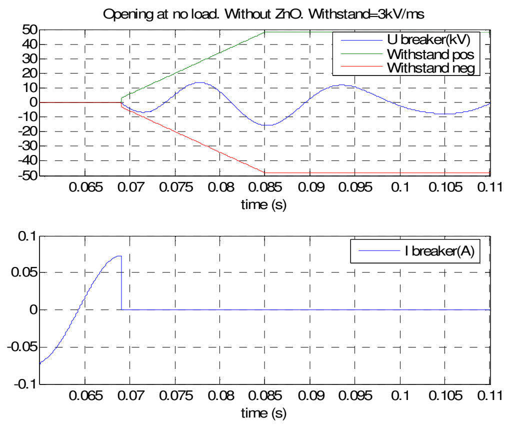

fig. 84. PSCAD: Opening at no load without 11kV ZnO. Tstep=0.05 µs

From these simulations the conclusions can be drawn:

- The no load current is very low: around 50mA rms.
- The simulated TRV (Transient Recovery voltage) differs from the measured TRV. This means that the model does not exactly resemble reality and either a capacitance or inductance value is not correctly estimated. The simulations show that the frequency of U_2 is higher than in measurements and the damping is lower.

In an ideal no-loss system the energy would transfer from the inductance to the capacitor and vice versa following an oscillating behaviour of frequency:

$$f = \frac{1}{2\pi \cdot \sqrt{LC}} \qquad \textbf{(eq. 44)}$$

According to this equation if the real frequency is lower than the simulated one then either L or C must be higher than in the model.

The current chopping level has been correctly chosen (3A) as it has been checked in the measurements (see test of day 2006-12-22 at 10:51:15 h)
If the expression of the TRV after current chopping is observed ($V_{peak}=I_0 \cdot sqrt[L/C]$) and knowing that the current chopping level is right, the inductance value must be lowered or the capacitor value increased in order to obtain a smaller voltage peak. If these statements are correct, then the real capacitor value is higher than the one in simulations.

According to fig. 78, the oscillation frequency of the load side voltage is 77.19 Hz.

$$f_{simulation} = \frac{1}{2\pi \cdot \sqrt{L_{\mathrm{mod}\,el} \cdot C_{\mathrm{mod}\,el}}} = \frac{1}{2\pi \cdot \sqrt{256.57H \cdot 16.57nF}} = 77.19Hz$$

The oscillation frequency measured from the simulations when opening at no-load is around 76.45 Hz, which means that the simulation results match the theoretical calculations based on the simulation file.

The measured real oscillation is much slower, 24.4 Hz.

Assuming that the capacitances have been correctly chosen, this means that the real equivalent inductance of the load side is 2568 H, approximately 10 times bigger than modelled.

$$\mathrm{L_{new}} = \frac{1}{\mathrm{C_{mod\,el}} \cdot (2\pi \cdot \mathrm{f_{measured}})^2} = \frac{1}{16.57\mathrm{nF} \cdot (2\pi \cdot 24.4\mathrm{Hz})^2} = 2568\mathrm{H}$$

On the other hand, presuming that the inductances have been correctly chosen, then this means that the real equivalent C of the load side is, approximately 10 times bigger than modelled.

$$\mathrm{C_{new}} = \frac{1}{\mathrm{L_{mod\,el}} \cdot (2\pi \cdot \mathrm{f_{measured}})^2} = \frac{1}{256\mathrm{H} \cdot (2\pi \cdot 24.4\mathrm{Hz})^2} = 166.2\mathrm{nF}$$

These values are both two big so it cannot be that only one element is incorrect. One of the parameters that could be changed is the magnetizing current, which has been estimated as 1% of the rated current. In some cases it can reach the 2% but this has to be checked. Another parameter that can be varied is the cable capacitance (depending of the layer thickness and material properties) but it is not possible to obtain a 10 times bigger value.

5.3.2 CLOSING AT NO LOAD

The simulations with and without ZnO have given the same results.

COMPARISON

Measurement: *PSCAD:*

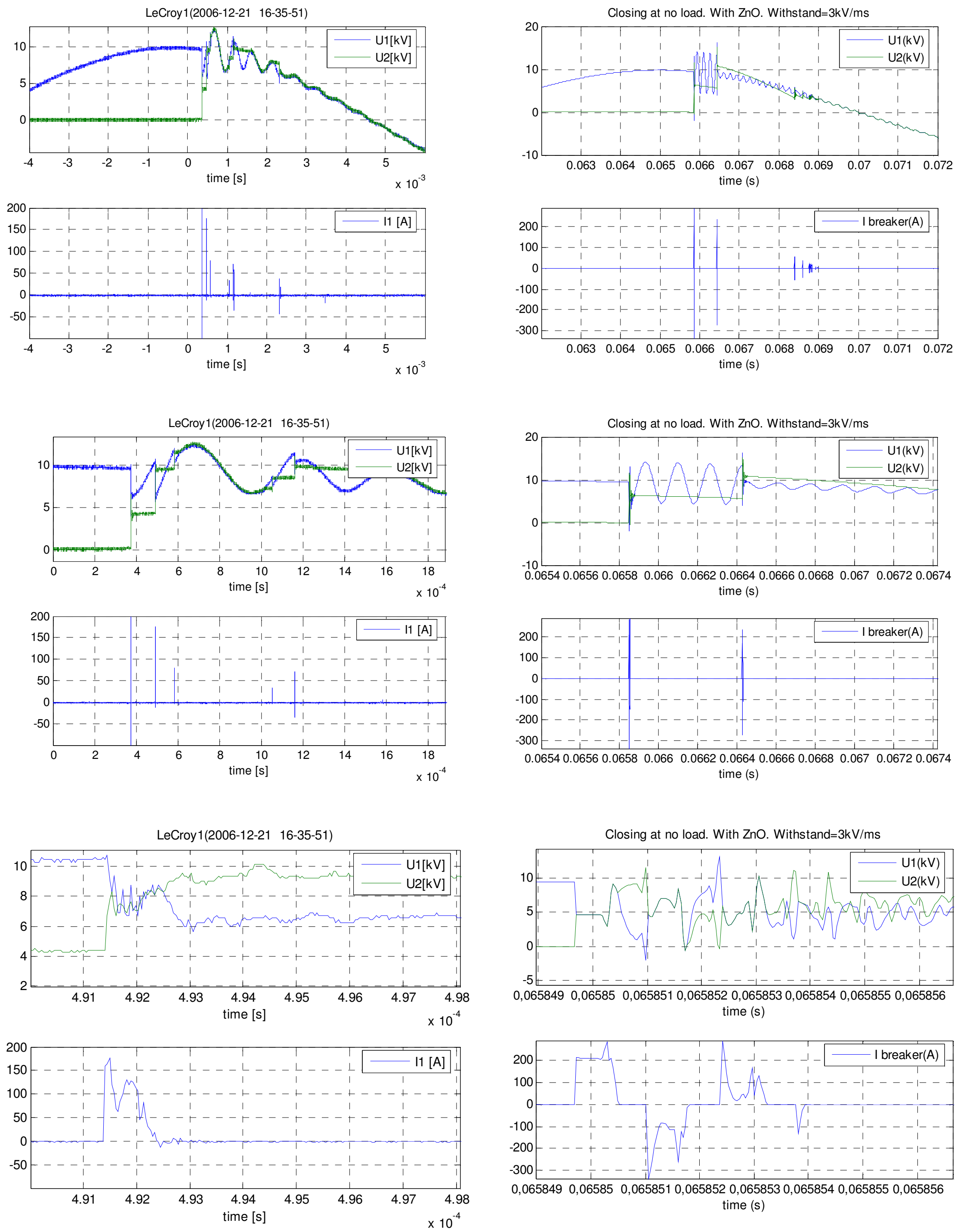

fig. 85. Comparison: Closing at no load with 11kV ZnO. 25 MS/s

In this case, as well as in the opening at no-load case a higher frequency oscillation is observed in the supply side voltage in simulations. This higher frequency and amplitude oscillation generates more pre-strikes than in reality.

COMPARISON

Measurement: *PSCAD:*

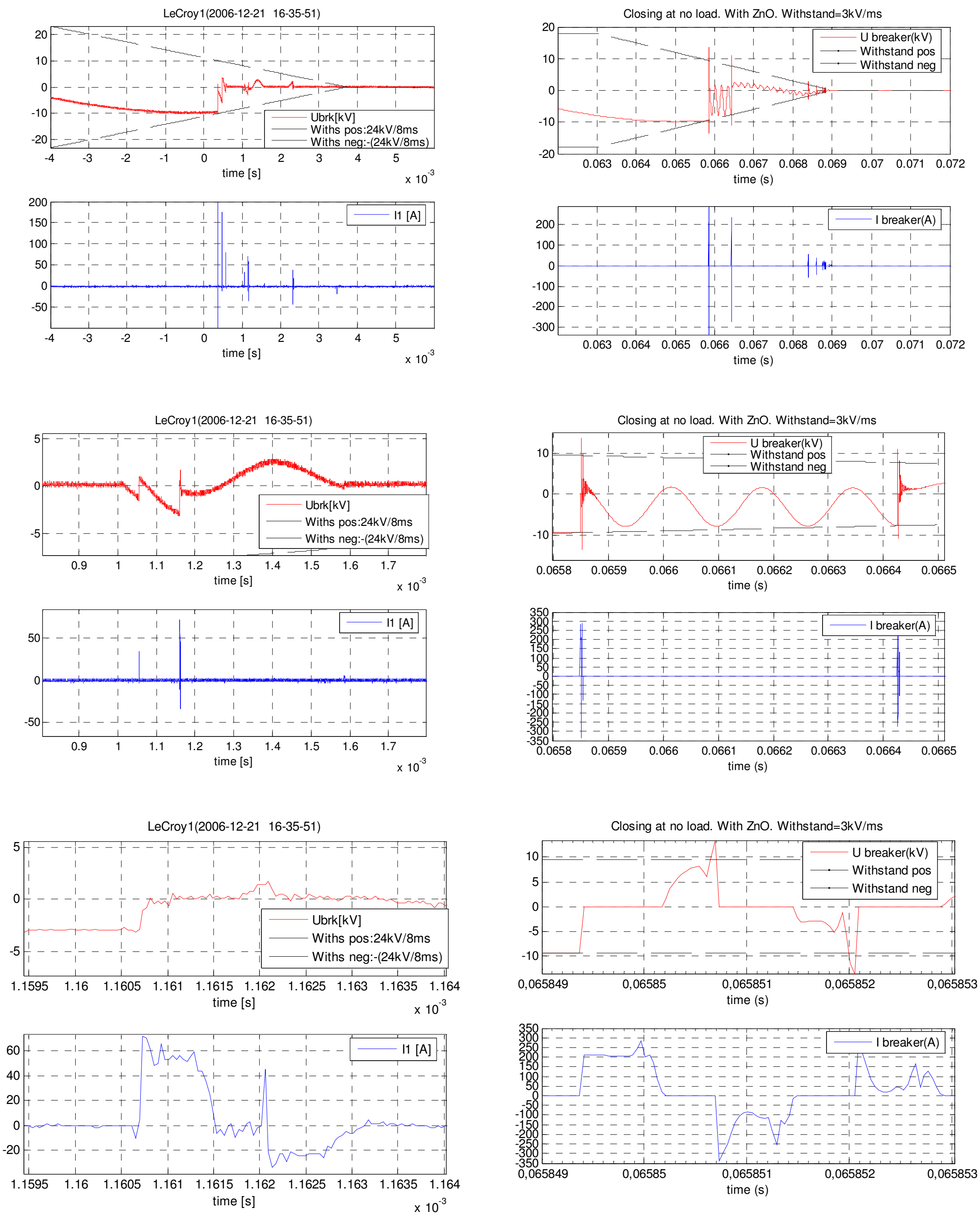

fig. 86. Comparison: Closing at no load with 11kV ZnO. 25 MS/s

It must also be observed that the model used does not make any difference between power frequency current and high frequency currents as far as current chopping is concerned. In reality current chopping does not happen at high frequencies and therefore the transient recovery voltage is much smoother than in simulations. In simulations the modelling of current chopping when the pre-strikes are extinguished causes more pre-strikes.

5.3.3 OPENING A RESISTIVE LOAD (R=0.5Ω)

The measurements performed with and without arrester show no difference. The arrester does not have influence on the system with this particular resistive load.

MEASUREMENTS

With ZnO:

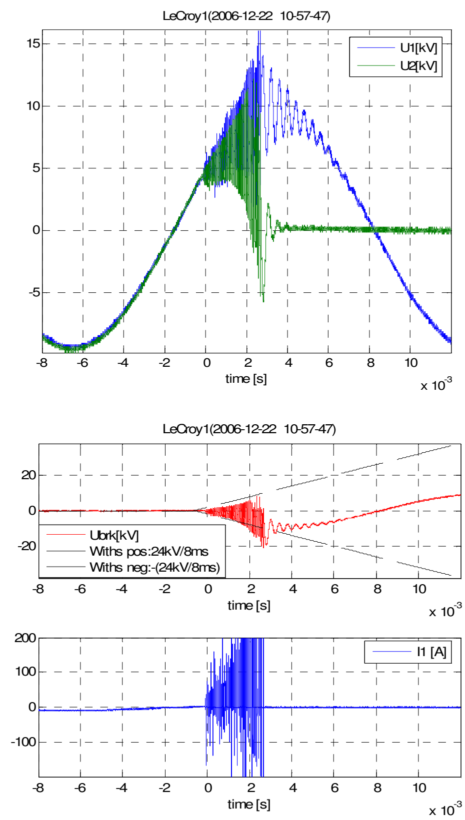

fig. 87. Test: Opening a resistive load (R=0.5Ω) with 11kV ZnO. 10 MS/s

Without ZnO:

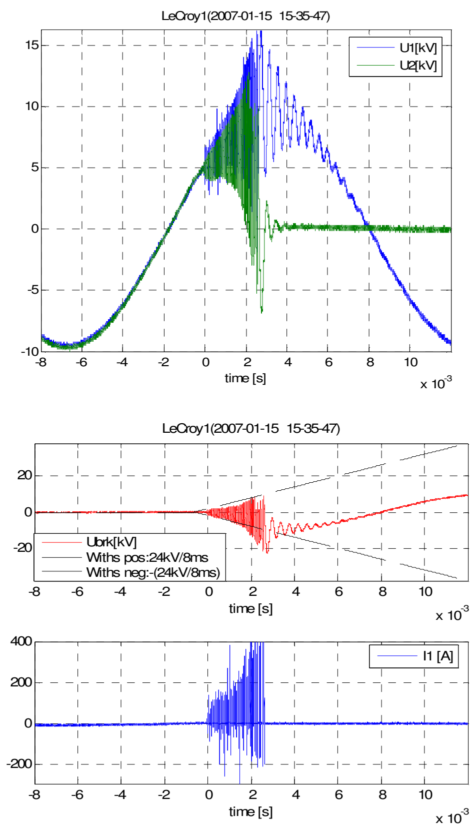

fig. 88. Test: Opening a resistive load (R=0.5Ω) without 11kV ZnO. 10 MS/s

The following comparisons take the arrester into account (all the measurements were done while the arrester was connected). The different records show the opening of a resistive load at several breaking times. It can be observed that the worst reignitions appear when the opening of the CB contacts starts just before the current becomes zero. Opening time “7” gives the worst scenario while opening times “3” and “4” are the smoothest ones. This behaviour can be explained as follows:

When the CB contacts receive the breaking command its contacts start to physically separate. However, while the current is not zero there is a current arc flowing through the contacts and therefore the voltage difference across the terminals is almost zero (few tens of volts). As soon as the current becomes zero the arc extinguishes and a voltage difference appears among both contacts, this is the so called transient recovery voltage (TRV). It is also known that the bigger the separation between contacts, the larger the voltage withstand capability is. For this reason, the longer time it takes for the current to annihilate the stronger the gap will become and the lesser reignitions that will take place.

MEASUREMENTS: OPENING TIME "1"

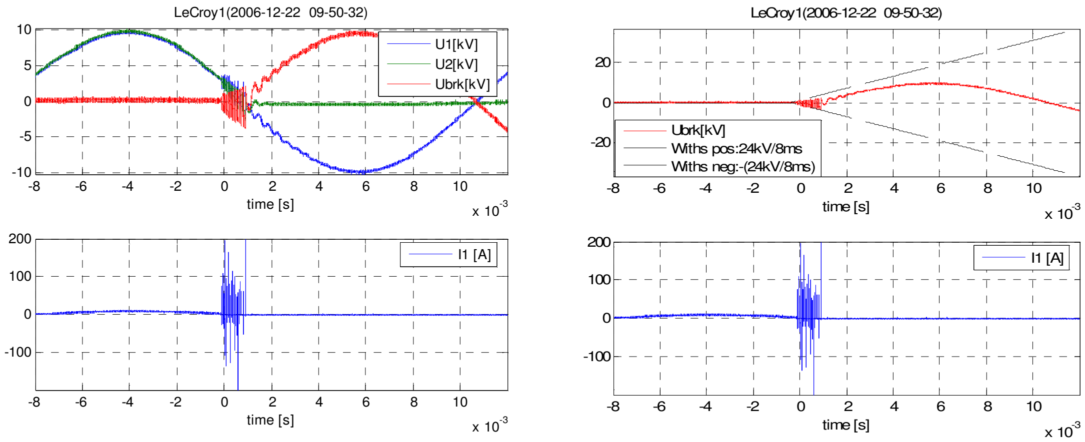

fig. 89. Opening a resistive load (R=0.5Ω). Opening time "1". With ZnO. 10MS/s

MEASUREMENTS: OPENING TIME "2"

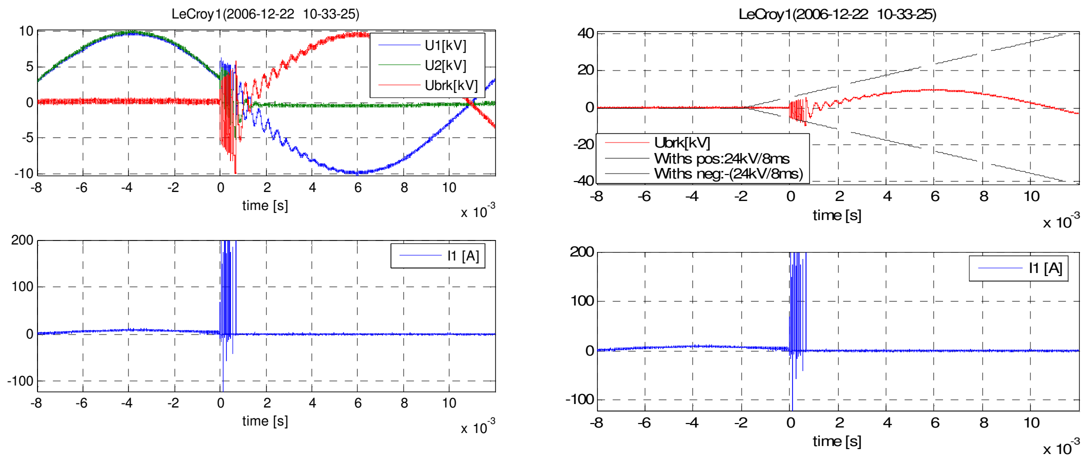

fig. 90. Opening a resistive load (R=0.5Ω). Opening time "2". With ZnO. 10MS/s

MEASUREMENTS: OPENING TIME "3"

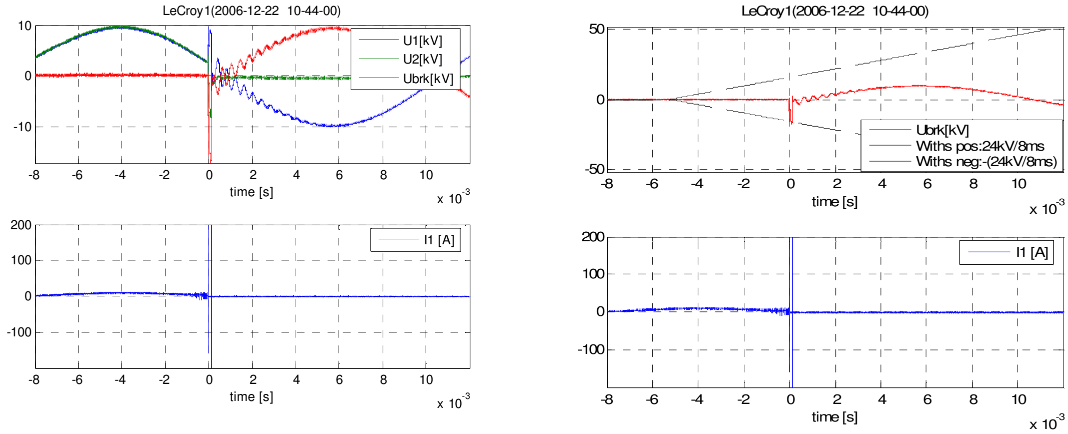

fig. 91. Opening a resistive load (R=0.5Ω). Opening time "3". With ZnO. 10MS/s

MEASUREMENTS: OPENING TIME "4"

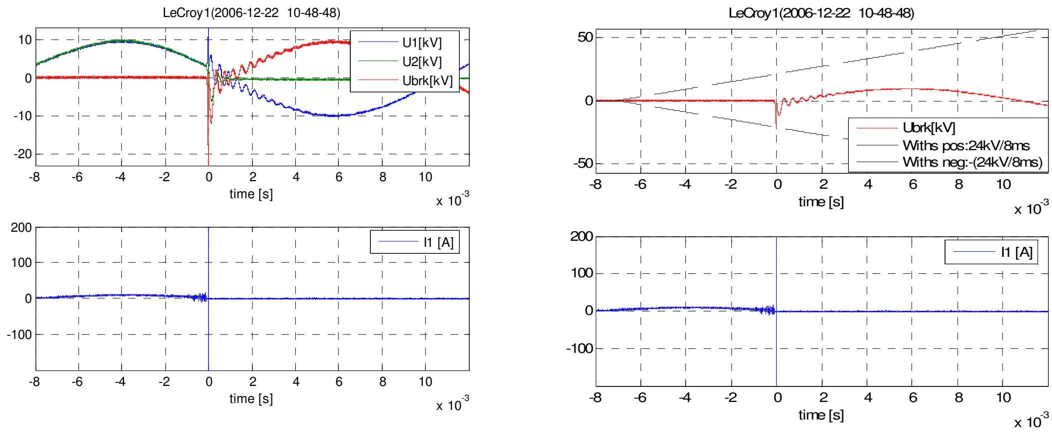

fig. 92. Opening a resistive load (R=0.5Ω). Opening time "4". With ZnO. 10MS/s

MEASUREMENTS: OPENING TIME "5"

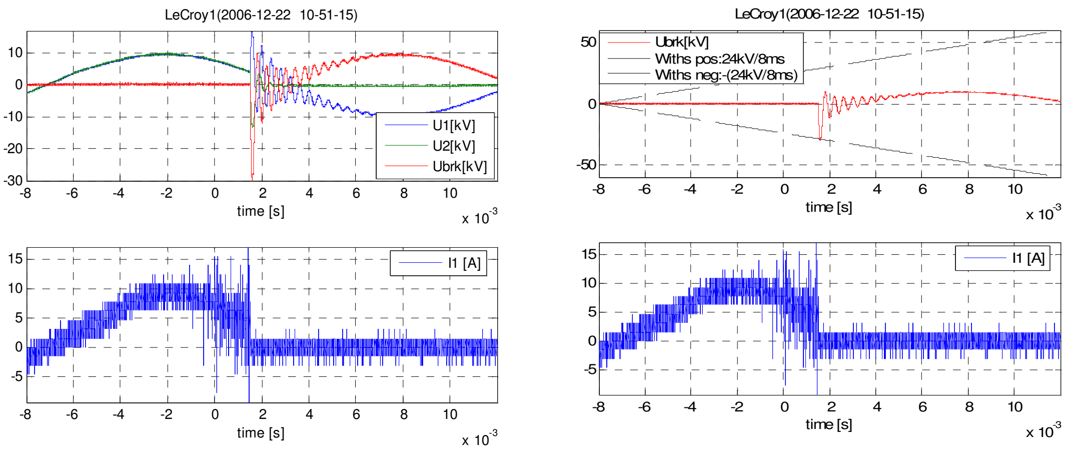

fig. 93. Opening a resistive load (R=0.5Ω). Opening time "5". With ZnO. 10MS/s

MEASUREMENTS: OPENING TIME "6"

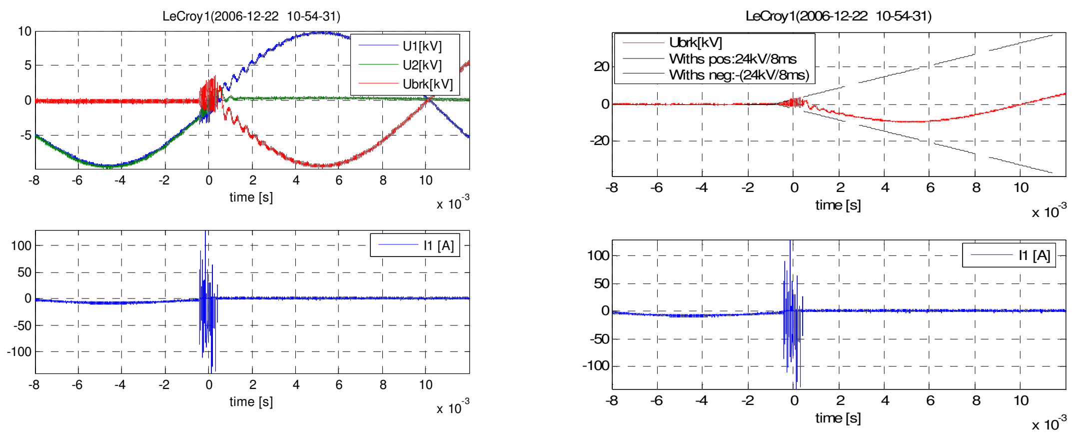

fig. 94. Opening a resistive load (R=0.5Ω). Opening time "6". With ZnO. 10MS/s

MEASUREMENTS: OPENING TIME "7"

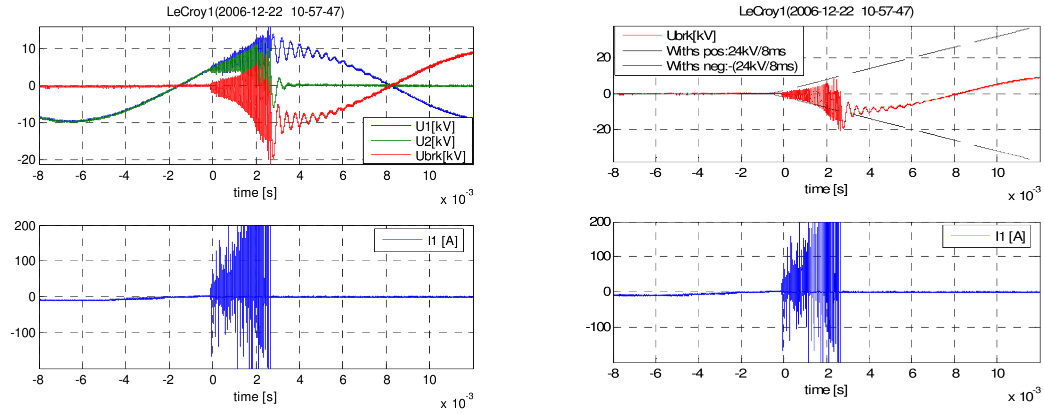

fig. 95. Opening a resistive load (R=0.5Ω). Opening time "7". With ZnO. 10MS/s

After gathering all measurements together, it has been possible to compare the effect of the opening time, and the result was as expected: the reignitions are worse when the opening time comes close to the crossing of the current zero.

The simulation of the PSCAD model has shown similar but not exactly equal results. Some important modelling constraints and other matters have been summarized:

- The values given to the components of the system are approximations and therefore it is very difficult to obtain an identical TRV. In addition, some components might be missing or are not correctly modelled, and it must not be forgotten that the frequency dependency of the system is not represented. Achieving a similar TRV is a very important issue for getting close results.

- The operation of the CB is modelled according to an estimated cold withstand curve. The hot withstand, which is also sensitive to the voltage rise rate of the TRV, has not been taken into account. The results are also dependant on the chosen rate of rise of the cold withstand curve. Moreover, there is certain evidence to think that the cold withstand curve does not follow a linear pattern as it has been modelled.

The PSCAD simulations in the case of a resistive load give the same results (fig. 96 and fig. 97) with and without arrester. The measurements have been performed with arrester consequently the PSCAD simulations explained will account for the arrester.

PSCAD SIMULATIONS (Opening time “7”)

Without arrester:

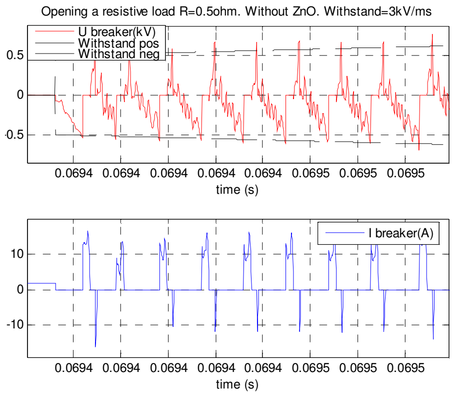

fig. 96. PSCAD: Opening a resistive load (R=0.5Ω) without 11kV ZnO. 10 MS/s

With arrester:

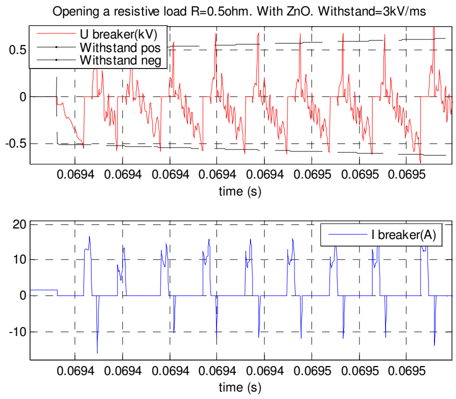

fig. 97. PSCAD: Opening a resistive load (R=0.5Ω) with 11kV ZnO. 10 MS/s

COMPARISON: OPENING TIME “1”

Measurement: *PSCAD:*

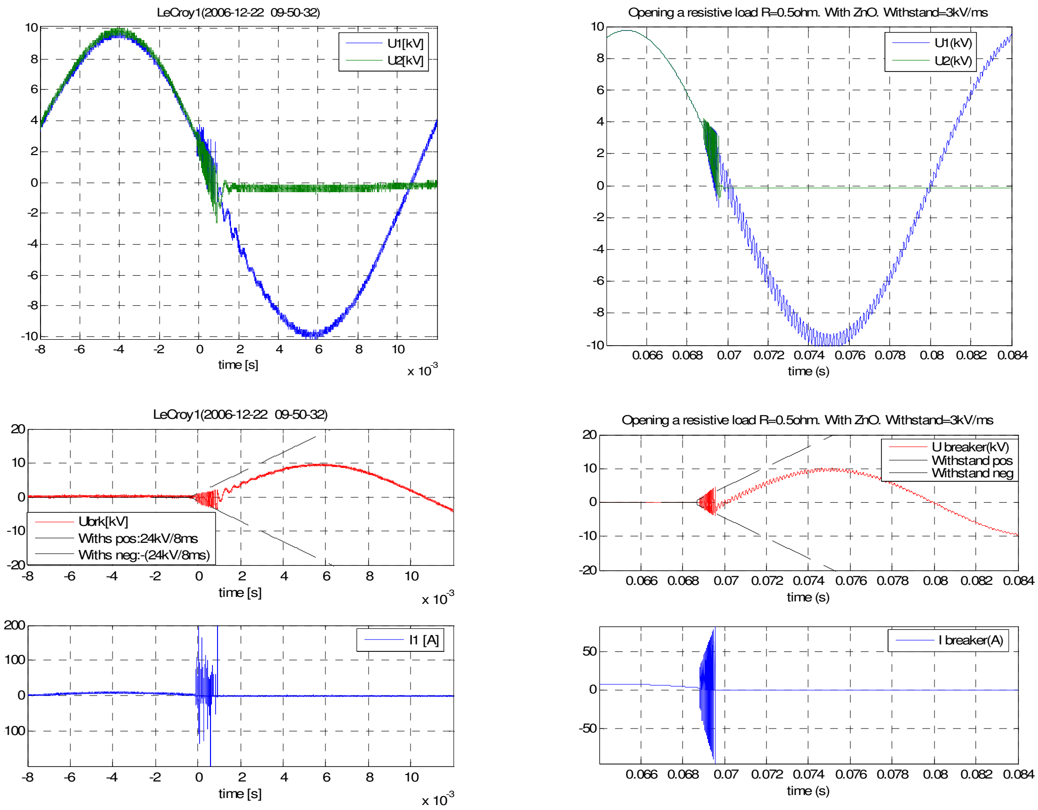

fig. 98. Comparison: Opening a resistive load (R=0.5Ω) with 11kV ZnO. Test: 10Mhz. PSCAD: 0.05µs

COMPARISON: OPENING TIME "1" (ZOOMS)

Measurement: *PSCAD:*

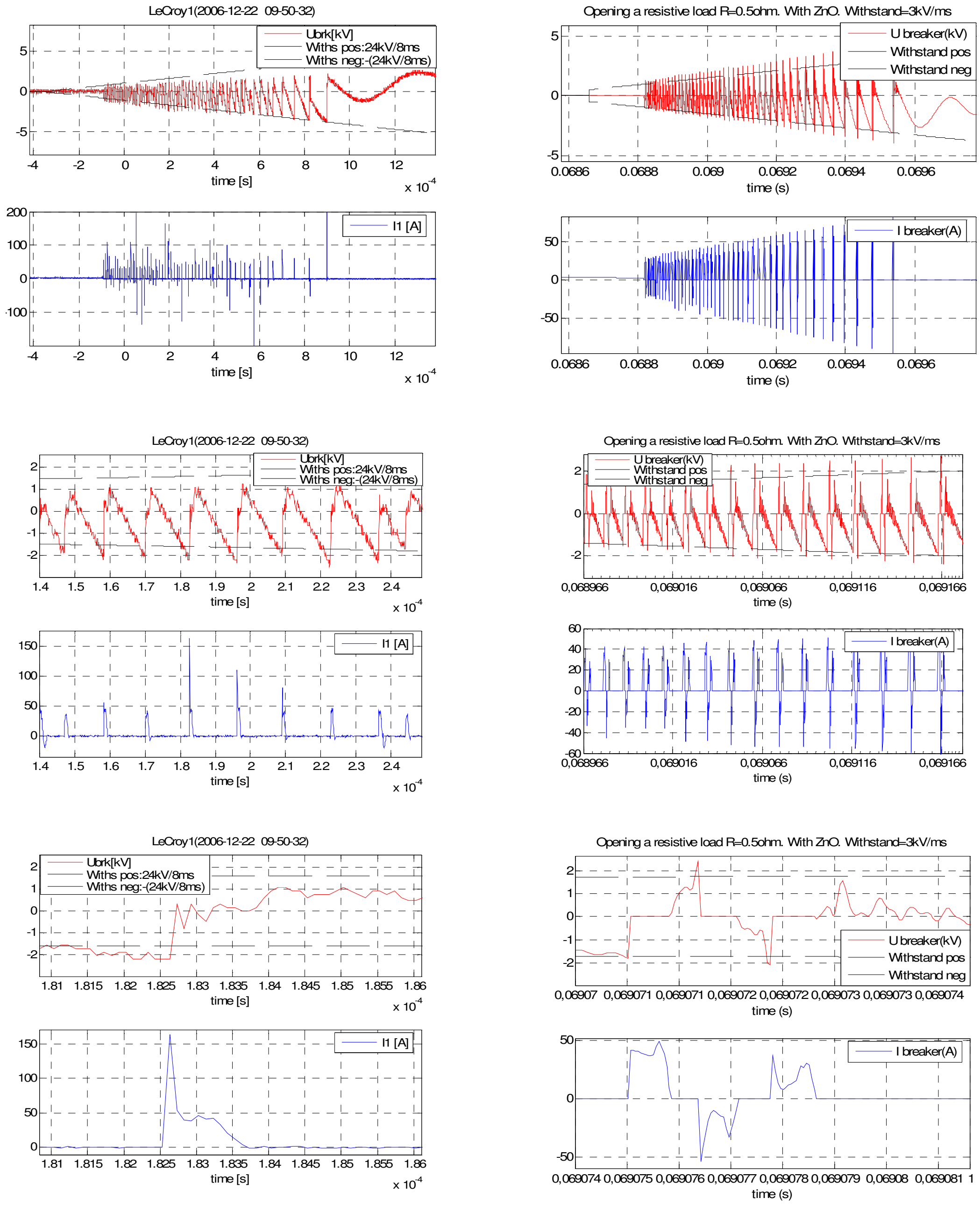

fig. 99. Comparison: Opening a resistive load (R=0.5Ω) with 11kV ZnO. Test: 10Mhz. PSCAD: 0.05µs

COMPARISON: OPENING TIME "2"

Measurement: *PSCAD:*

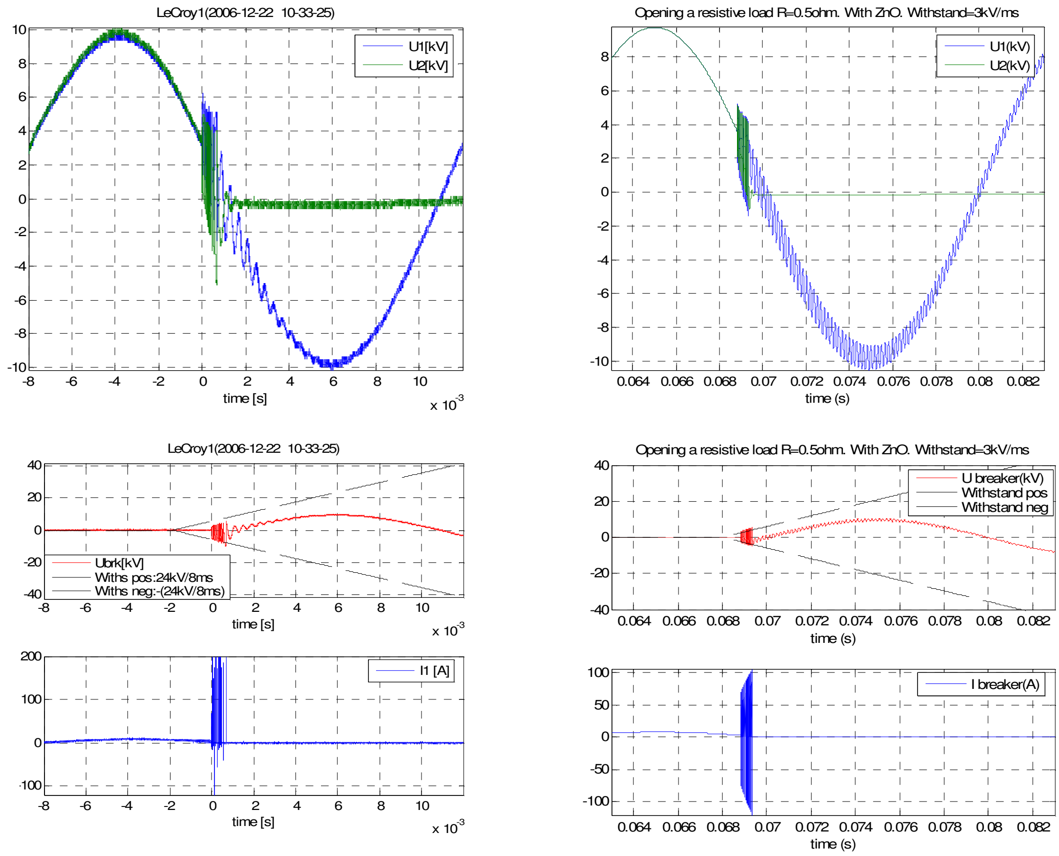

fig. 100. Comparison: Opening a resistive load (R=0.5Ω) with 11kV ZnO. Test: 10Mhz. PSCAD: 0.05μs

COMPARISON: OPENING TIME "3"

Measurement: *PSCAD:*

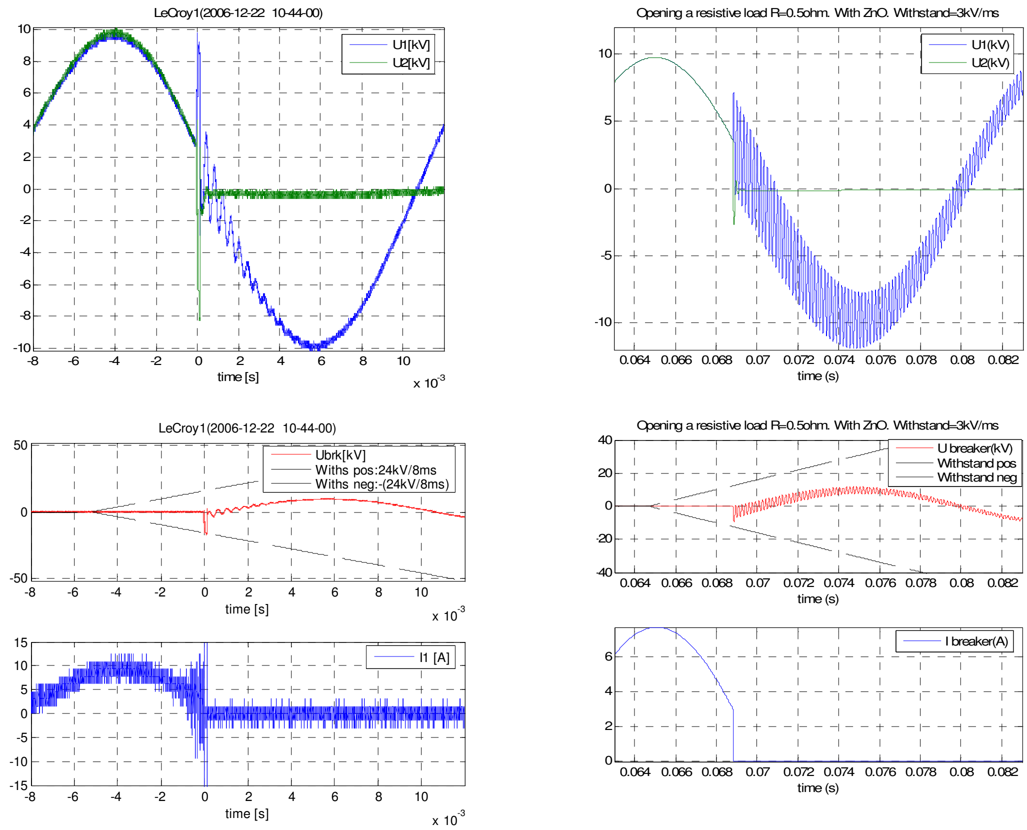

fig. 101. Comparison: Opening a resistive load (R=0.5Ω) with 11kV ZnO. Test: 10Mhz. PSCAD: 0.05µs

COMPARISON: OPENING TIME "4"

Measurement: *PSCAD:*

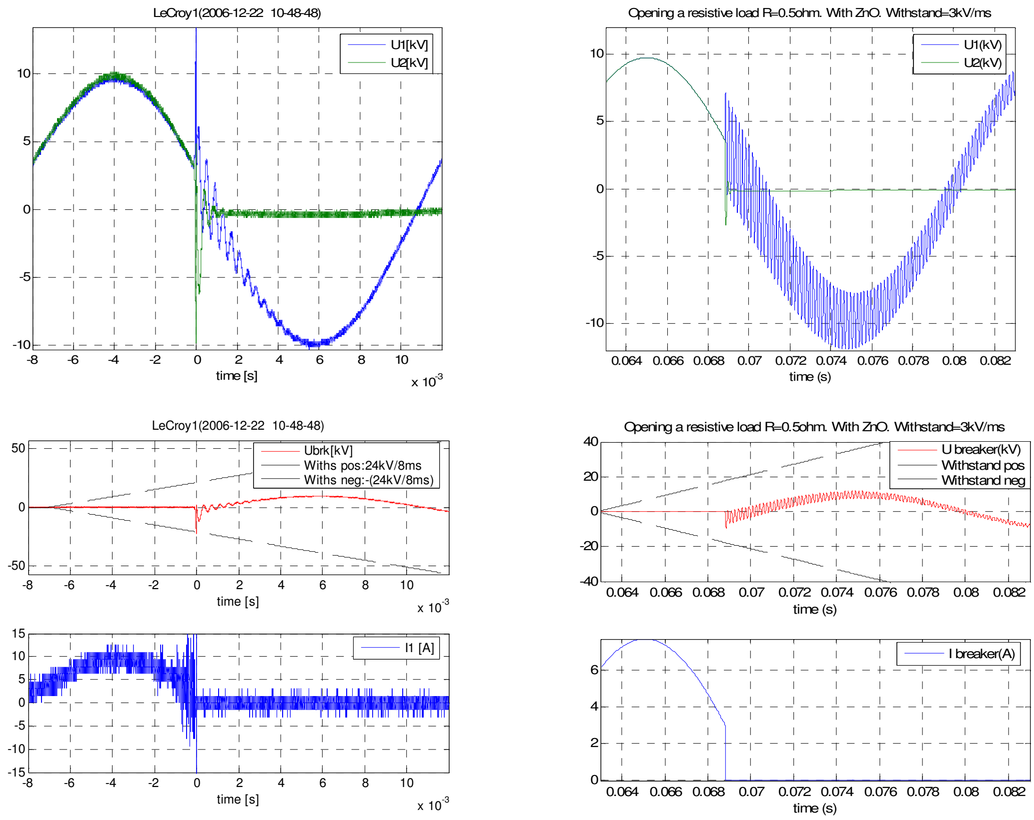

fig. 102. Comparison: Opening a resistive load (R=0.5Ω) with 11kV ZnO. Test: 10Mhz. PSCAD: 0.05μs

COMPARISON: OPENING TIME “5”

Measurement: *PSCAD:*

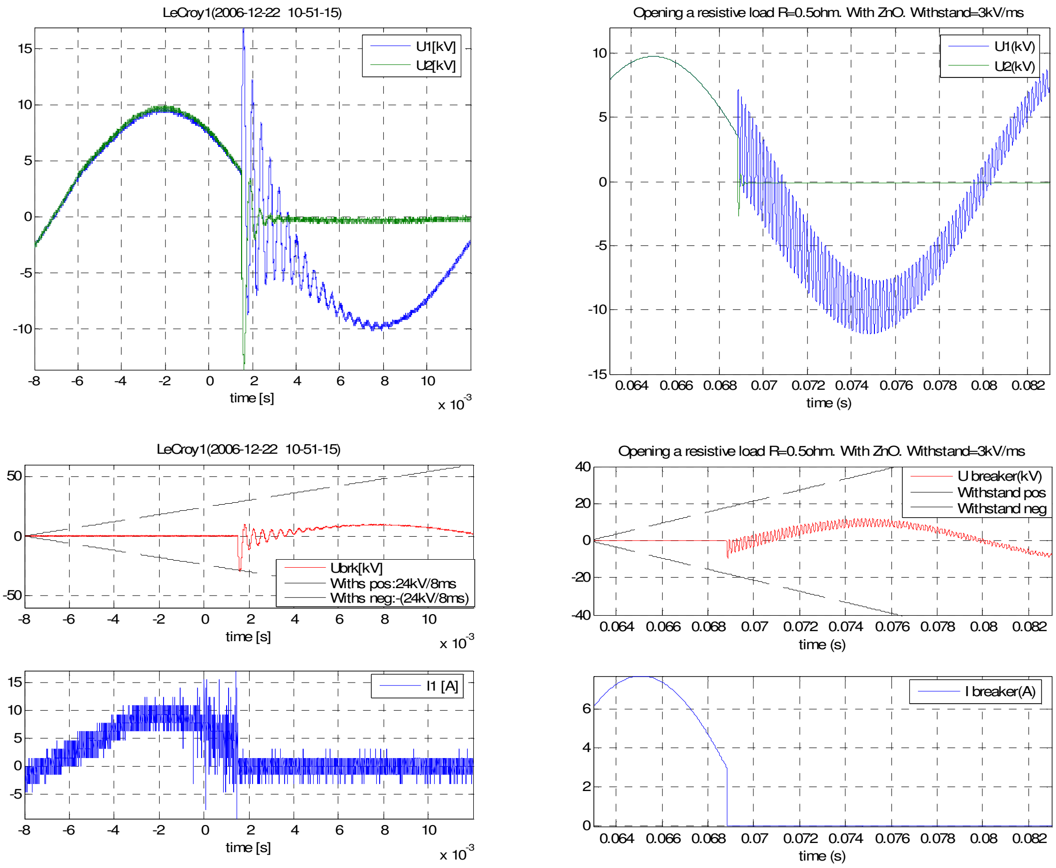

fig. 103. Comparison: Opening a resistive load (R=0.5Ω) with 11kV ZnO. Test: 10Mhz. PSCAD: 0.05µs

COMPARISON: OPENING TIME “6”

Measurement: *PSCAD:*

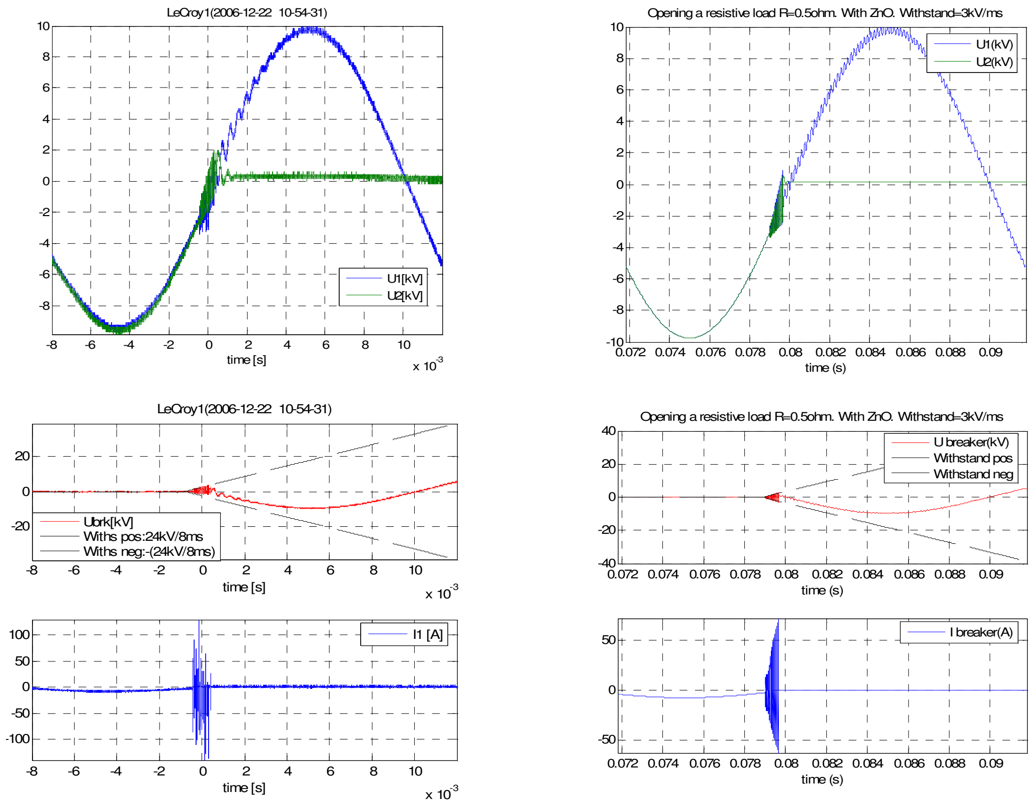

fig. 104. Comparison: Opening a resistive load (R=0.5Ω) with 11kV ZnO. Test: 10Mhz. PSCAD: 0.05μs

COMPARISON: OPENING TIME "7"

Measurement: *PSCAD:*

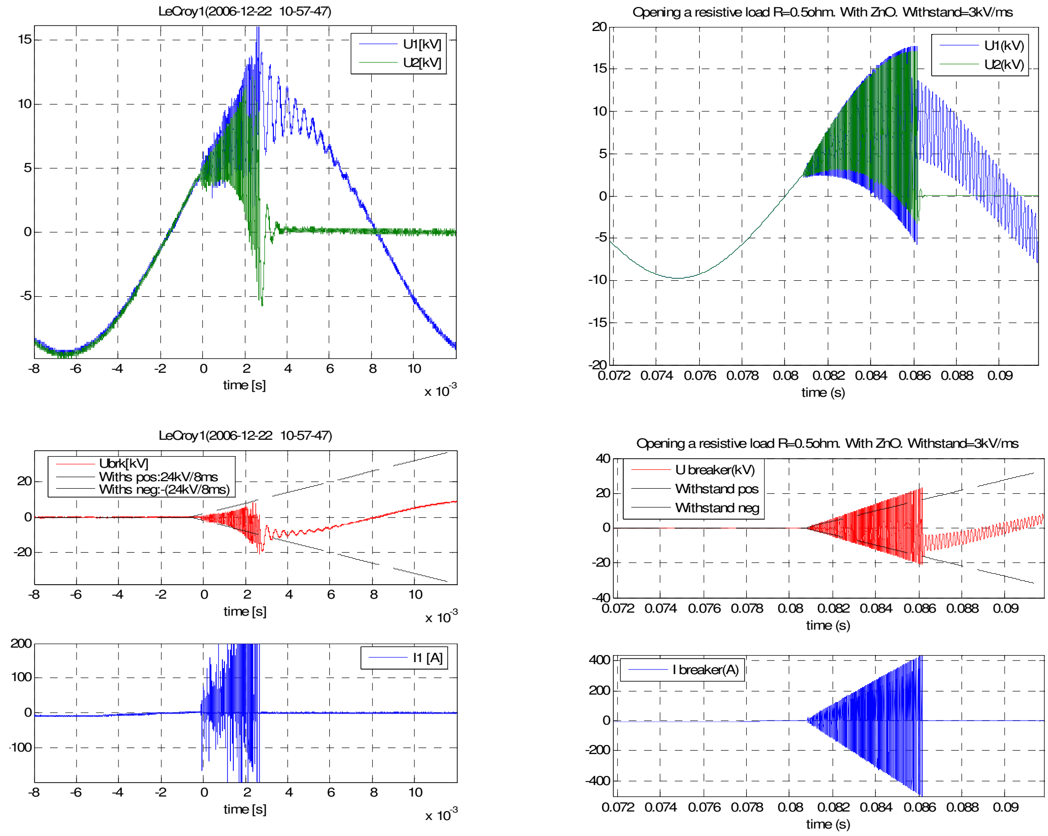

fig. 105. Comparison: Opening a resistive load (R=0.5Ω) with 11kV ZnO. Test: 10Mhz. PSCAD: 0.05μs

5.3.4 CLOSING A RESISTIVE LOAD (R=0.5Ω)

It is not straight forward to estimate if the arrester influences the results in the case of closing a resistive load because the closing does not happen at the same exact moment. Nonetheless the waveshapes seem to follow the same pattern and therefore the arrester is believed not to be active.

MEASUREMENTS

With ZnO(load at phase c):

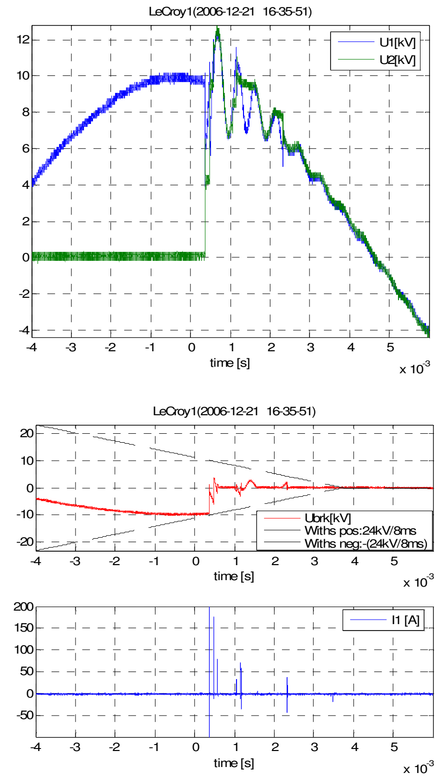

fig. 106. Test: Closing a resistive load (R=0.5Ω) with 11kV ZnO. 10 MS/s

Without ZnO(load at phase b):

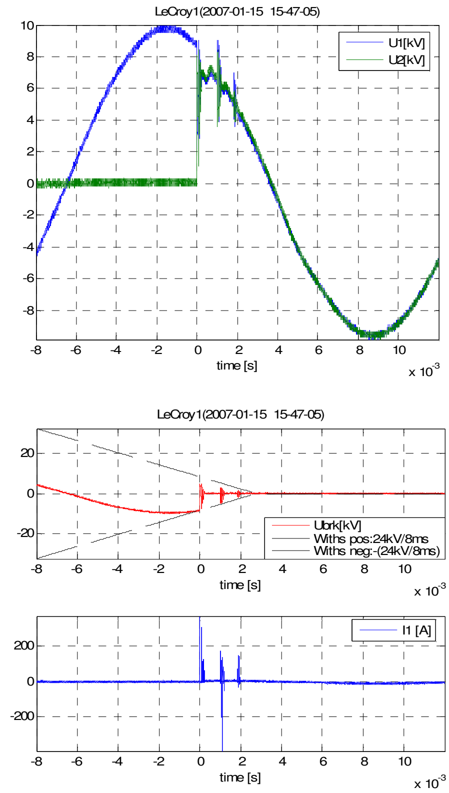

fig. 107. Test: Closing a resistive load (R=0.5Ω) without 11kV ZnO. 10 MS/s

COMPARISON: CLOSING A RESISTIVE LOAD (without ZnO)

Measurement: *PSCAD:*

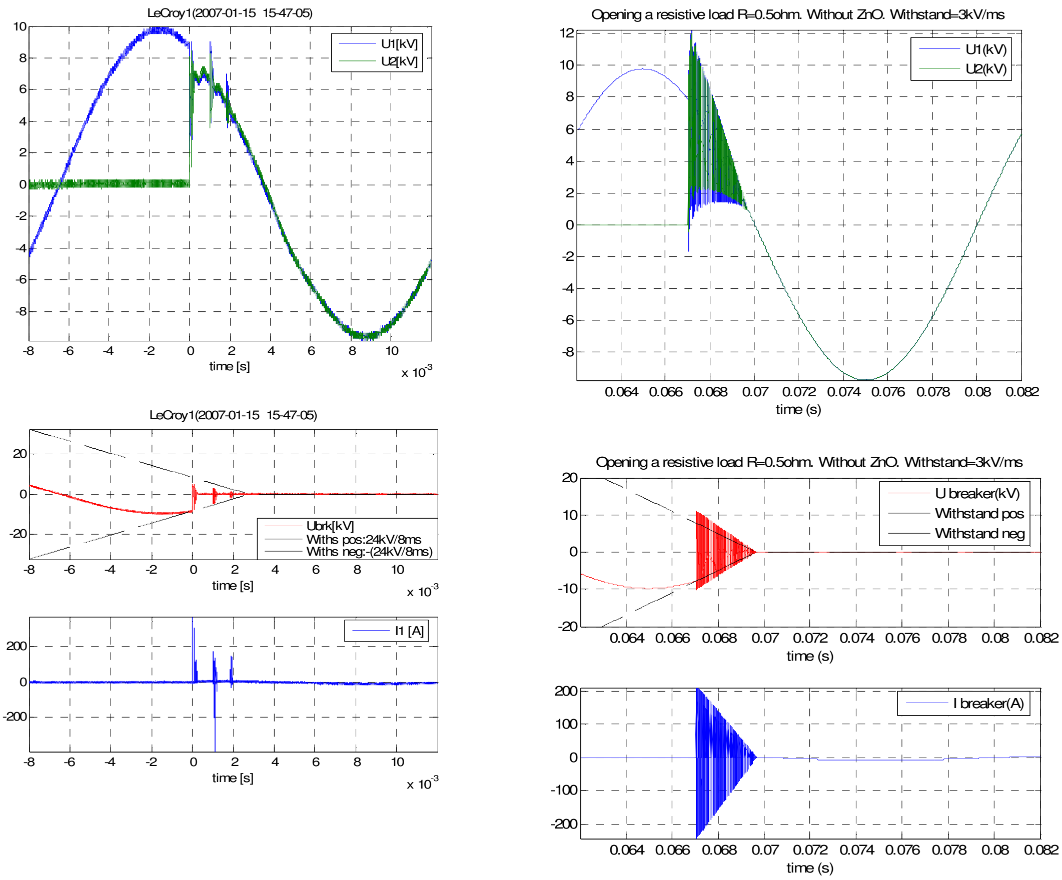

fig. 108. Comparison: Closing a resistive load (R=0.5Ω) without 11kV ZnO. Test: 10Mhz. PSCAD: 0.05µs

5.3.5 CONCLUSIONS

The model of the laboratory setup does not exactly resemble reality. The main differences are the following:

– The damping reflected in the simulations is too low. In reality oscillations are much faster damped. Modelling the damping when the frequency spectrum is broad is difficult because the AC resistance changes according to the operation frequency and the real circuit has always many resistive elements that are not considered in the model.

– The frequency of oscillations is higher in the simulated cases compared to the measurements. This evidences that either the equivalent inductance or capacitance of the circuit has not been correctly modelled. The following equipment is suspected not to be adequately tuned:

- **Cables**

  The cable capacitance is estimated according to the thickness and material of its insulating layer (between conductor and shield). It might be that the real cable has other insulation layer values and properties.

The ground wire (which lays at a distance of 10cm in parallel to the cable) adds some capacitance to the system. However, this capacitance is believed to be much lower than the capacitance between the conductor and the shield.

The cable is not laid straight ahead from the transformers to the breaker and it makes some curves. These half-loops might add some inductance to the circuit but it is thought to be negligible compared to the magnetizing inductance of the transformer.

- **Transformer**

  The magnetizing curve of the transformer is not linear. The experiments are being run at a voltage level three times lower than the rated voltage and, although this point is supposed to still be in the linear region, it might show some differences. The simulation results shown here do not take into account the non-linearities and therefore consider the rated magnetizing inductance (the magnetizing current is assumed to be 1% of the rated current). The real magnetizing curve must be obtained and introduced in the model in order to get a more reliable result.

– There is a noticeable difference in the CB operation in the simulations and in reality. In reality current chopping only occurs just before the power frequency current zero crossing but if the current chopping is enabled in the CB model it chops all currents, including the high frequency ones. This means that the simulated results show a much higher density of multiple reignitions. In the simulations, every time that a reignition takes place and the current is close to reach the zero, the current is chopped and the TRV is so steep that it generates another reignition. In reality this fast TRVs do not appear because the high frequency current is not chopped. This dysfunction can be observed in the simulations in the form of groups of 2 or 3 current spikes in each reignition while in the lab measurements the current spike is, most of the times, only one (unipolar).

– The CB model uses a cold-withstand curve. The cold withstand curve is not given by breaker manufacturers and must be estimated. Moreover, even if the curve is assumed to be linear, is not exactly linear so the simulation diverts from the real records. In real operation the breaker is also exposed to the effects of the hot gap, that decreases the withstand characteristic and it is not modelled.

– The chopping level has been correctly chosen to be 3A.

– At circuit opening the worst reignitions are obtained when the contacts start to separate just before the zero crossing. At circuit closing it is difficult to point out which is the most critical closing time.

– All the simulations and recordings have been stored in matlab figures so they can be further analysed in later studies.

6. 3 PHASE CABLE SIMULATIONS

Although the original aim of the laboratory experiments was to use three phase cables but due to several problems the preliminary laboratory setup has been exposed to successive variations. The lack of a three phase cable has lead to a series of single phase experiments that were not planned in the beginning. For this reason the results obtained after the following simulations cannot be compared with the experimental measures for the moment. Nevertheless, these simulations can be used later on when the three phase cable is available.

6.1 STRUCTURE

Two different circuit configurations will be simulated and analysed. These circuits represent a small branch of the collection grid of an offshore WP.
The **first** configuration (fig. 109) is comprised of two three phase cables of similar lengths (65m and 50m) separated by a VCB. The left hand side transformer is a step up transformer that raises the voltage from 240 V to 12 kV and the right hand side transformer, which is a step down transformer, is connected to the load.

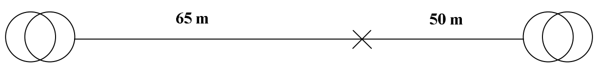

fig. 109. Schematic drawing of Configuration I

The **second** configuration (fig. 110) is almost identical to the first configuration with the only difference of a capacitor attached to the high voltage side of the supply transformer. The purpose of this capacitor is to emulate the feeders and cables that surround this small system and that constitute the collection grid. The capacitor does not exactly behave as a charged cable but it can provide a good approximation as long as the results are correctly interpreted.

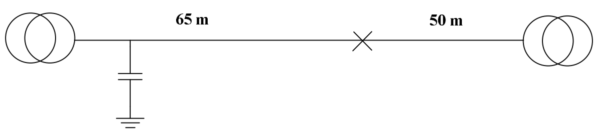

fig. 110. Schematic drawing of Configuration II

Each of these configurations has been simulated in different situations and load types. They have been compared and conclusions have been drawn.

6.2 OPERATIONS

The following operations will be simulated:

i) Energizing at no load
ii) Opening
 a.- No load
 b.- A resistive load
 c.- An inductive load
 d.- A fault:
  - Single-line-to-ground (SLG)
  - Two-phase-to-ground (2ph-gnd)

- Three-phase-to-ground (3ph-gnd)
- Two-phase (2ph), three-phase (3ph)

6.3 DESCRIPTION OF THE SIMULATION FILE

The simulation file used is very similar to the laboratory experiment simulation file, see fig. 113. The main differences are in the cables, which now are three phase, and in the CB settings.

6.3.1 The cables

The cable data introduced in these simulations does not exactly correspond to the laboratory cable data. The reason is that when the simulations were done the data of the experiment components was not known yet. As it can be observed in fig. 111 the longest cable (65m) is assumed to have a cross section of 185mm^2, an aluminium conductor and a copper shield while the shortest cable (54m) is assumed to have a cross section of 95mm^2, an aluminium conductor and a copper shield.

Cross-section of conductor	Diameter of conductor	Insulation thickness	Diameter over insulation	Cross-section of screen	Outer diameter of cable	Cable weight (Al-conductor)	Cable weight (Cu-conductor)	Capacitance	Charging current per phase at 50 Hz	Inductance
mm²	mm	mm	mm	mm²	mm	kg/m	kg/m	µF/km	A/km	mH/km
Table 38										
Three-core cables nominal voltage 20 kV (U_m = 24 kV)										
25	5.8	5.5	18.4	10	47	1.7	2.2	0.15	0.6	0.43
35	7.0	5.5	19.6	16	50	2.0	2.6	0.17	0.6	0.40
50	8.0	5.5	20.6	16	52	2.2	3.2	0.18	0.7	0.39
70	9.6	5.5	22.2	16	56	2.6	3.9	0.20	0.7	0.37
95	11.2	5.5	23.8	25	60	3.1	4.9	0.22	0.8	0.35
120	12.8	5.5	25.2	25	63	3.5	5.8	0.24	0.9	0.33
150	14.2	5.5	26.8	35	67	4.1	6.9	0.26	1.0	0.32
185	15.9	5.5	28.4	35	70	4.7	8.1	0.28	1.0	0.31
240	18.0	5.5	30.7	35	76	5.6	10.1	0.31	1.2	0.30

Cable 2 (54m)
Cable 1 (65m)

fig. 111. XLPE Cable Guide Table chosen as guideline

The geometrical layout and thickness of the layers of the cables used in these simulations is shown in fig. 112.

Cable1	Cable2

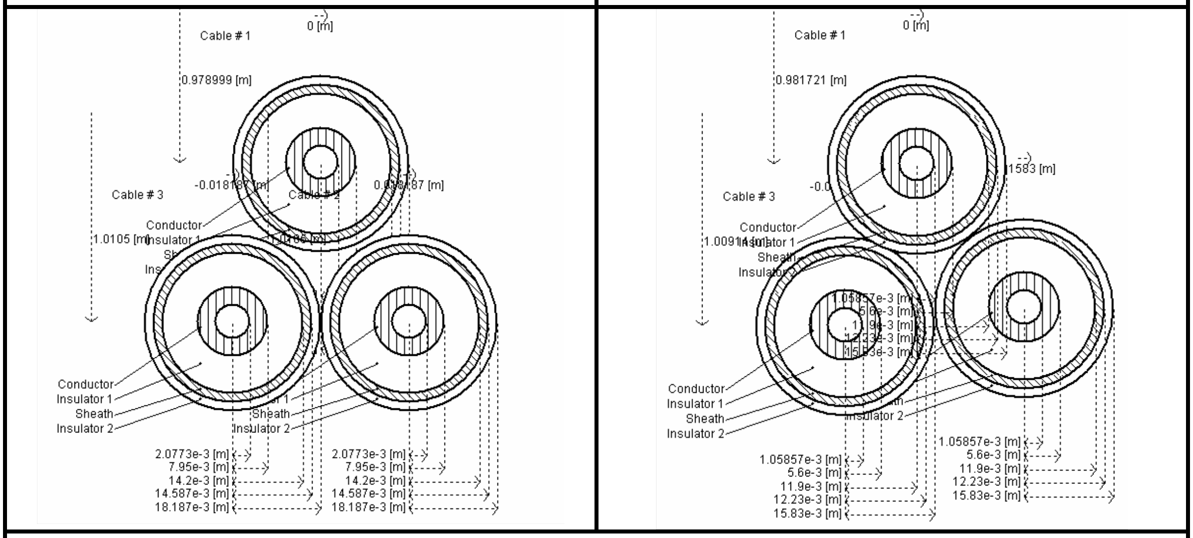

fig. 112. Cable layer diameters and geometrical layout

6.3.2 CB settings

The CB settings are not the same as the ones used to simulate the laboratory experiments. In most of the simulations (unless it is mentioned) the current chopping is not enabled and the withstand capability is a linear curve of 25kV/ms (8 times higher than the slope used for simulating the laboratory experiments). Unfortunately the laboratory experiments showed later that the withstand curve was smaller. This means that precaution must be taken when interpreting the following results: it can be that some simulations do not show any reignition but there might be in reality.

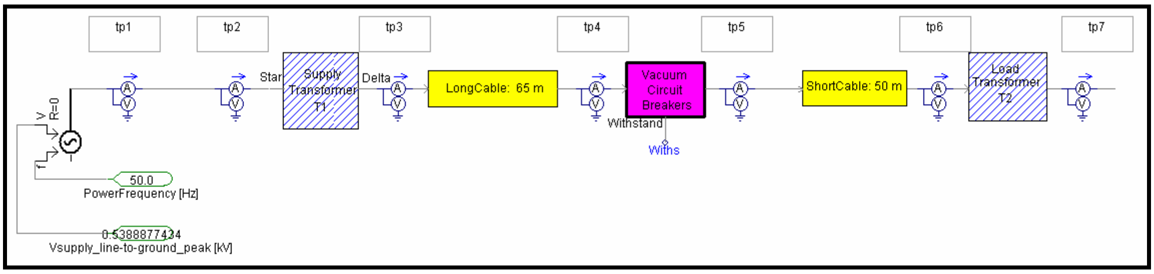

fig. 113. Main simulation file used for the three phase simulations

6.4 CONFIGURATION I

6.4.1 DESCRIPTION

The first configuration, observe fig. 114, is formed by two three phase cables of 65m and 50m length joined by a VCB. The lengths of the cables have been chosen to be the same as the available cables at the moment. The system voltage has been chosen to be 12 kV to meet the ratings of the lab breaker although this specific CB can also work at 33 kV. For this reason, transformers will mostly work in their unsaturated region and saturation need not be modelled. Nevertheless, the influence of saturation has been analysed.

The system is fed by a 1.25 MVA step up transformer and the load by a 1 MVA transformer. Both transformers are Dyn11 connected.

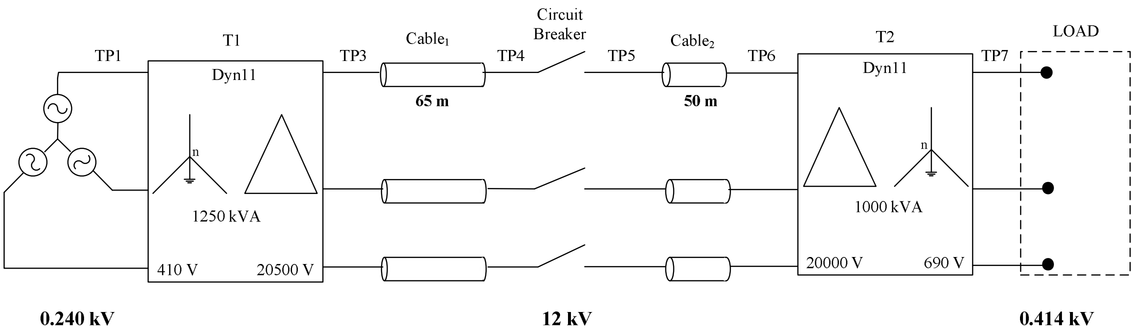

fig. 114. Simulated circuit: Configuration I

6.4.2 ENERGIZING THE TRANSFORMER AT NO LOAD

Fast transient analysis requires various consecutive zooms to observe different phenomena. Choosing the right zoomed shot of these simulations is difficult because at each moment there is a different need and a different time period might be interesting to see. For this reason various zooms are presented to fit various examination needs. Following all the sequence might be tough for the reader.

The voltages and currents in the most relevant points of the system are shown in fig. 115. The first pre-strike occurs in phace c.

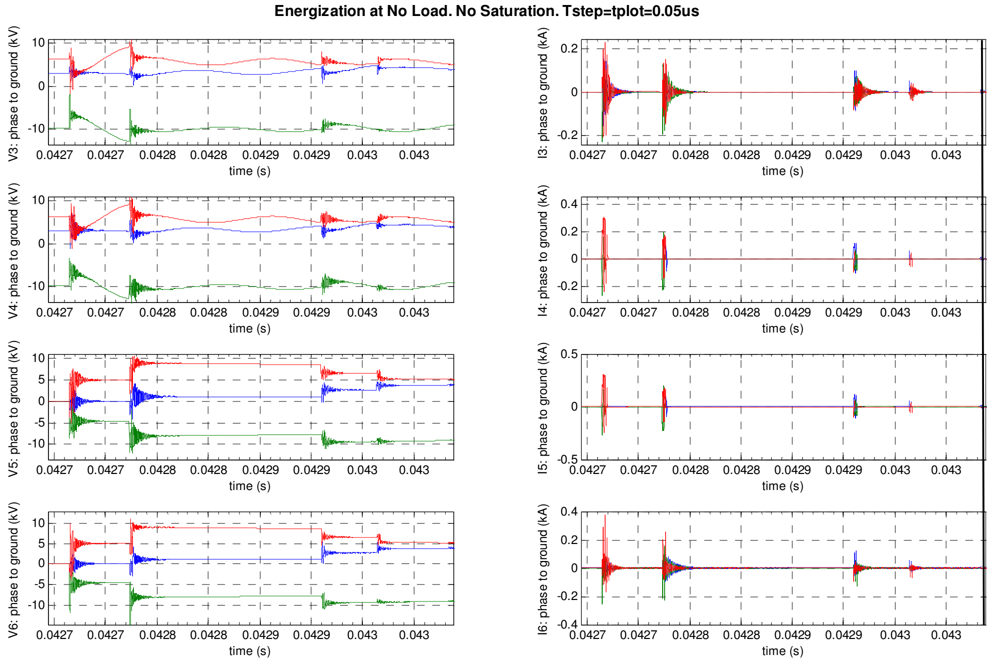

fig. 115. Voltages and Currents in different test points. Energizing at No Load. No Saturation. Tstep=Tplot=0.05µs

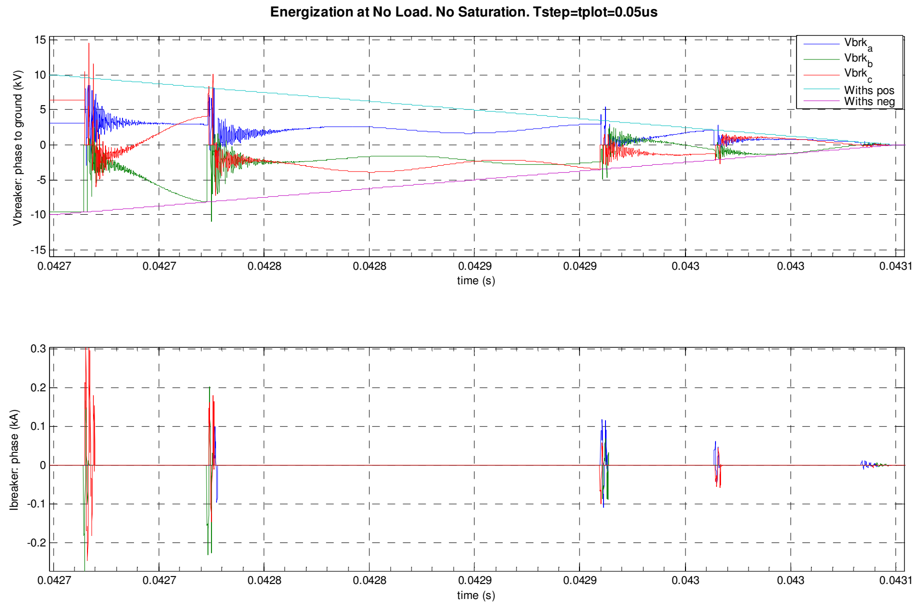

fig. 116. Voltage and Current across the CBs. Energizing at No Load. No Saturation. Tstep=Tplot=0.05µs

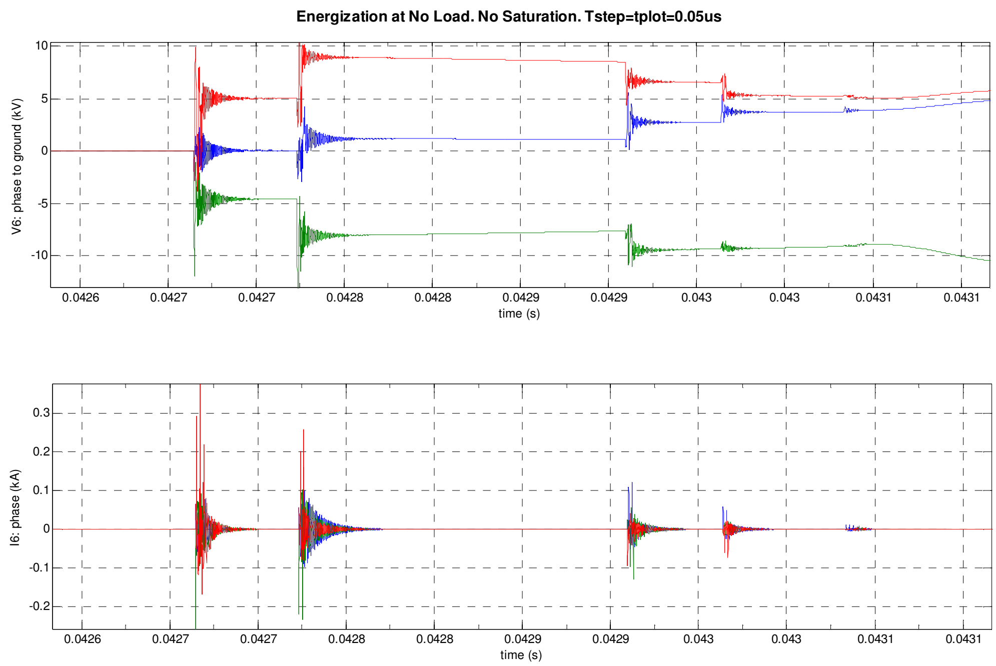

fig. 117. Voltage and Current at point 6. Energizing at No Load. No Saturation. Tstep=Tplot=0.05µs

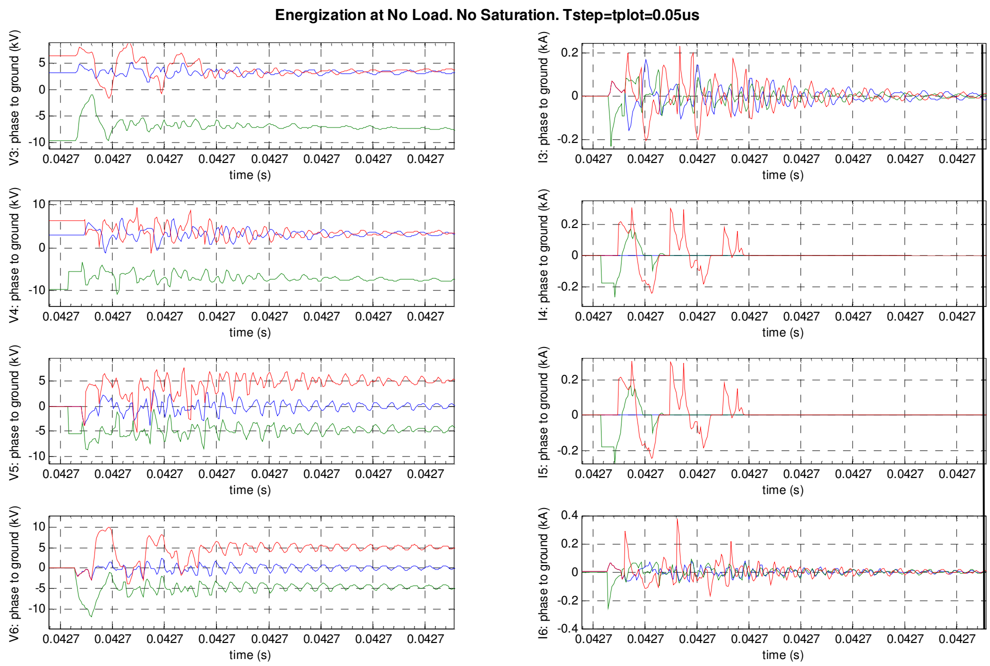

fig. 118. Voltages and Currents in different test points. Energizing at No Load. No Saturation. Tstep=Tplot=0.05µs

When the saturation is enabled the almost identical results are obtained (fig. 119 and fig. 120):

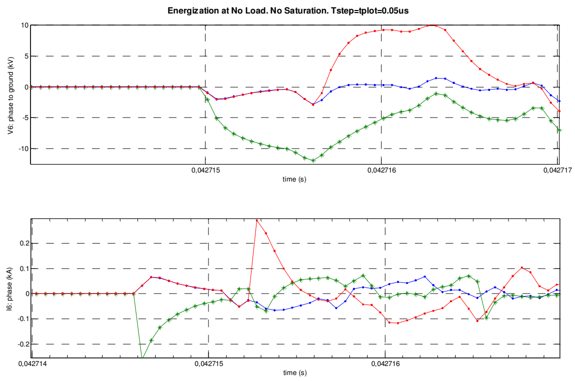

fig. 119. Voltages and Current at point 6. Energizing at No Load. No Saturation. Tstep=Tplot=0.05µs. (V=12kV)

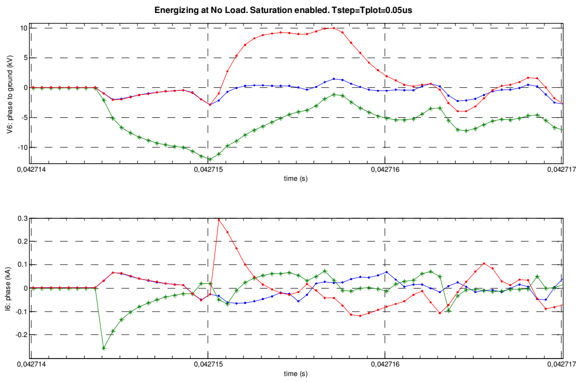

fig. 120. Voltages and Current at point 6. Energizing at No Load. Saturation Enabled. Tstep=Tplot=0.05µs. (V=12kV)

The question is when the saturation does influence the results. In these simulations the supply level is lower than the rated voltage of the transformers. This means that the transformer will work at a lower magnetization level.

The same simulation but using a higher supply voltage level (33kV line to line rms in the breaker side) has been performed both with saturation option enabled and disabled. No noticeable difference has been observed (fig. 121 and fig. 122).

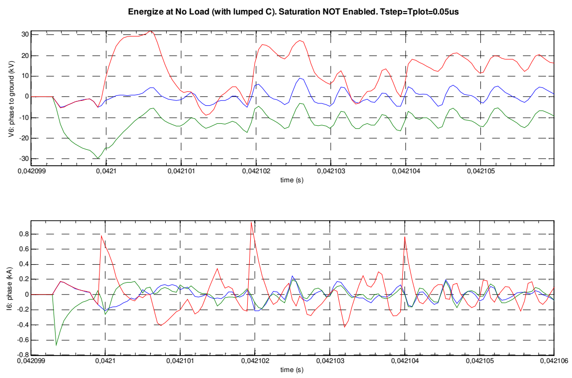

fig. 121. Voltages and Current at point 6. Energizing at No Load. No Saturation. Tstep=Tplot=0.05µs. V=33Kv

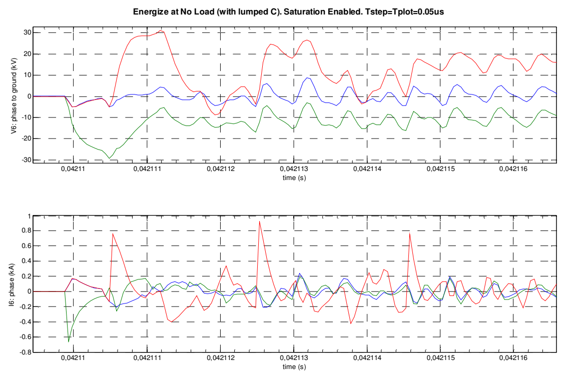

fig. 122. Voltages and Current at point 6. Energizing at No Load. Saturation Enabled. Tstep=Tplot=0.05µs. V=33kV

6.4.3 OPENING

For the opening of the circuit three main options have been studied: breaking at no load, with a load and after a fault. In case of a loaded system an inductive and a resistive load have been analysed.

6.4.3.1 NO LOAD

At no load the current flowing in the circuit is very low (≈ 100 mA). This is mostly due to the large value of the magnetizing inductance which is in the order of a couple hundreds of henrys per phase. It can be observed (fig. 123) that the current follows the voltage 90º behind.

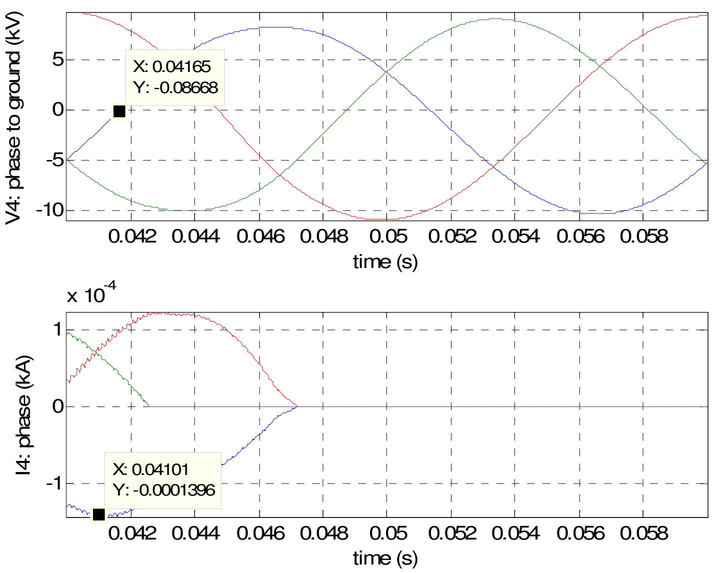

fig. 123. Voltage and current at TP4 when opening at no load

The value of the current can be easily obtained if all the capacitances and inductances of the system are known. The values used in fig. 124 are approximated equivalent values of the capacitances and inductances to ground (observe that the transformers are delta-wye connected).

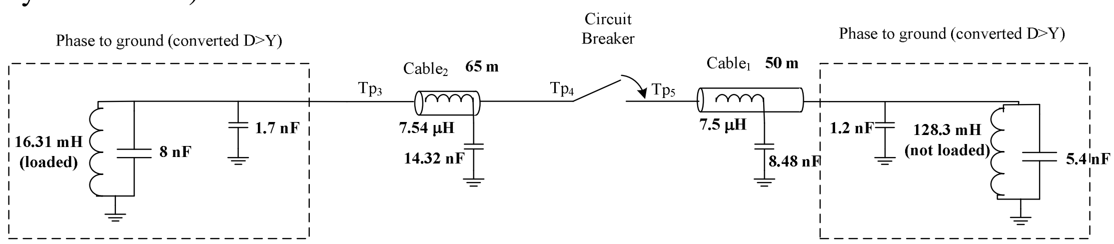

fig. 124. Voltage and current at TP4 when opening at no load

Assuming that C_{eq}=39.13nF, L_{eq}=144.61mH, V=12kV/sqrt(3)= 6.9282 kV and f=50Hz:

$$Z_C = \frac{1}{j\omega C_{eq}} = -j8.1355 \cdot 10^4 \Omega \quad \textbf{(eq. 45)}$$

$$Z_L = j\omega L_{eq} = j4.5431 \cdot 10^4 \Omega \quad \textbf{(eq. 46)}$$

$$Z_{TOT} = Z_C // Z_L = j1.0288 \cdot 10^5 \Omega \quad \textbf{(eq. 47)}$$

$$I_{phase} = \frac{V}{Z_{tot}} = \text{-j}0.0673\ \text{A} \quad \textbf{(eq. 48)}$$

$$I_{line\text{-}to\text{-}line} = I_{phase} \cdot \sqrt{3} = \text{-j}0.1166\ \text{A} \quad \textbf{(eq. 49)}$$

It is reasonable to think that such small current values will not lead to any reignitions because the charge trapped in the systems is too low.

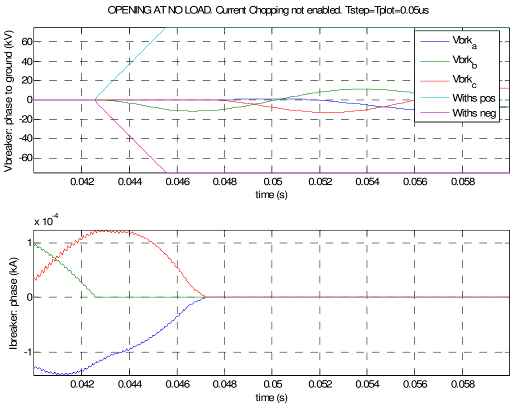

fig. 125. Voltage and current across the breaker when opening at no load (no current chopping enabled)

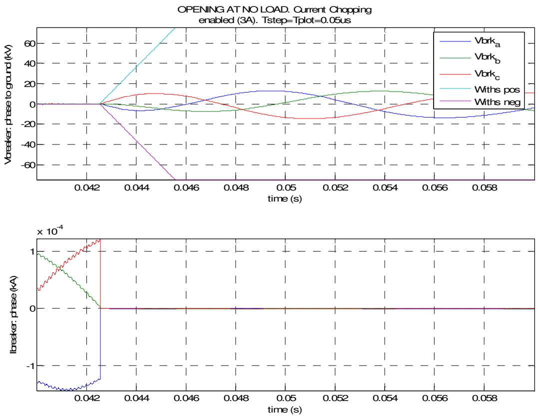

fig. 126. Voltage and current across the breaker when opening at no load (current chopping at 3A)

In this simulation the current chopping has not been considered. However, even if the current chopping is taken into consideration and set to a value of 3A, no reignition is observed (fig. 126). The high withstand curve slope must be also regarded.

6.4.3.2 LOAD

When operating at no load the CB does not produce any reignitions. In order to analyse how loads affects reignitions a resistive and an inductive load have been simulated.

– **Resistive**

The load transformer is rated at 1MVA. If the load is fully resistive it is possible to calculate the value of the resistance the transformer to operate at rated power, all the apparent power will be dissipated as active power. Assuming that the load is star connected:

$$R = \frac{{V_{\text{line-to-line}}}^2}{S_{3\text{ph}}} = \frac{(414\text{V})^2}{1\text{MW}} = 171.4\text{m}\Omega \qquad \textbf{(eq. 50)}$$

After several simulations with different resistor values it has been observed that reignitions appear only when the resistance value is lower than the calculated one for a rated transformer operation at rated power. For values higher than 0.1Ω no reignition is observed. The high value of the withstand curve must be taken into account, if it was slower, then reignitions might be observed.

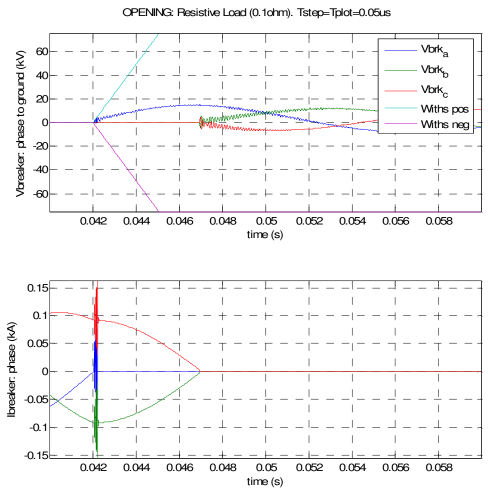

fig. 127. Voltage and current across the breaker when opening a resistive load (0.1Ω)

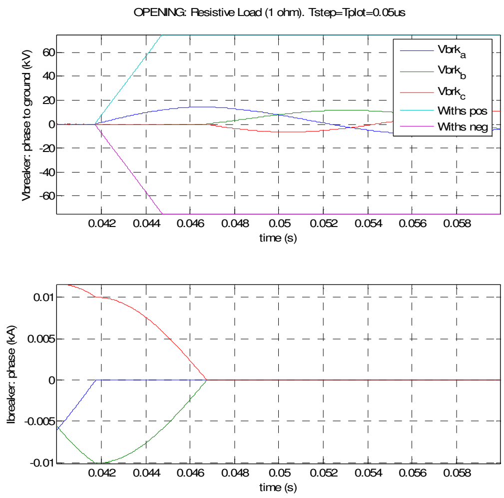

fig. 128. Voltage and current across the breaker when opening a resistive load (1Ω)

The simulation of fig. 127 takes into consideration the current chopping and this can be a reason for observing some almost unnoticeable reignitions.

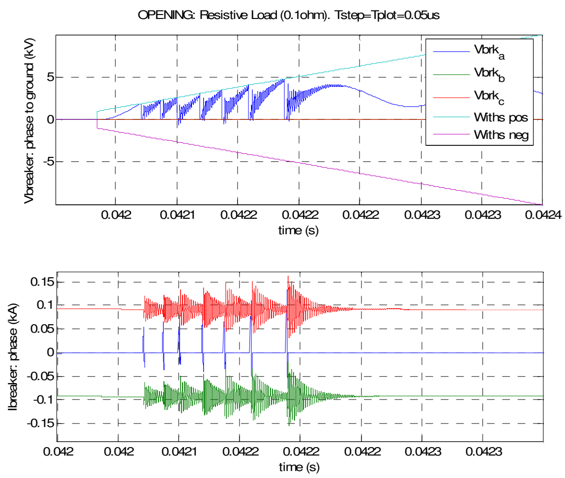

fig. 129. Zoom of voltage and current across the breaker when opening a resistive load (0.1Ω)

– **Inductive**

A 4mH inductance has been used as the inductive load. In order for the load transformer to be working at its maximum power the inductance should be 0.54557mH. Nevertheless, this means that when the inductance value is lower than 4mH the inductive current flowing through the circuit is even higher than the simulated one and the more multiple reignitions appear.

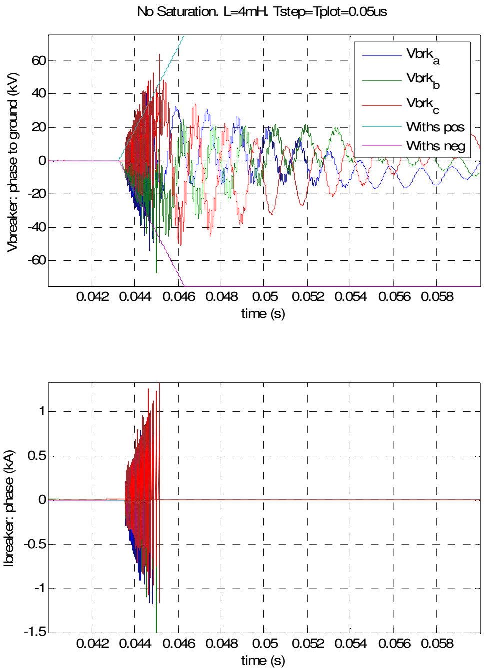

fig. 130. Opening and inductive circuit L=4mH. Saturation Not Enabled

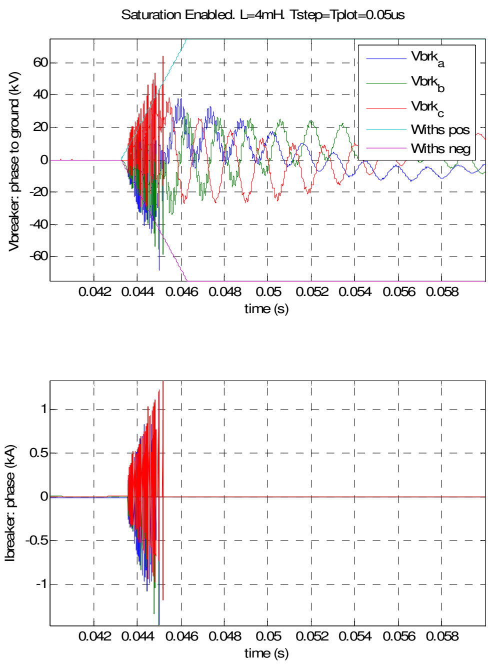

fig. 131. Opening and inductive circuit L=4mH. Saturation Enabled

Two cases have been simulated to analyse the influence of modelling the saturation of the iron core of the transformers. A slight difference has been observed where the model in which the saturation has not been taken into consideration shows a worse behaviour in what reignitions refers.

6.4.3.3 FAULTS

The short circuits have been simulated using a mainly inductive load with a small percentage of resistance: R_{load}=100 mΩ and L_{load}= 4 mH. It is believed that the type of load used does not change the intensity of the fault, and therefore does not affect the reignitions. However, if voltage dips or other effects were to be studied the load must be regarded.

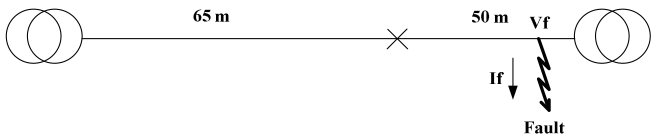

fig. 132. Fault happening in the low voltage side of the load transformer

When simulating short circuits one of the questions that arise is how to model the short circuit. In PSCAD short circuits are modelled by means of a constant value resistance to ground although in reality this resistance will vary.

PSCAD uses a default resistance value of 10mΩ. Different values of resistances have been simulated and it has been observed that the value affects the damping of the fault current: the larger the resistance the faster it attenuates. The following figures (fig. 133 and fig. 134) show the damping difference between two fault resistance values in a SLG fault type.

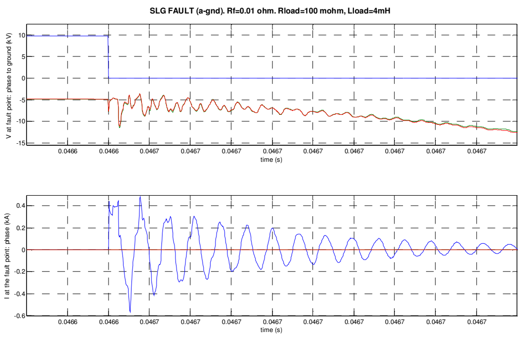

fig. 133. Voltage and Current at the fault (pt 6). Rf=1Ω

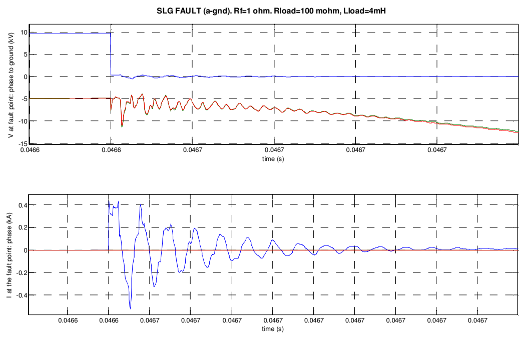

fig. 134. Voltage and Current at the fault (pt 6). Rf=10mΩ

– **SLG (Single Line to Ground fault)**

The following graphs show the voltage and current at the fault point when a SLG fault happens. The fault point has been chosen to be the high voltage side of the load transformer and the fault resistance has been set to 10mΩ.

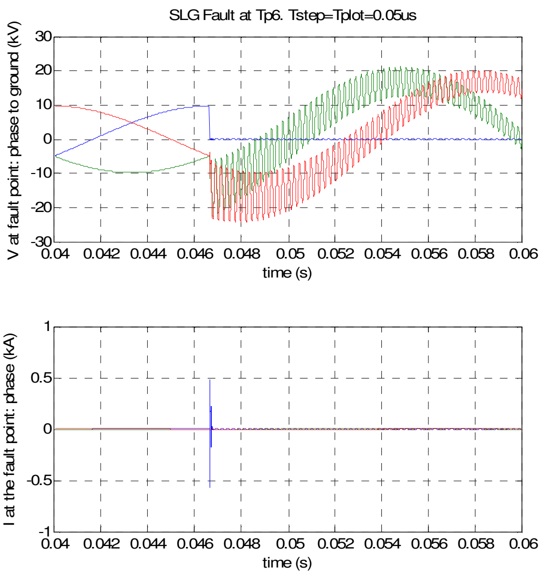

fig. 135. Voltage and Current at the fault (pt 6). Rf=10mΩ

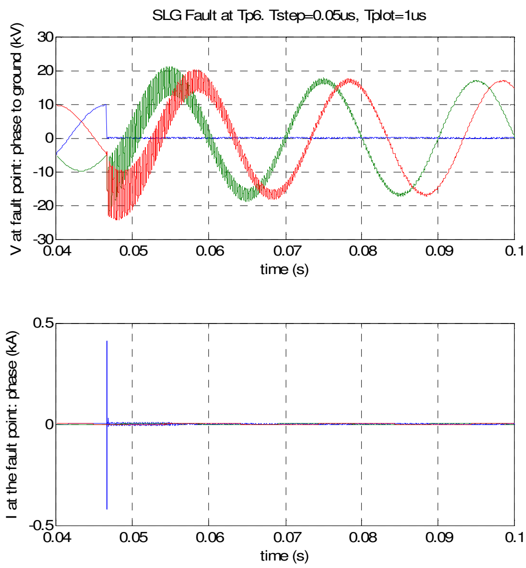

fig. 136. Voltage and Current at the fault (pt 6). Rf=10mΩ

The first current peak is approximately 400-600A and takes ≈70µs to attenuate the initial fault current.

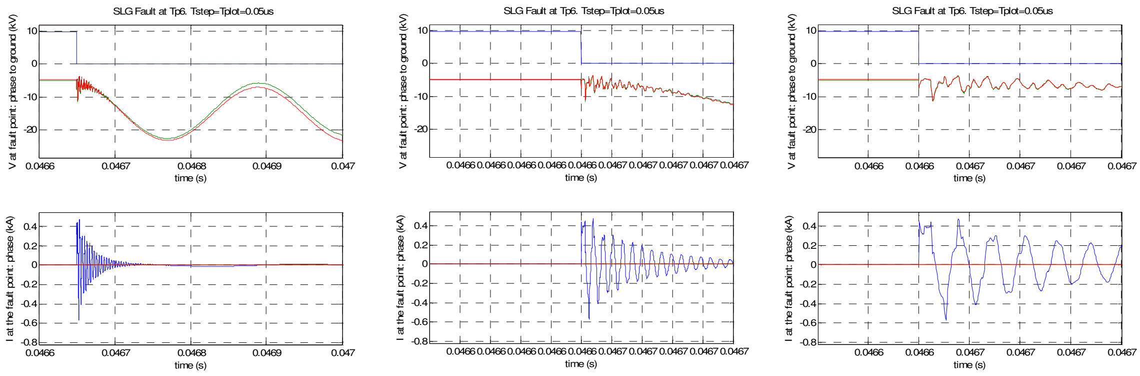

fig. 137. Voltage and Current at the fault (pt 6). Rf=10mΩ

The effects of breaking a fault are different depending on the moment in which the breaker opens. For this reason, different opening times have been studied.

Break Point 1 (t_{open}=0.046653 s): Opening just after the first current peak (before a current zero crossing)

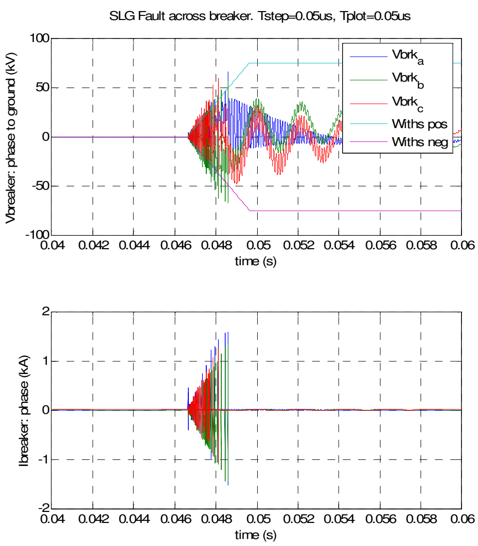

fig. 138. Voltage and Current across the breaker. Break Point 1

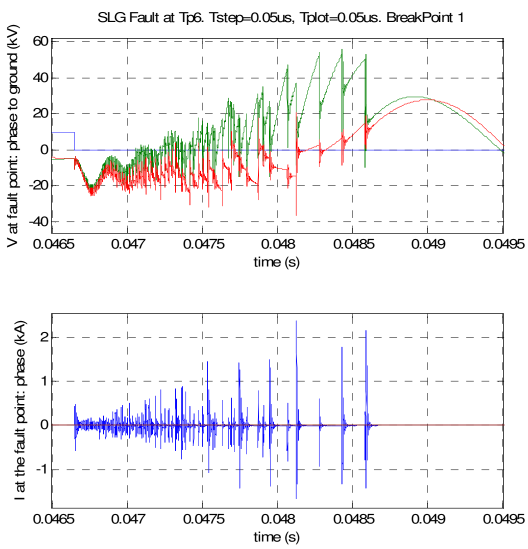

fig. 139. Voltage and Current at the fault. Break Point 1

Break Point 2 (t_{open}=0.046669 s):

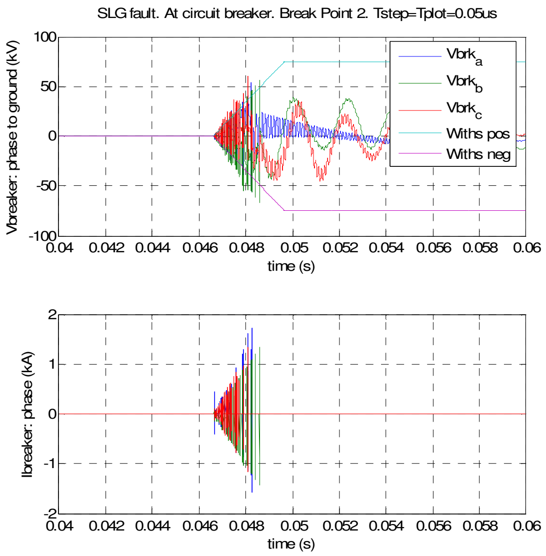

fig. 140. Voltage and Current across the breaker. Break Point 2

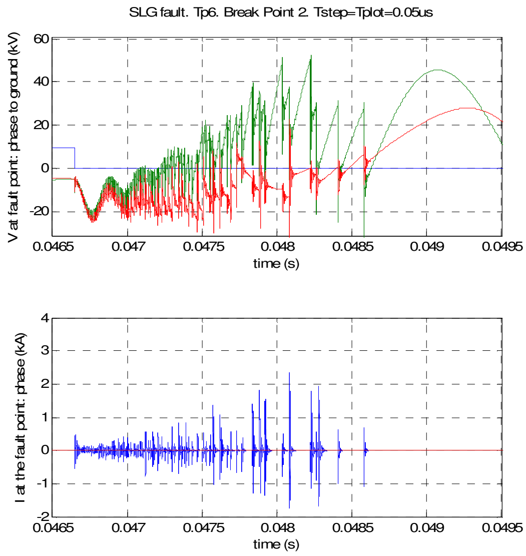

fig. 141. Voltage and Current at the fault. Break Point 2

Break Point 3 (t_{open}=0.047023 s):

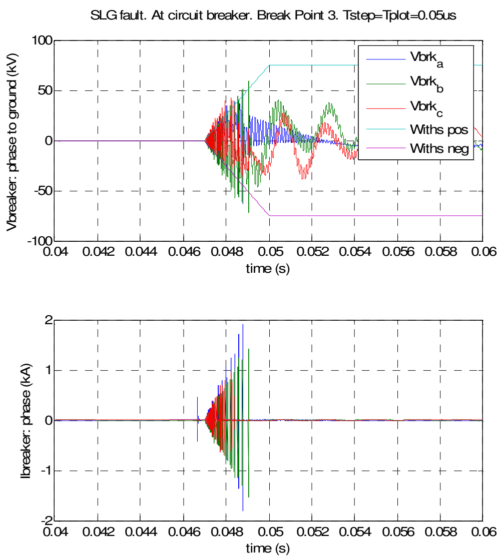

fig. 142. Voltage and Current across the breaker. Break Point 3

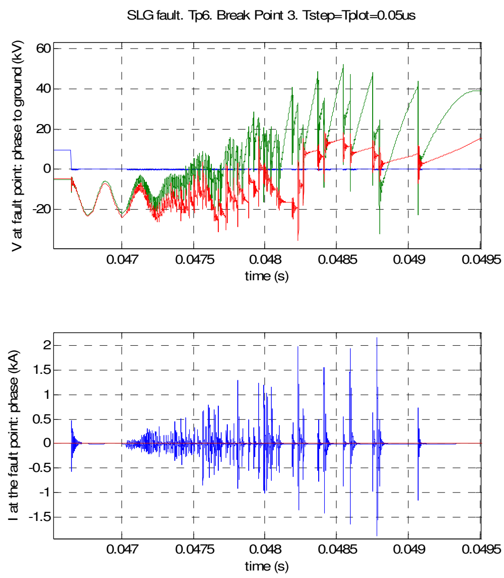

Fig. 143. Voltage and Current at the fault. Break Point 3

Break Point 4 (t_{open}=0.049710 s):

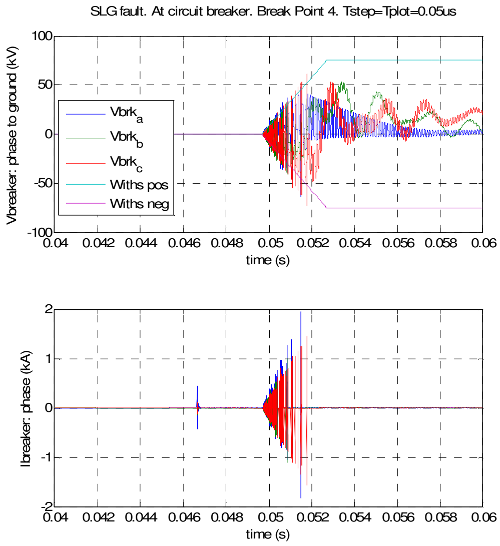

fig. 144. Voltage and Current across the breaker. Break Point 4

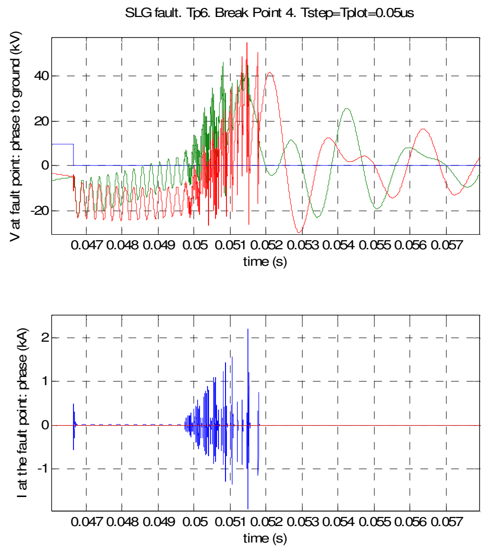

fig. 145. Voltage and Current at the fault. Break Point 4

Break Point 5 (t_{open}=0.056574 s):

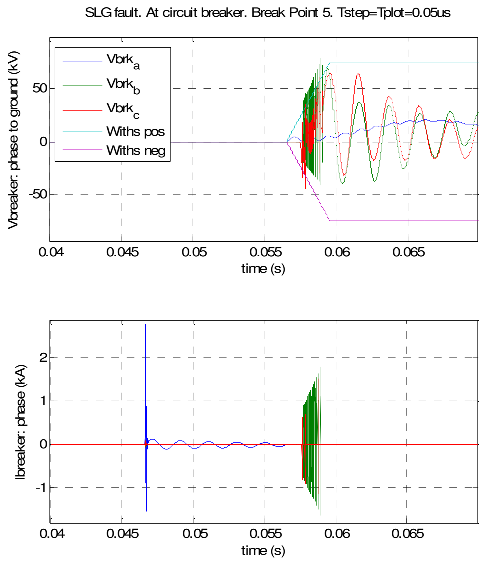

fig. 146. Voltage and Current across the breaker. Break Point 5

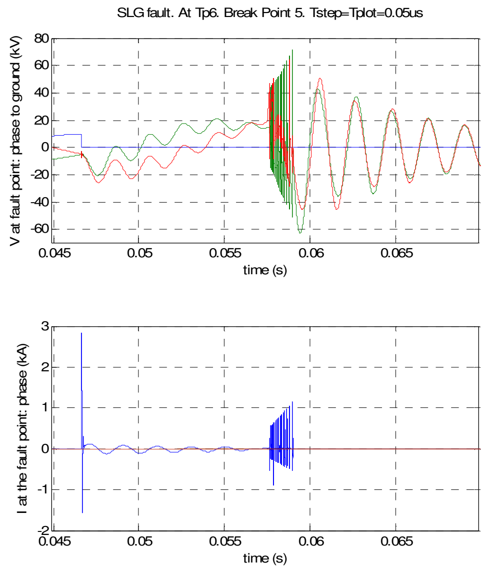

fig. 147. Voltage and Current at the fault. Break Point 5

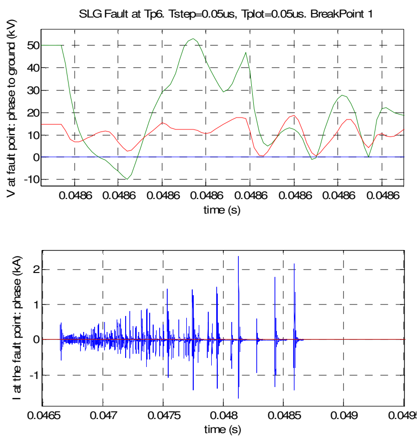

fig. 148. Voltage and Current at fault. Break Point 1

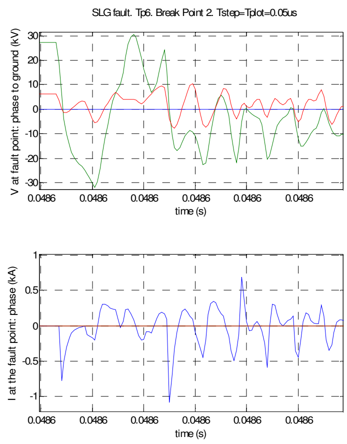

fig. 149. Voltage and Current at fault. Break Point 2

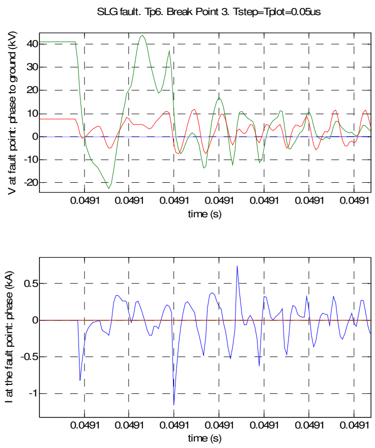

fig. 150. Voltage and Current at fault. Break Point 3

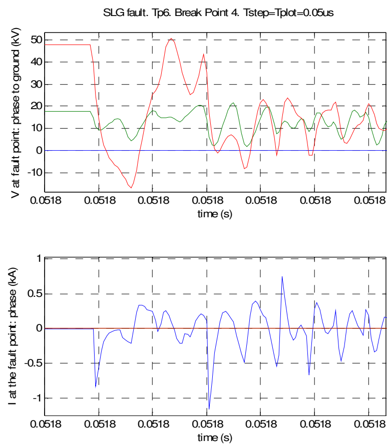

fig. 151. Voltage and Current at fault. Break Point 4

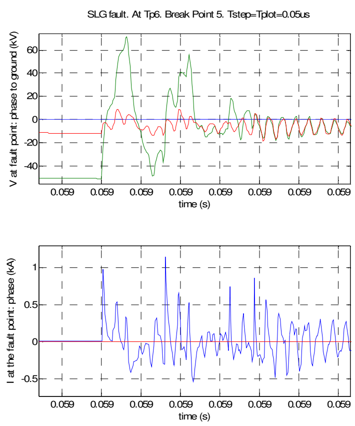

fig. 152. Voltage and Current at fault. Break Point 5

The five figures above show a zoom of the voltages at the fault location where it is observed that all the time derivatives and amplitudes are approximately the same:

Break point 1:

[53.1789-(-9.8493)] kV/0.75µs=63.02 kV/0.75µs=84.03 kV/µs

Break point 2:

[30.5446-(-31.7939)] kV/0.75µs=62.33 kV/0.75µs=83.11 kV/µs
Break point 3:
[43.7935-(-20.9854)] kV/0.8µs=64.67 kV/0.8µs=80.97 kV/µs
Break point 4:
[50.64-(-16.76)] kV/0.75µs =67.40 kV/0.75µs=89.87kV/µs
Break point 5:
[70-(-50)] kV/ 1.35µs =120 kV/1.35µs=89.05kV/µs

This means that the point where the breaker is opened does not affect very much the rise time of the voltage at the fault location but it does affect the magnitude (observe that the magnitude at break point 5 is doubled).

– **2Ph (Two Phase fault)**

When a two phase fault happens, the following graphs are obtained:

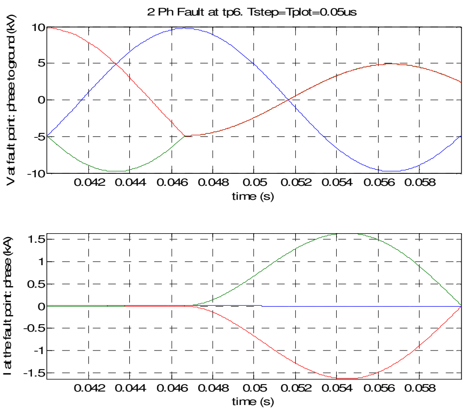

fig. 153. Voltage and Current at the fault

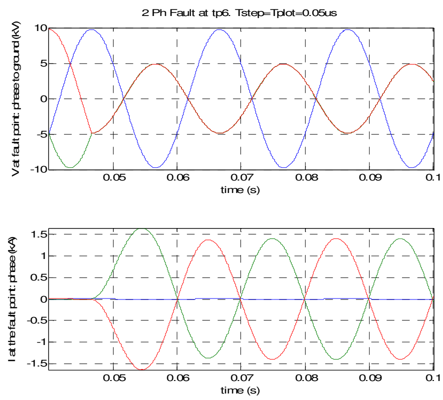

fig. 154. Voltage and Current at the fault

The worst point to open the fault is just before the current zero crossing (break point 1). However, an opening at the current peak (break point 2) will also be performed.

Break Point 1 (t_{open}=0.06002s: before the current zero):

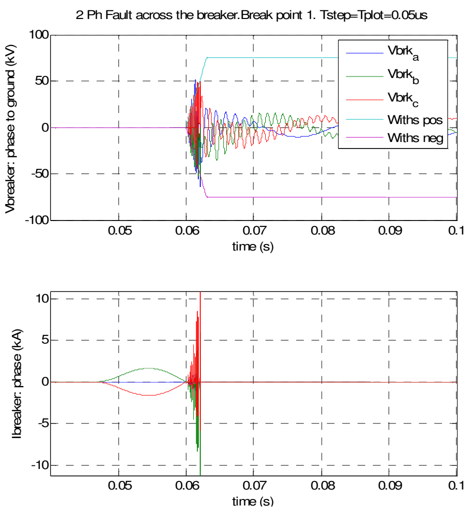

fig. 155. Voltage and Current across the breaker when opening at break point 1

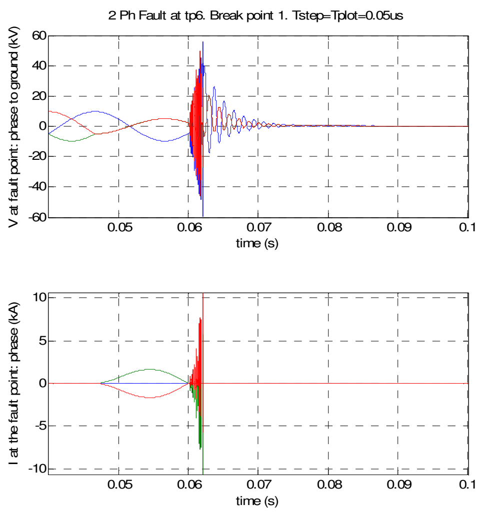

fig. 156. Voltage and Current at tp6 when opening at break point 1

Break Point 2 (t_{open}=0.0545s: at the current peak):

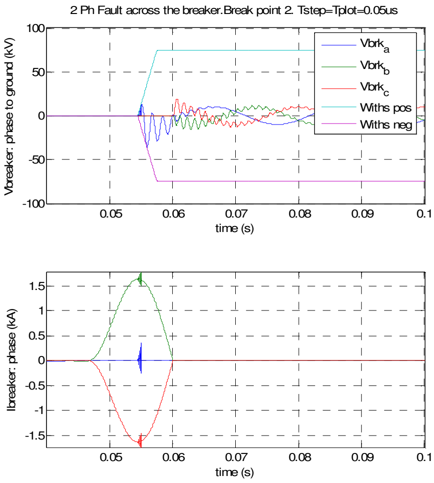

fig. 157. Voltage and Current across the breaker when opening at break point 2

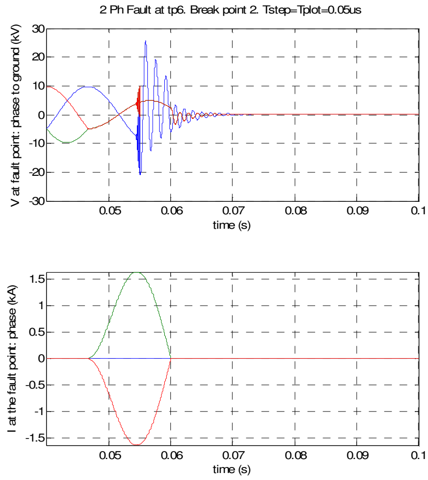

fig. 158. Voltage and Current at tp6 when opening at break point 2

The next figures show a comparison between the voltages at the fault location when breaking at point 1 or 2. The voltage rise is steeper when breaking just before the current zero crossing as it can be seen in the figures.

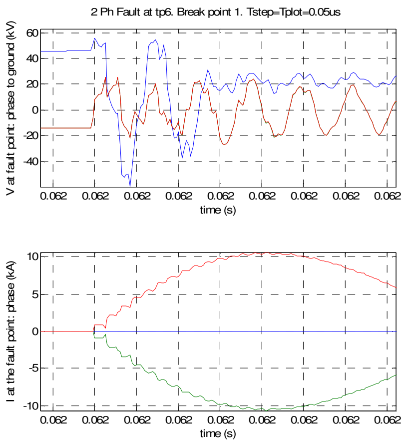

fig. 159. Voltage and Current at fault when opening at break point 1

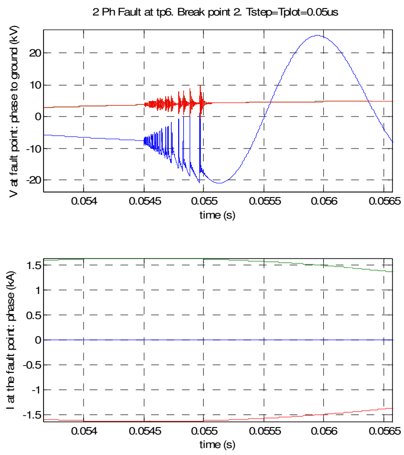

fig. 160. Voltage and Current at fault when opening at break point 2

Break point 1:
[54.7830-(-59.4016)] kV/1.2μs=114.1846 kV/1.2μs=95.15 kV/μs
Break point 2:
[3.1673-(-20.9140)] kV/1.2μs=24.0813 kV/1.2μs=20.07 kV/μs

– **3Ph (Three Phase fault)**

When a three phase fault happens, the following graphs are obtained:

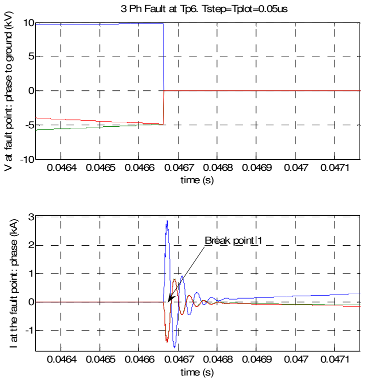

fig. 161. Voltage and Current at the fault

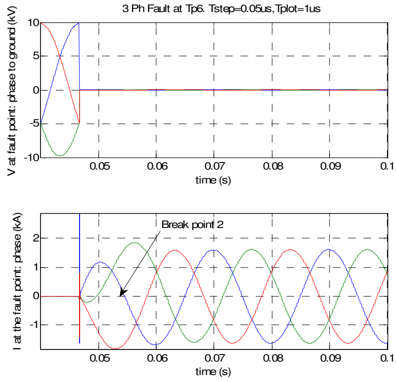

fig. 162. Voltage and Current at the fault

Break Point 1 (t_{open}=0.046682s):

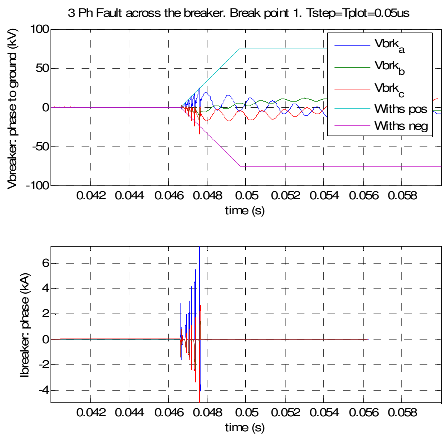

fig. 163. Voltage and Current across the breaker when opening at break point 1

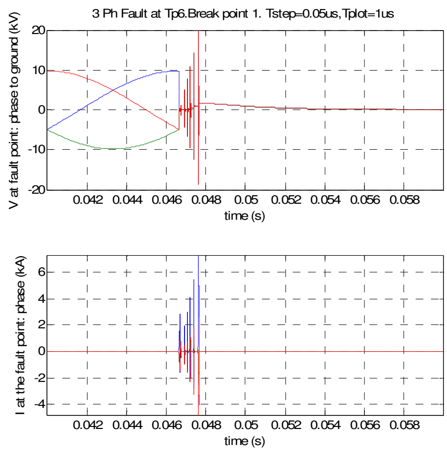

fig. 164. Voltage and Current at tp6 when opening at break point 1

Break Point 2 (t_{open}=0.054504s):

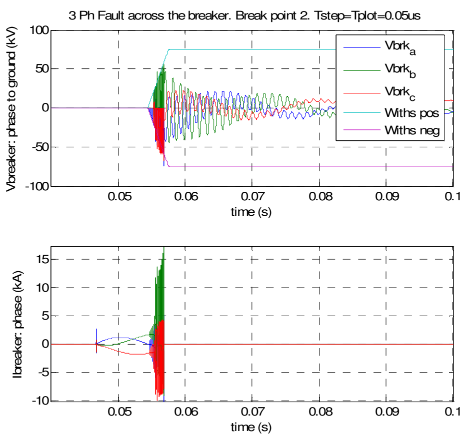

fig. 165. Voltage and Current across the breaker when opening at break point 2

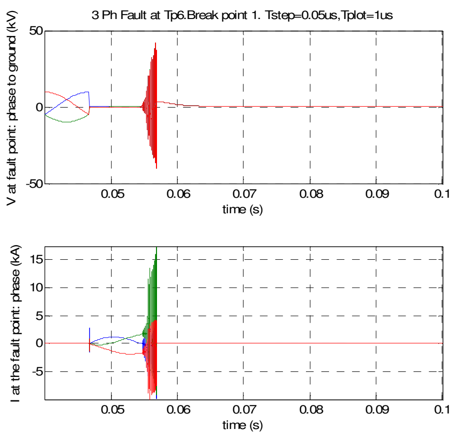

fig. 166. Voltage and Current at tp6 when opening at break point 2

The worst results are obtained when breaking at point 2. The steepness of the voltage at the fault is doubled.

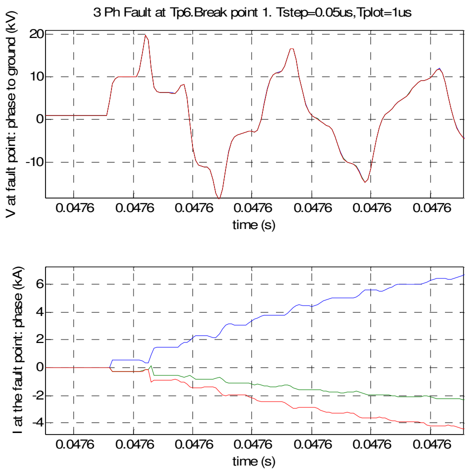

fig. 167. Voltage and Current at fault when opening at break point 1

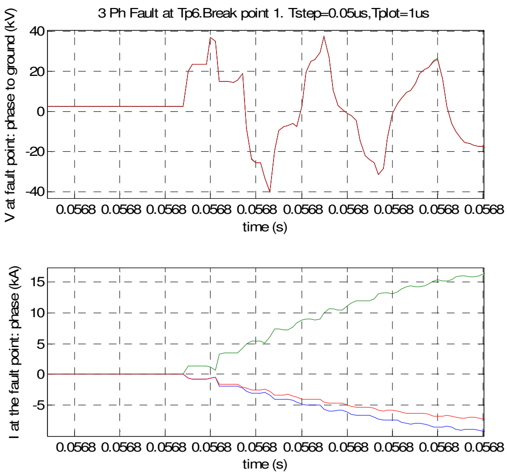

fig. 168. Voltage and Current at fault when opening at break point 2

Break point 1:
[19.7736-(-17.2211)] kV/1.2μs=36.9947kV/1.2μs=30.83 kV/μs
Break point 2:
[37.4380-(-40.2971)] kV/1.2μs=77.7350 kV/1.2μs=64.78 kV/μs

– **2Ph-gnd (Two Phase to Ground fault)**

When a two phase to ground fault happens, the following graphs are obtained:

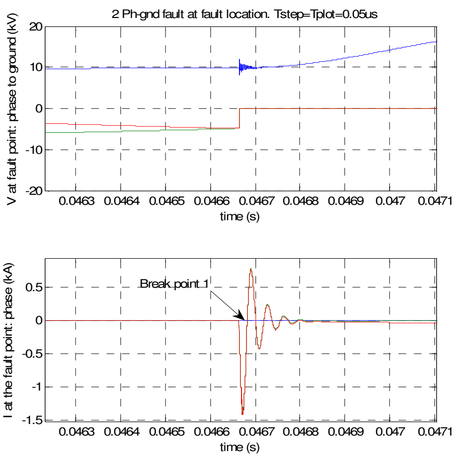

fig. 169. Voltage and Current at the fault

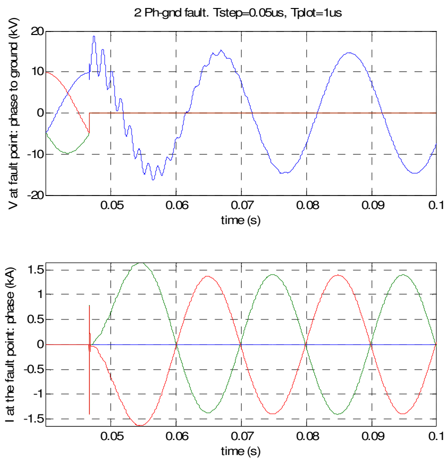

fig. 170. Voltage and Current at the fault

Break Point 1 (t_{open}=0.046682s):

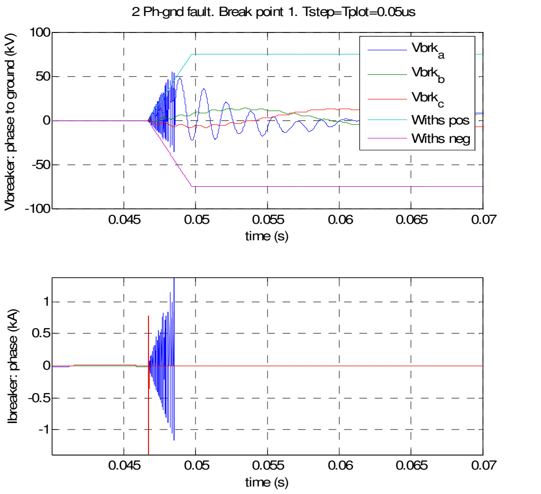

fig. 171. Voltage and Current across the breaker when opening at break point 1

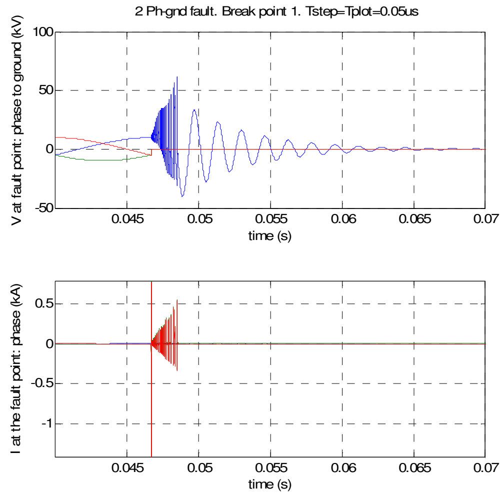

fig. 172. Voltage and Current at tp6 when opening at break point 1

Break Point 2 (t_{open}=0.054611s):

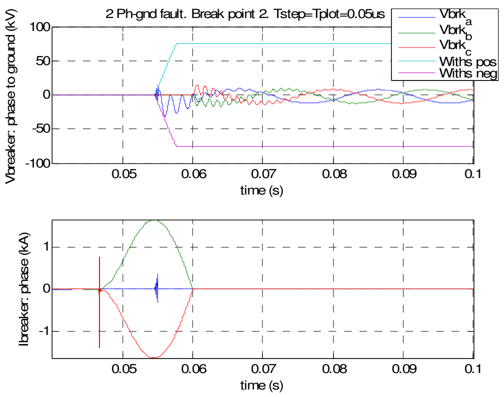

fig. 173. Voltage and Current across the breaker when opening at break point 2

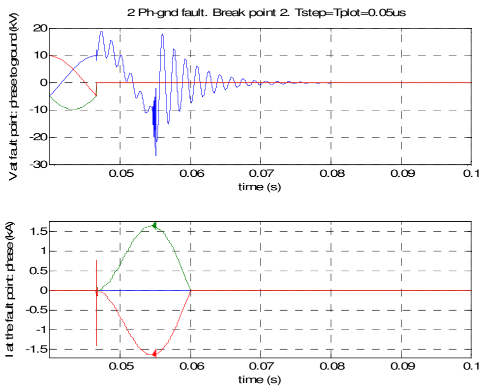

fig. 174. Voltage and Current at tp6 when opening at break point 2

Break Point 3 (t_{open}=0.059818s):

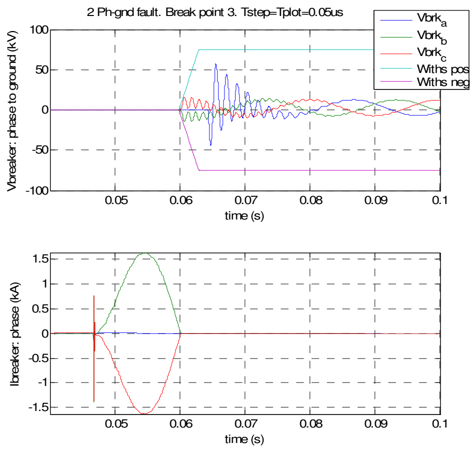

fig. 175. Voltage and Current across the breaker when opening at break point 3

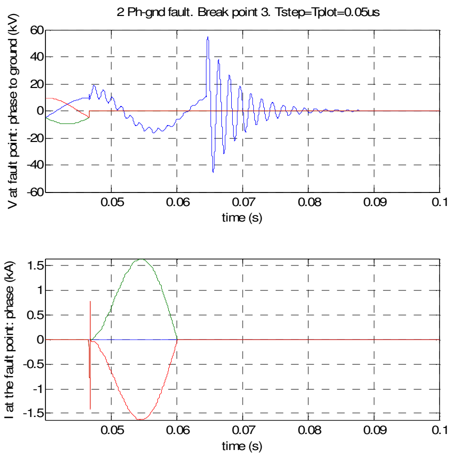

fig. 176. Voltage and Current at tp6 when opening at break point 3

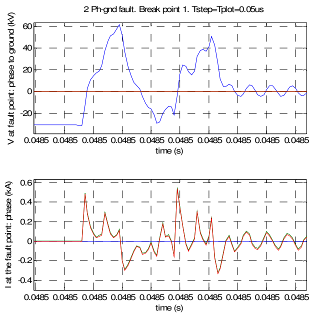

fig. 177. Voltage and Current at tp6 when opening at break point 1

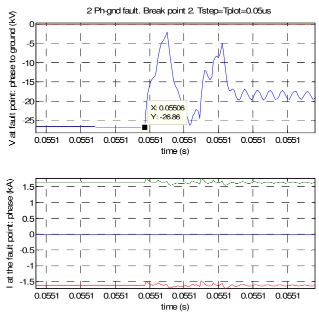

fig. 178**. Voltage and Current at tp6 when opening at break point 2**

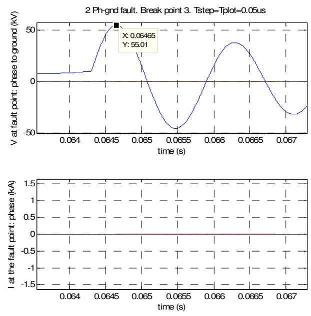

fig. 179**. Voltage and Current at tp6 when opening at break point 3**

Break point 1:
[19.7736-(-17.2211)] kV/1.2µs=36.9947kV/1.2µs=30.83 kV/µs
Break point 2:
[-2.1100-(- 26.8572)] kV/1.3µs= 24.7472 kV/1.3µs=19.04 kV/µs
Break point 3:
[-45.4584-(+55.0072)] kV/ 814.90µs=100.4655 kV/814.90µs =0.12329 kV/µs

The steepest voltage is at break point 1 but the highest overvoltage is found at break point 3.

– **3Ph-gnd (Three Phase to Ground fault)**

When a three phase to ground fault happens, the following graphs are obtained:

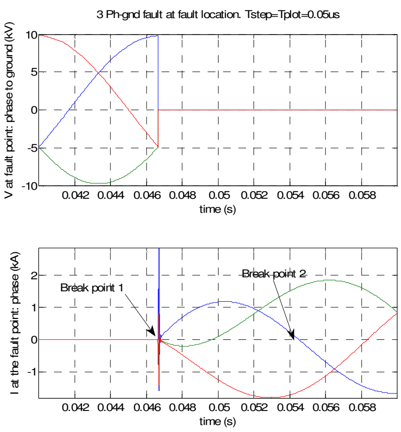

fig. 180. Voltage and Current at the fault

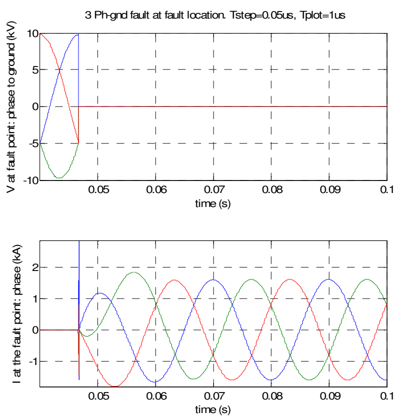

fig. 181. Voltage and Current at the fault

Break Point 1 (t_{open}=0.046682s):

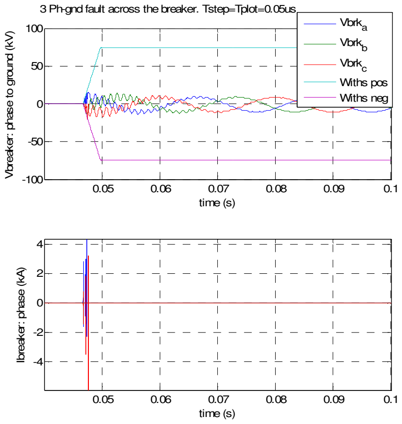

fig. 182. Voltage and Current across the breaker when opening at break point 1

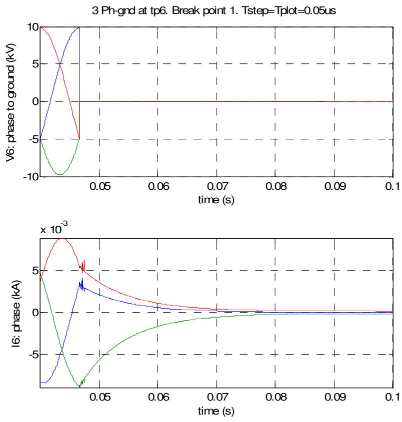

fig. 183. Voltage and Current at tp6 when opening at break point 1

Break Point 2 (t_{open}=0.0545049s):

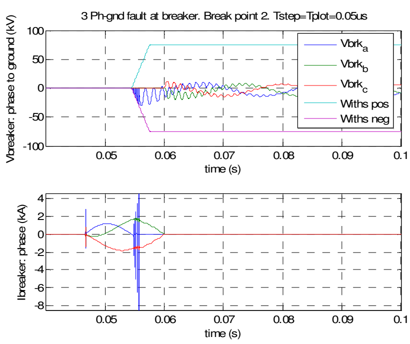

fig. 184. Voltage and Current across the breaker when opening at break point 2

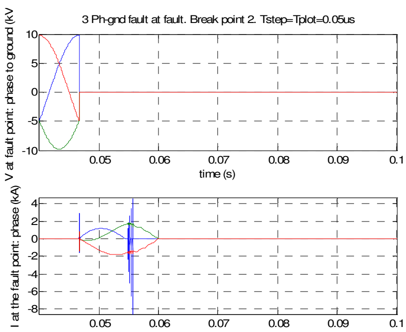

fig. 185. Voltage and Current at tp6 when opening at break point 2

In both cases the reignitions are not numerous and they are more evident when breaking at point 2. However, the voltage is instantaneously made zero (10 kV/ 0.1µs=100 kV), which gives a very high and dangerous voltage change rate.

6.4.4 CONCLUSIONS

The following conclusions have been derived:

- The chosen length of the cables in the simulations does not correspond to the real lengths of the cables that are laid in the seabed. The actual lengths should be around 660m for the inter-turbine distance and 80m for the nacelle tower. This means that the simulations should show a worse scenario than the real windpark since the simulated lengths are shorter. Thus, shorter cables produce faster propagating waves and therefore, more frequent reflections.
- The simulated configuration (Configuration I) does not represent a real branch of a collection grid because the influence of the surrounding cables is not taken into account. Configuration II gives an alternative way of modelling the charged cables that form the rest of the distribution grid by means of a capacitor.
- At high frequencies modelling the saturation of the iron core is not relevant and can be skipped. However, the PSCAD model incorporates this option and it is rather simple to use. The effect of saturation would be more evident if the

voltage level would be higher than the rated voltage of the transformers but the simulation voltage is much lower than the rated value and as a consequence the transformer core works in its linear region.

- Energizing the transformer always produces pre-strikes even if it is performed at no-load. It is due to the fact that energizing is a sudden energy transfer. The shapes of the first travelling waves have been analysed (section 3.6) in order to see the reflection and refraction of the waves.
- No reignitions have been observed when opening at no load. At no load the current flowing through the circuit is very small in magnitude and it is mainly inductive. Even if the current chopping is enabled no reignitions are seen. It must also be mentioned that this simulations have been performed assuming a withstand curve 8 times steeper than the one observed experimentally. This means that care must be taken when interpreting these simulations. The same applies for the opening of the resistive load, where no reignitions have been observed in most of the cases.
- When opening the circuit with a resistive load it is very unusual to observe reignitions. Only if the resistance has a very small value and the current chopping is enabled little reignitions can be viewed.
- If the load is inductive reignitions are assured almost everytime. Only when the inductance takes a large value reignitions are not perceived.
- The insulation of an electrical apparatus is damaged when either the voltage magnitude or rate of rise across its terminals is exceeded. For this reason these two factors must be analysed when breaking a fault.
- The instant in which the fault is cleared it is relevant as far as reignitions and voltage rate of rise are concerned. It has been observed that SLG (Single Line to Ground) faults are the ones that are most sensitive and the reignition number is very high independently of when is the breaker opened. For the rest of fault types the reignitions can be as considerable as in the SGL case if the fault is broken just before a current zero crossing. However, in the most of the cases the reignitions are not so severe.

6.5 CONFIGURATION II

6.5.1 DESCRIPTION

The second configuration (fig. 188) is identical to the first configuration except for a lumped capacitor that has been added at the high voltage side of the supply transformer. The duty of this capacitor is to simulate the effect of the cables of the adjacent grid and its value has been set to C_{lumped}=2μs because the feeder capacitance is estimated to be in the range of 2-3μs, see fig. 186.

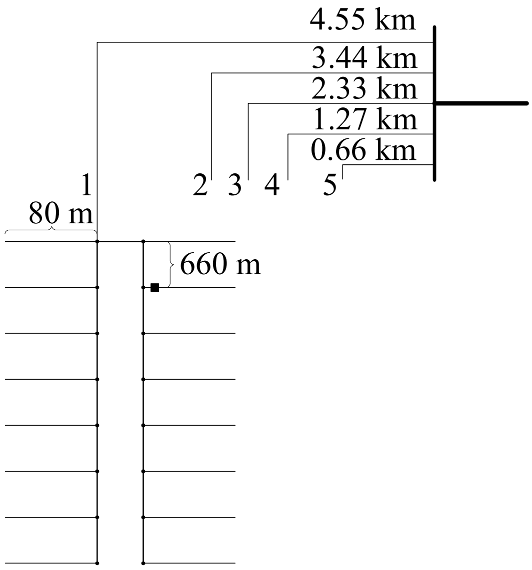

fig. 186. Schematic view of the cable distribution of the windpark under study

If it is assumed that the interturbine length is 660m and the length of the tower from the bottom of the sea to the nacelle is 80m, and if the capacitance per unit length of the cables is presumed to be ≈ 200 pF/m, the equivalent capacitances can be calculated.

$$l_{TT} = 660m$$

$$l_{WT} = 80m$$

$$l_{seen\_at\_bottom\_of\_WT} = \left[\sum_{1}^{15} l_{TT} + \sum_{1}^{15} l_{WT}\right] + l_{feeder}$$

$$\left[\sum_{1}^{15} l_{TT} + \sum_{1}^{15} l_{WT}\right] = 15 \cdot 660m + 15 \cdot 80m = 11.1km$$

table 16. Lengths and equivalent lumped capacitances of the windpark cables

Feeder number	Length (km)	Equivalent Capacitance (µF)
1	**11.1 + 4.55 = 15.65**	**3.130**
2	**11.1 + 3.44 = 14.54**	**2.908**
3	**11.1 + 2.33 = 13.43**	**2.686**
4	**11.1 + 1.27 = 12.37**	**2.474**
5	**11.1 + 0.66 = 11.76**	**2.352**

However, it must be mentioned that the lumped capacitance does not exactly behave as a long charged cable. While the cable provides a step shaped current (a sudden shot of charges) the capacitor gives a current with a first order function profile. This difference must be borne in mind. Fig. 187 shows the difference between charging a line from a charged cable or from a capacitor (observe Vload2 of the left graph and Vload of the right graph).

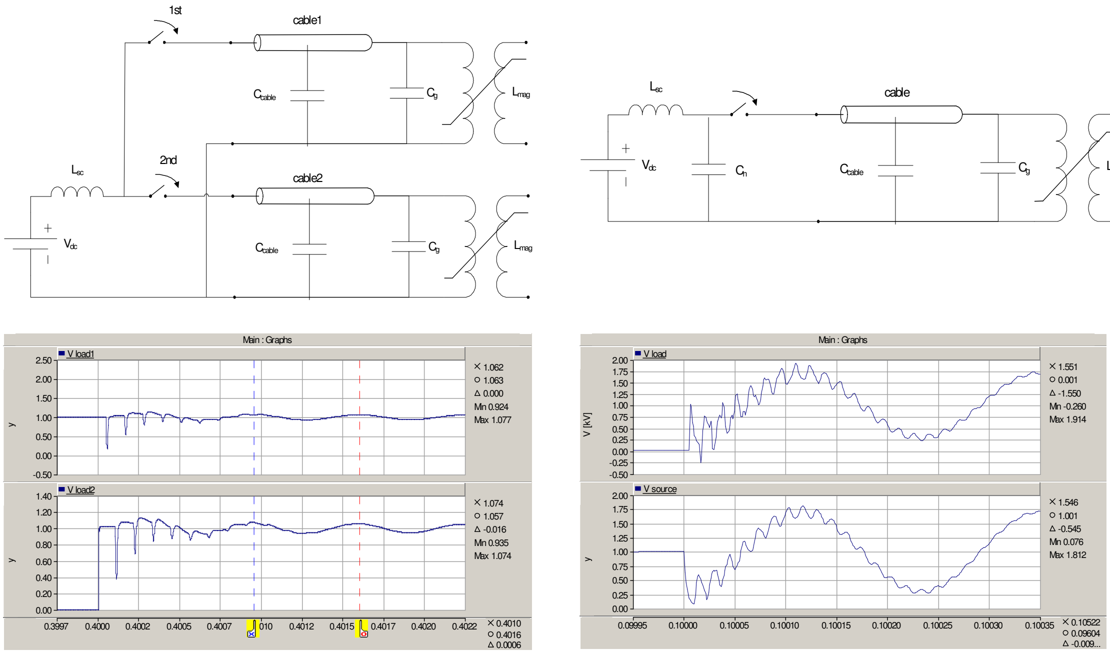

fig. 187. Charging of the line by a cable (left) and by a lumped capacitor (right)

In the cable charged case, the voltage front increases immediately while in the capacitor case the very first voltage increase is not instantaneous. The greater voltage oscillations in the second case must not be regarded because the length of the cable and the capacitor value has been chosen quite randomly and are not equivalent. The oscillations are due to resonance in the circuit.

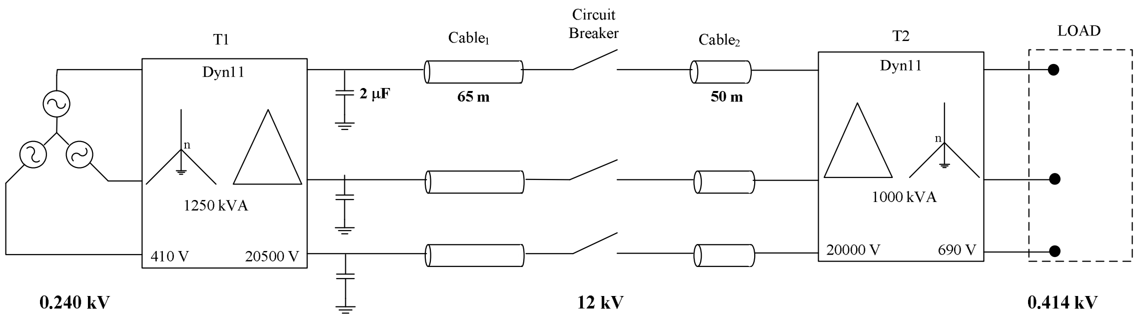

fig. 188. Simulated circuit: Configuration II

6.5.2 OPERATIONS

6.5.2.1 ENERGIZING

The energizing is performed at no load. The importance of saturation has been analysed at two different voltage levels: 12 kV and 33 kV but modelling the saturation seems not to have any effect at high frequencies. However, saturation is always enabled in the following simulations because at lower frequencies it does have any larger influence.

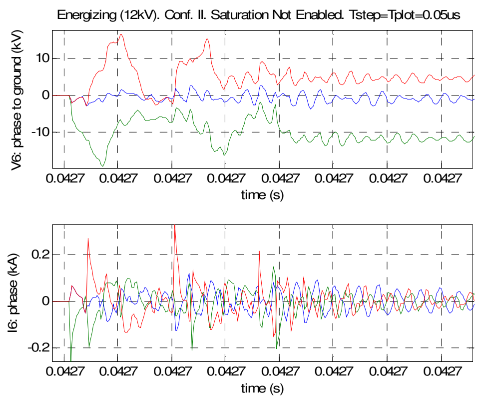

fig. 189. Voltage and Current at tp6 when energizing at no load (12 kV). Saturation not modelled

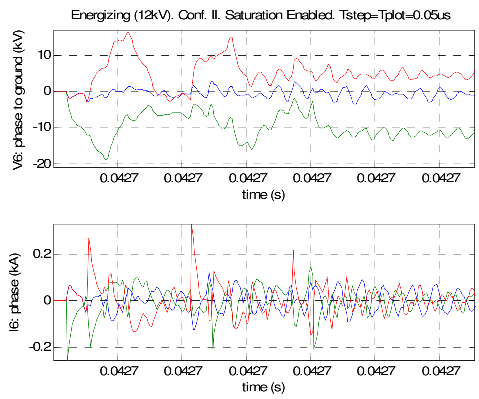

fig. 190. Voltage and Current at tp6 when energizing at no load (12 kV). Saturation modelled

At 12 kV the transformers work in their linear region but at 33 kV their operating point rises and gets closer to saturation.

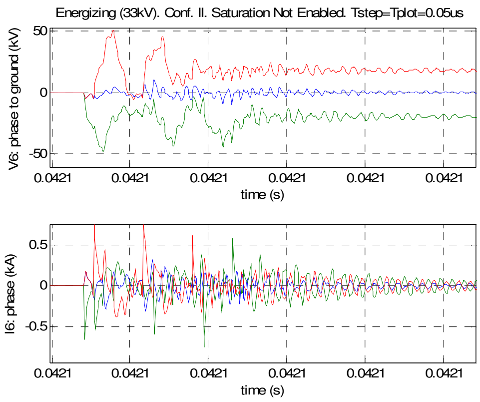

fig. 191. Voltage and Current at tp6 when energizing at no load (33 kV). Saturation not modelled

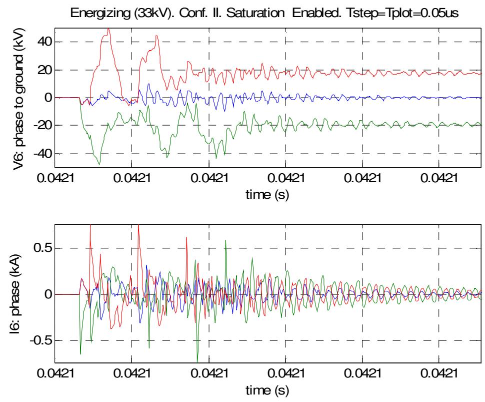

fig. 192. Voltage and Current at tp6 when energizing at no load (33 kV). Saturation modelled

It seems that the addition of a capacitance decreases the number of pre-strikes (fig. 193 and fig. 194). However, if the first series of pre-strikes is zoomed (fig. 195 and fig. 196) the number of pre-strikes is higher in the second case. This could be due to the fact that for high frequency reflections the capacitor provides a fast charge while at lower frequencies keeps the voltage at a steady power frequency.

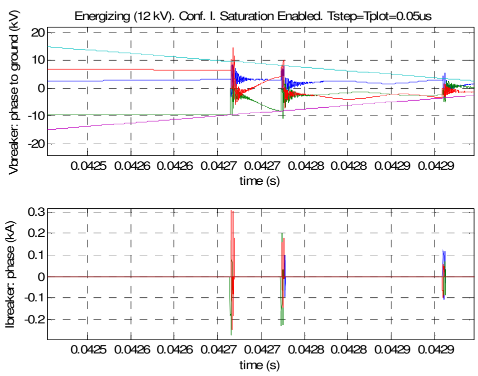

fig. 193. Voltage and Current across the breaker when energizing at no load (12 kV). Configuration I

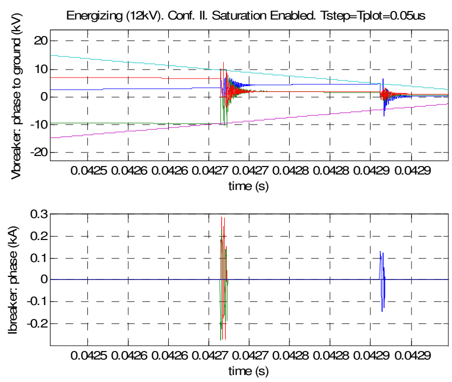

fig. 194. Voltage and Current across the breaker when energizing at no load (12 kV). Configuration II

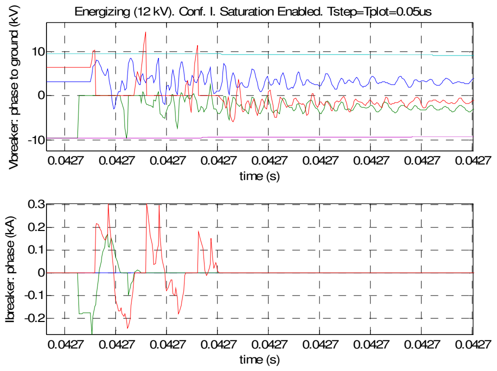

fig. 195. Voltage and Current across the breaker when energizing at no load (12 kV). Configuration I (zoomed)

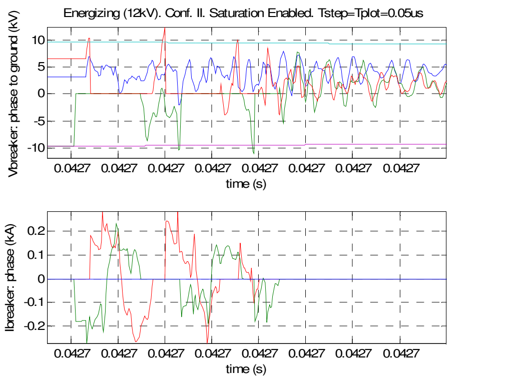

fig. 196. Voltage and Current across the breaker when energizing at no load (12 kV). Configuration II (zoomed)

6.5.2.2 OPENING

6.5.2.2.1 NO LOAD

When opening at no load the same behaviour as in configuration I is observed: there is no reignition because the current flowing through the circuit is too low. The only difference between both configurations is the “waving” of the current due to the capacitor resonating with other elements of the circuit.

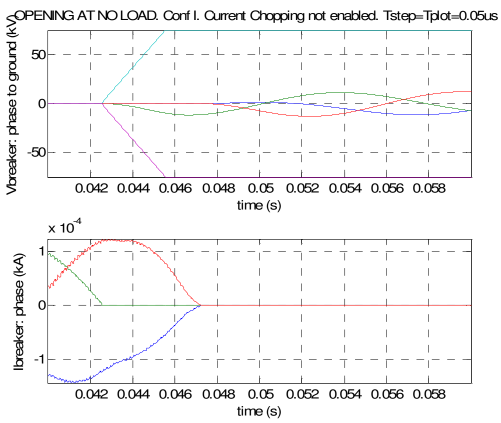

fig. 197. Voltage and Current across the breaker when opening at no load (12 kV). Configuration I

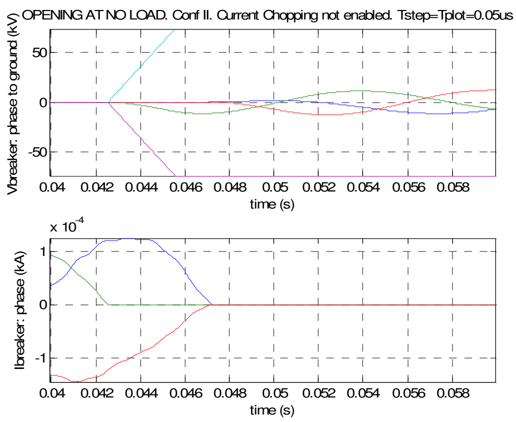

fig. 198. Voltage and Current across the breaker when opening at no load (12 kV). Configuration II

If the current chopping is modelled very similar results are obtained (the transient recovery voltage rises a little faster) so the next simulations do not model the current chopping.

For a better analysis of the effect of the lumped capacitor, the loaded cases need to be studied.

6.5.2.2.2 LOAD

– **Resistive**

The resistance value has been chosen to be as low as to be able to absorb enough current to create reignitions. Moreover, current chopping has been set to 3A. In this case, configuration I gives worse results than configuration II. It seems that the lumped capacitor produces a slower transient recovery voltage and thus less reignitions.

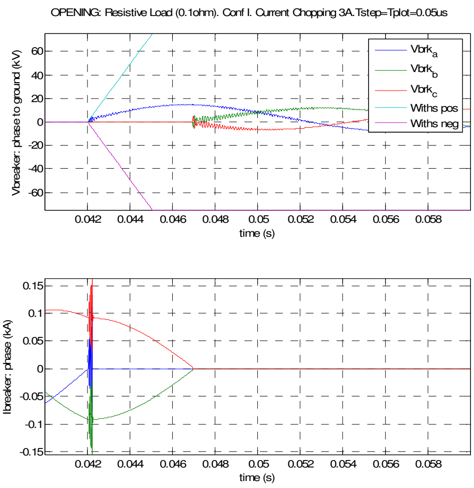

fig. 199. Voltage and Current across the breaker when opening a resistive load (0.1 Ω). Current chopping modelled. Configuration I

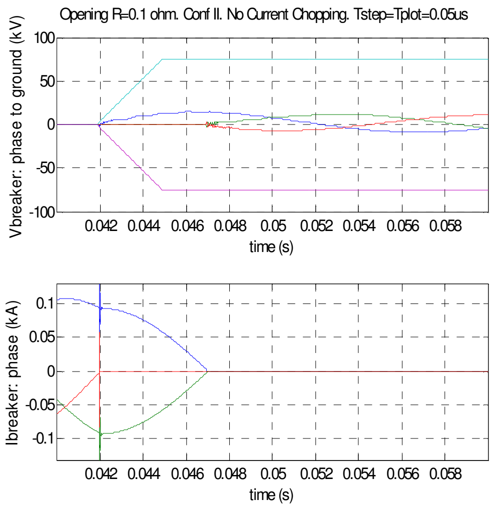

fig. 200. Voltage and Current across the breaker when opening a resistive load (0.1 Ω). Current chopping modelled. Configuration II

– **Inductive**

The inductance used in these simulations has been arbitrarily chosen (4 mH) not to be too big or too small.

After simulating both cases (with and without lumped capacitance) it is difficult to decide which one that gives the worst results.

The case without lumped capacitance gives more density/quantity of reignitions especially when the contacts start to separate but their sharpness at the high voltage side of the load transformer is lower than in the capacitor case.

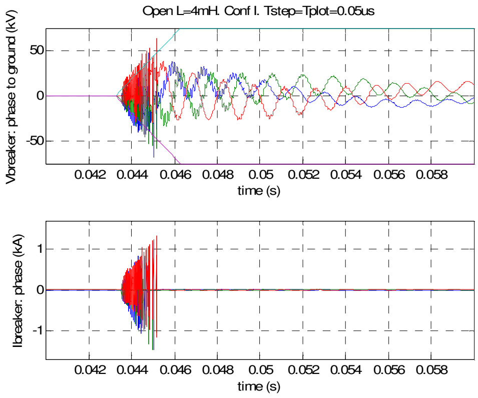

fig. 201. Voltage and Current across the breaker when opening an inductive load (4 mH). Saturation Enabled. Configuration I

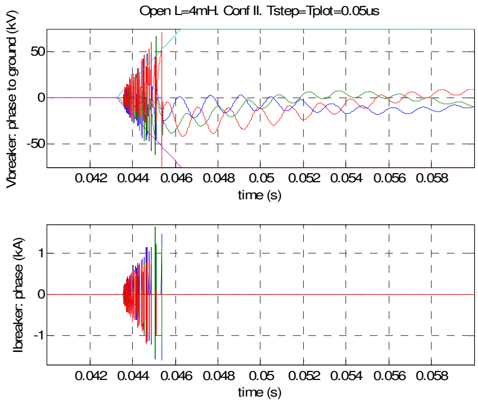

fig. 202. Voltage and Current across the breaker when opening an inductive load (4mH). Saturation Enabled. Configuration II

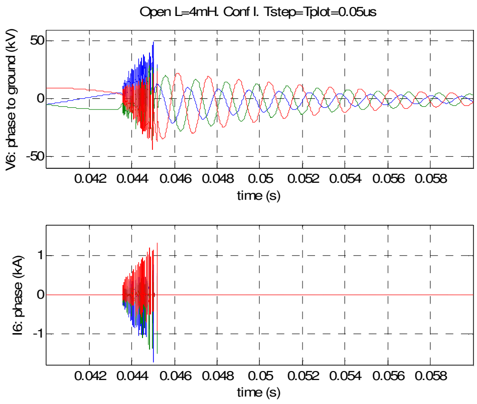

fig. 203. Voltage and Current at tp6 when opening an inductive load (4 mH). Saturation Enabled. Configuration I

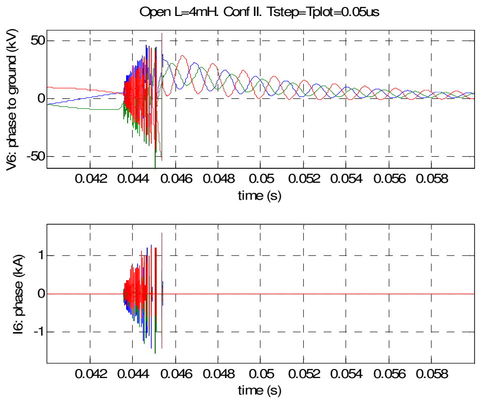

fig. 204. Voltage and Current at tp6 when opening an inductive load (4mH). Saturation Enabled. Configuration II

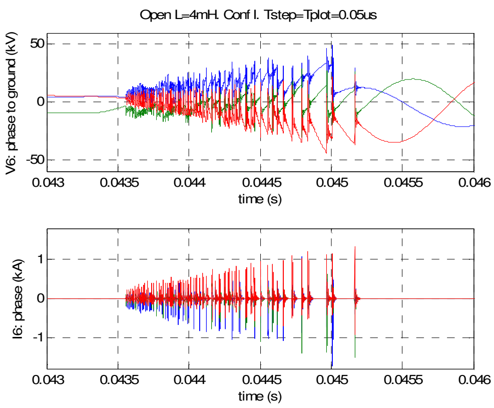

fig. 205. Voltage and Current at tp6 when opening an inductive load (4 mH). Saturation Enabled. Configuration I (zoomed)

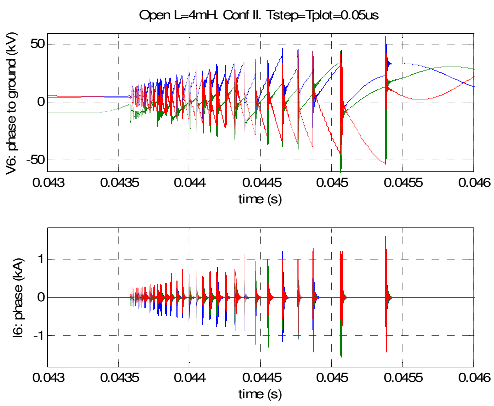

fig. 206. Voltage and Current at tp6 when opening an inductive load (4mH). Saturation Enabled. Configuration II (zoomed)

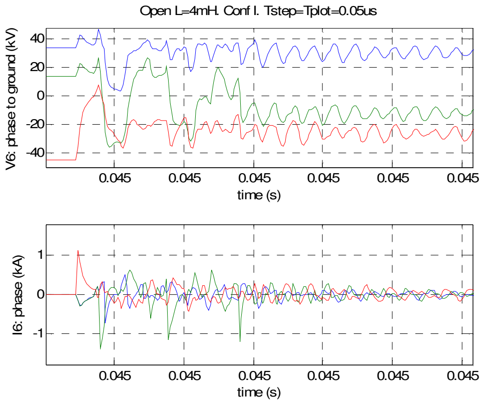

fig. 207. Voltage and Current at tp6 when opening an inductive load (4 mH). Saturation Enabled. Configuration I (zoomed)

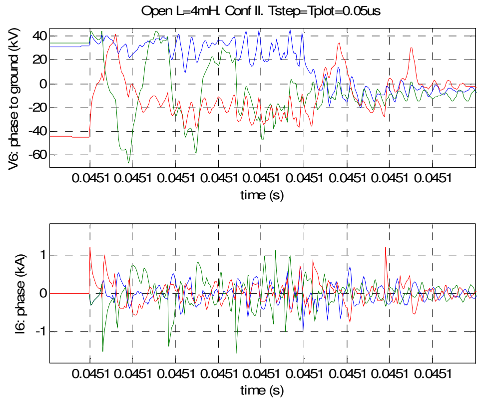

fig. 208. Voltage and Current at tp6 when opening an inductive load (4mH). Saturation Enabled. Configuration II (zoomed)

6.5.2.2.3 FAULTS

From all the types of faults the SLG fault is the most harmful as far as fast transients are concerned. For this reason, even if every fault has been simulated and the results saved, the single line to ground fault type will be analysed and compared.

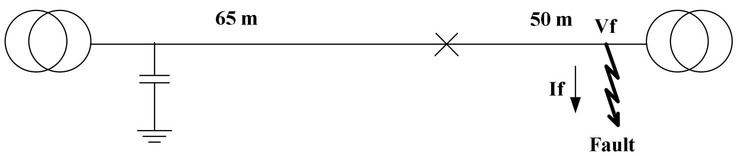

fig. 209. Schema of the fault

– **SLG (Single Line to Ground fault)**

The differences between the first configuration and the second configuration are the following:

- In the case with the lumped capacitance the initial current is almost six times higher than in the case without capacitance.
- The oscillation frequency of the voltage after the fault is lower in the second case.

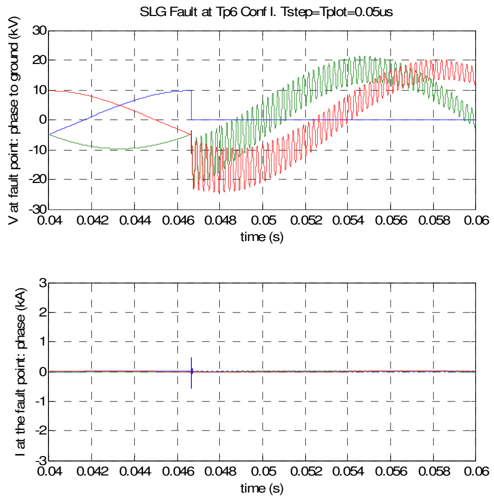

fig. 210. Voltage and Current at tp6 when a SLG fault happens. Configuration I

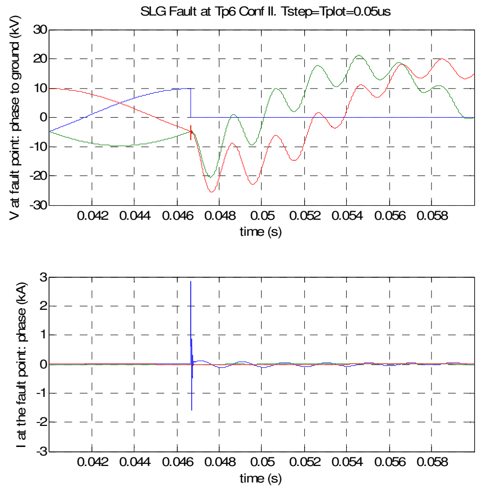

fig. 211. Voltage and Current at tp6 when a SLG fault happens. Configuration II

For the case in which the fault breaks in one of the first zero-crossings the results are shown in fig. 212, fig. 213, fig. 214, fig. 215, fig. 216 and fig. 217:

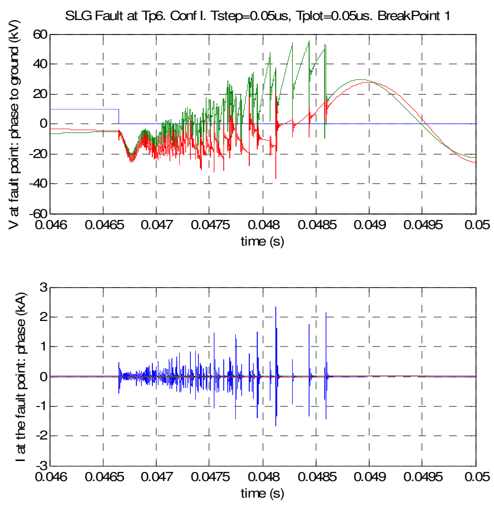

fig. 212. Voltage and Current across the breaker after opening a SLG fault . Configuration I

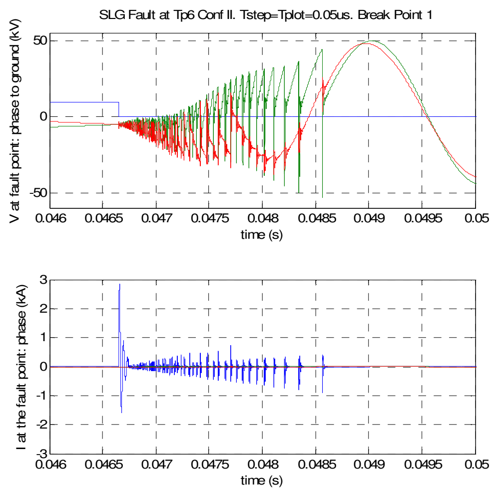

fig. 213. Voltage and Current across the breaker after opening fault. Configuration II

In this case it is also difficult to evaluate which is the configuration that gives the most harmful results. Nevertheless, if the voltage and current at the fault point are zoomed some conclusions can be drawn:

- The steepness of the voltage is higher in the second configuration. Observe the difference between positive and negative values.
- The amplitude of the voltage after the reignition series is higher in the second configuration.
- After breaking the fault, the fault current value is lower in the second configuration.

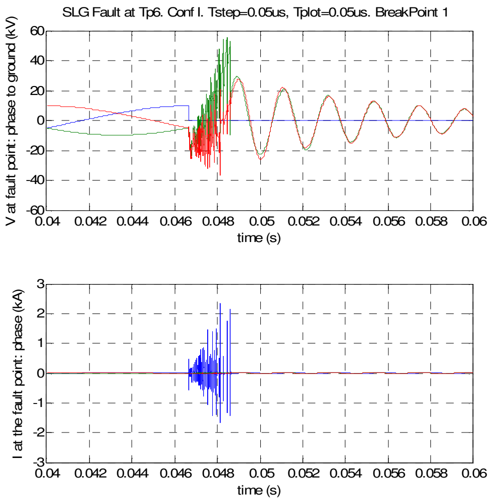

fig. 214. Voltage and Current across the breaker after opening a SLG fault . Configuration I

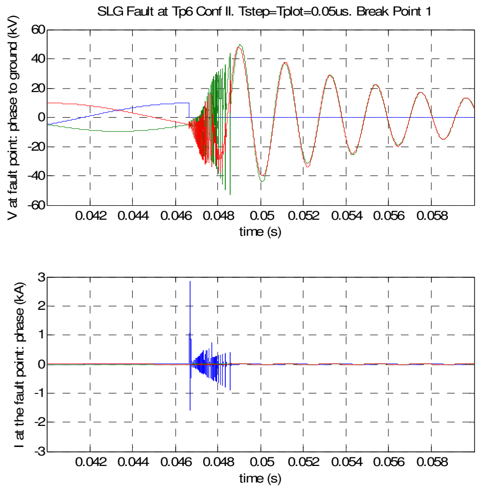

fig. 215. Voltage and Current across the breaker after opening fault. Configuration II

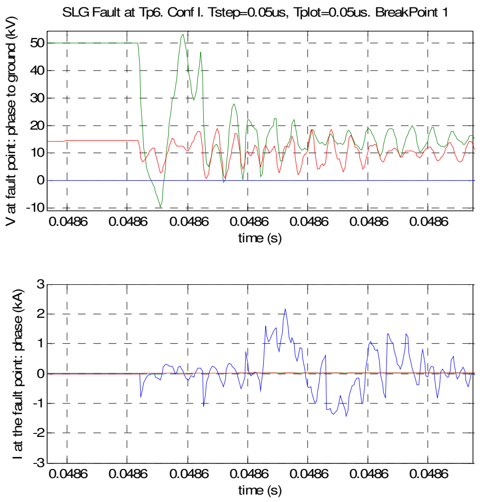

fig. 216. Voltage and Current across the breaker after opening a SLG fault . Configuration I

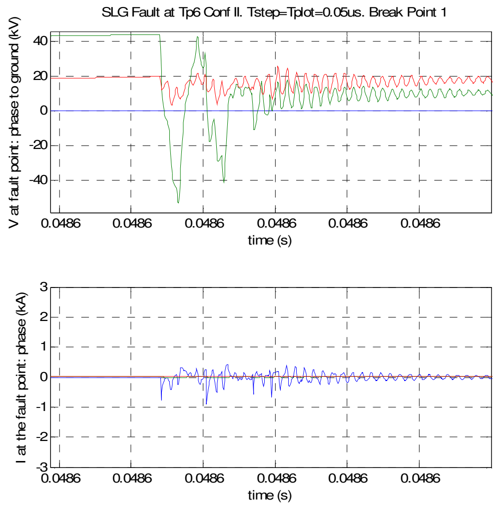

fig. 217. Voltage and Current across the breaker after opening fault. Configuration II

6.5.3 CONCLUSIONS

It is not straightforward to say which of the two configurations gives the most harmful results. However, it seems that the second configuration, which considers the charging of the surrounding cables, gives a steeper voltage rise in the high voltage side of the load transformer.

7. CONCLUSIONS AND FUTURE WORK

The continuous development of larger and larger wind parks increases the interest for studying large cable grids. The interaction between cables and VCB is a source of fast transient overvoltages that damages the electrical insulation of the WP equipment. A good understanding of these fast transient phenomena is required in order to decide the most adequate measures: change the design specifications of the insulation materials, think about the most cost-efficient preventive or corrective methods et cetera.

7.1 MODELLING

Power system equipment models are optimized to operate at power frequencies. However, fast transients occur at a wide range of frequencies and hence, the usual models for power frequencies are not valid anymore. Most of the models used to represent fast transients must take into consideration the frequency dependency of the parameters. This fact makes model designing much more complex requiring good command of mathematical tools.

On the other hand, fast transients are caused by several different phenomena. This means that the model must be chosen to better represent a particular phenomenon because it is not possible to design a "universal" model for fast transients.

The simulation software used is called PSCAD/EMTDC and it is a good simulation package overall. Nevertheless some disadvantages have been found:

- Most of the PSCAD library models are designed to work at power frequencies. The models are written in FORTRAN and therefore it is requires some programming skills to create custom models.
- Some of the components that need to be adapted in order to work with fast transients are the VCB and the transformer. Cables are quite well modelled but they can be further improved (the armour, for example, is not taken into account).
- The simulation step is constant. For fast transient analysis this can be a drawback because both power frequency and high frequency components are subjects for investigations. Simulating a couple of power frequency periods at an appropriate sampling rate that also allows examining high frequencies can take a long time.
- Due to the small sampling times the generated simulation file can be so large that it can be impossible to read from another program such as Matlab. Saving the plots in Matlab figures is very time consuming but it gives the possibility of dynamically zooming the simulations (necessary to analyse fast transients). Another possibility is to save them in PSCAD using a custom made program and read them again from PSCAD or to plot them using TOP (The Output Processor).

7.2 SINGLE PHASE LABORATORY EXPERIMENTS AND SIMULATIONS

These laboratory experiments are the first stage of a long run experimental project in which a real branch (with real parameters) of a WP is to be studied. It has taken more time than expected to gather all the necessary material but finally it was possible to run a few tests.

Although, before running the tests there was a certain concern about whether the single phase configuration would give problems or not, it has been demonstrated that it works perfectly. Moreover, it can be useful to have single phase experiments because the coupling between phases can not occur and thus the results are easier to examine.

The comparison of the measured results with the simulated results has shown that there is a high degree of similarity but it they are not exactly the same. The divergence could be due to the following facts:

- The CB model used gives the possibility of enabling/disabling the current chopping. If the chopping is enabled (that is the case of these simulations) then the current is always chopped no matter the frequency. In reality current chopping is only observed at power frequencies so if the current is chopped also at higher frequencies the consequent TRV after each current zero is steeper than in reality and the reignition number and frequency increases. In simulations the reignition density is higher.
- The cold withstand curve is deduced from the measurements and modelled as a two point linear curve. However, the real withstand is not linear and it also depends in the hot gap withstand characteristics.
- The oscillation frequencies of the supply side and of the load side (separately) of the circuit are higher in simulations than in reality. This evidences that some parameter(s) have not been correctly chosen. Some possibilities are:
  - The saturation curve of the transformer has not been enabled because the experiments have been run at voltages far below the rated voltage. However, it can be that a fast overshot reaches the saturation region. In addition, the value of the magnetizing current has been guessed (1% of the rated current) because the real saturation curve could not be provided.
  - The cable parameters might be slightly different giving different values of per-unit length capacitances and inductances.
  - The cables are not laid straight in the cellar. A big effort has been made to keep them as straight as possible but they are inevitable slightly bend.
  - Although the copper conductor used as return conductor has also been modelled, it can be that the model does not observe all the implications of its presence.

7.3 SIMULATIONS OF THREE PHASE CIRCUIT

The following conclusions have been extracted from the simulations performed with three phase cables:

- Energizing at no-load always gives re-strikes.
- The worst moment to open a CB is always when the current is close to become zero.
- Opening at no-load does not generate reignitions because the no-load current is very small.
- Opening a resistive load only gives reignitions when the resistor is very small.
- Opening and inductive load always creates reignitions unless the inductance is so large that the current is too small.
- Depending on the fault type different voltage and current profiles are obtained. It seems that the worst reignitions are obtained when a single phase to ground is broken. The resulting current has such a strong high frequency component that the reignitions are as severe no matter when the fault is opened. In other kinds of faults the current is much slower and the probability of reignitions is reduced because they appear when the breaker is near the current zero crossing.
- The addition of a capacitor in the high voltage side of the supply transformer increases the steepness of the voltage fronts but the difference is not very noticeable.

7.4 FUTURE WORK

The laboratory experiments have shown that the models must be further improved. The following is suggested:

- A frequency dependent transformer model.
- A vacuum circuit model that includes a better characterization of the current chopping and an analysis of high frequency current quenching methods.
- An experimental determination of the cold-withstand curve.
- Analysis of the existing cable model and design of improvements (armour).

An additional suggestion is to study methods to improve simulation speed and storage of simulation file data.

Regarding the laboratory experiments it is advisable to set the necessary measures to avoid high frequency interference in the recording equipment before continuing with other simulations. Besides, it is also helpful to gather as much information as possible around the laboratory experiments:

- A detailed diary of experiments (this has been done) that can be read and understood by any person that was not present during the experiments.
- A database with all the information (reference number, name and characteristics…) of the equipment used in the lab.

8. References

[1] IEC 56 Standard

[2] IEEE Std C37.011™-2005, IEEE Application Guide For Transient Recovery Voltage

[3] A. Morched, L. Martí, J. Ottevangers, "A High Frequency Transformer Model for the EMTP", IEEE Transactions on Power Delivery, Vol. 8, No.3, July 1993

[4] M.Popov, "Switching Three-Phase Distribution Transformers with a VCB. Analysis of Overvoltages and the Protection Equipment", PhD Thesis, Delft University of Technology

[5] A. Greenwood, "Electrical Transients in Power Systems", 2nd Edition, Wiley-Interscience

[6] L. M. Wedepohl, "Theory of Natural Modes in Multi-Conductor Transmission Lines", Course Notes, May 1989.

[7] L. M. Wedepohl, "Transient Analysis of Underground Transmission Systems", Proc. IEE, Vol. 120, No. 2, Feb. 1973.

[8] J. Marti, "Accurate Modeling of Frequency Dependent Transmission Lines in Electromagnetic Transients Simulation", IEEE Transactions on Power Apparatus and Systems, PAS-101, #1, pp. 147-155, Jan. 1982.

[9] L. Marti, "Simulation of Electromagnetic Transients in Underground Cables with Frequency Dependent Modal Transformation Matrices", Ph.D. Thesis, University of British Columbia, 1986.

[10] PSCAD HELP

[11] A. Morched, B. Gustavsen, M. Tartibi, "A Universal Line Model for Accurate Calculation of Electromagnetic Transients on Overhead Lines and Cables", Paper PE-112-PWRD-0-11-1997.

[12] B. Gustavsen, G. Irwin, R. Mangelrod, D. Brandt, K. Kent, "Transmission Line Models for the Simulation of Interaction Phenomena Between Parallel AC and DC Overhead Lines", IPST '99 Proceedings, pp. 61-67, 1999.

[13] P.G. Slade, "Vacuum Interrupters: The New Technology for Switching and Protecting Distribution Circuits", IEEE Transactions On Industry Applications, Vol. 33, No. 6, November/December 1997

[14] J. Helmer, M.Lindmayer, "Mathematical Modeling of the High Frequency behaviour of Vacuum Interrupters and Comparison with Measured Transients in Power Systems", XVIIth International Symposium on Discharges and Electrical Insulation in Vacuum-Berkeley-1996

[15] L. Liljestrand, A. Sannino, H. Breder, S. Johansson, "Transients in Collection Grids of Large Offshore Wind Parks", Nordic Wind Power Conference, 22-23 May 2006, Espoo, Finland

[16] IEEE Std C37.011™-2005. IEEE Application Guide for Transient Recovery Voltage for AC High-Voltage CBs

[17] M.Popov, L. Van Der Sluis, "Improved Calculations for No-Load Transformer Switching Surges", IEEE Transactions on Power Delivery, Vol. 16, No. 3, July 2001

[18] M.Popov, L. Van Der Sluis, G. C. Paap, "Investigation of the CB Reignition Overvoltages Caused by No-load Transformer Switching Sources", ETEP, Vol. 11, No. 6, November/December 2001

[19] T. Yu, J. Martí, “A robust Phase-Coordinates Frequency-Dependent Underground Cable Model (zCable) for the EMTP”, IEEE Transactions on Power Delivery, Vol. 18, No. 1, January 2003

[20] J. Lopez-Roldan, G.Campos, H. de Herdt, J. Min, R. Van Velthoven, T. Sels, J. Karas, M. Popov, “Fast Transient Overvoltages Produced By Switching Distribution Transformers With A VCB: Simulation and Testing”, Power Quality Conference, EA Technology, Chester, UK, May 2nd, 2002

[21] Fishbane, Gasirowicz, Thornton, “Física Para Ciencias e Ingeniería”, Vol. II, Prentice-Hall Hispanoamericana

[22] Technical documentation, “ABB XLPE Cables User’s Guide,” available from www.abb.com.

APPENDIX I. PSCAD 3 PHASE TRANSFORMER (UMEC)

1. OBJECTIVE

The main objective of this appendix was to explain how the PSCAD transformer parameter table should be filled in order to represent adequately the performance of a chosen transformer.

An equivalent transformer model will be deduced starting from the nameplate data of the real transformer and both the pscad predefined model and the custom made model will be simulated in order to check the validity of the calculations.

The explanations will be based on two particular examples (the transformers used in the laboratory experiments).

2. TRANSFORMERS' (TX1 and TX2) NAMEPLATES' DATA

Both transformers are oil filled three-phase distribution transformers. Transformer TX1 IS used as a step up transformer and TX2 as step down transformer directly connected to the load. The nameplate data of both transformers is gathered in table 17 and table 18.

table 17. Nameplate data of transformer TX1

No. 5214242		1999
CTMU 24 HA 1250		IEC 76
1250 kVA	Dyn11	50 Hz
20500 ± 2×2.5 % V		35.2 A
410 V		1760 A
U 125AC50/AC8 kV		ONAN
Zk 5.4 %		2885 kg
Pk 11971 W		605 kg
Po 1455 W		

table 18. Nameplate data transformer TX2

No. 5210667		1997
CTMU 24 HM 1000		IEC 76
1000 kVA	Dyn11	50 Hz
20000 ± 2×2.5 % V		28.87 A
690 V		836.7 A
U 125AC50/AC8 kV		ONAN
Zk 5.1 %		2670 kg
Pk 10260 W		505 kg
Po 1223 W		

3. PSCAD MODEL FOR THREE PHASE TRANSORMERS

PSCAD offers two different models for three phase transformers: the classical approach and the UMEC model. The difference between them is not big.

The UMEC (Unified Magnetic Equivalent Circuit) transformer model is based primarily on core geometry. Unlike the classical transformer model, magnetic coupling between windings of different phases, in addition to coupling between windings of the same phase, are taken into account.

The UMEC transformer models treat core saturation differently than the classical models: Here, the piecewise linear technique is used to control the model equivalent branch conductance.

The non-linearity of the core is entered directly into the model as a piece-wise linear V-I curve, which makes full use of the interpolation algorithm for the calculation of exact instants in changing of state range.

The classical model represents saturation using a compensating current source across the winding wound closest to the core.

For this explanation the UMEC model have been chosen.

3.1. TRANSFORMER TX1

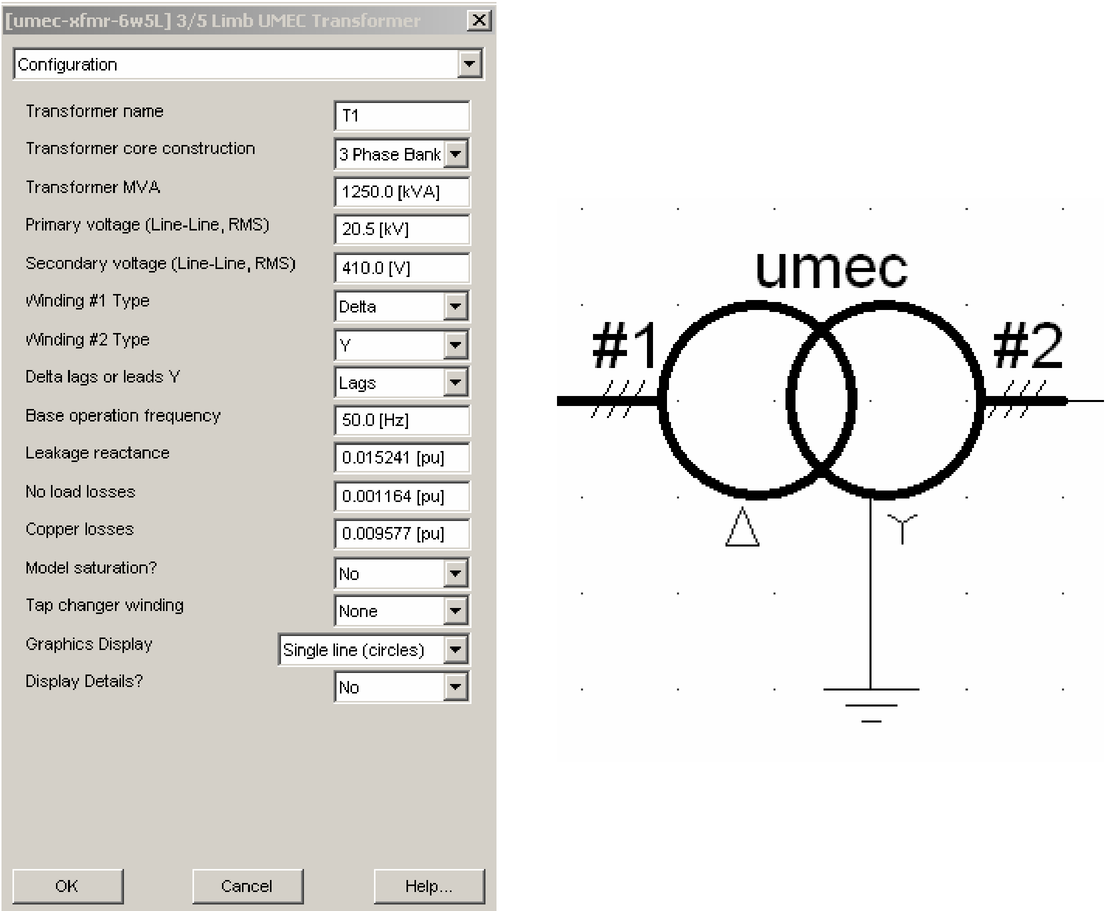

fig. 218. PSCAD transformer 1 configuration table

Most of the parameters are inserted straightforward from the nameplate data. In this case, if saturation is not modelled, the only parameters that need to be modified are the leakage reactance, the no-load losses and the copper losses.

The total no-load losses and the copper losses are given in the nameplate but must be scaled to to per unit values. The base power is the rated transformer power, 1250 kVA.

$$S_{\text{base}} = 1250\text{kVA}$$

$$P_0(\text{p.u}) = \frac{P_0}{S_{\text{base}}} = \frac{1455\text{W}}{1250\text{kVA}} = 0.001164\text{p.u}$$

$$P_k(\text{p.u}) = \frac{P_k}{S_{\text{base}}} = \frac{11971\text{W}}{1250\text{kVA}} = 0.009577\text{p.u}$$

The leakage reactance can be calculated using the short-circuit power (P_k) and per-unit short-circuit impedance (z_k (pu)).

Attention must be paid here to the used base system. In three phase systems the base systems is often calculated as follows:

$$S_{base} = S_{rated} = 1250\text{kVA}$$
$$U_{base} = U_{rated} = 20500\text{V}$$

where,

$$I_{base} = \frac{S_{base}}{\sqrt{3}\cdot U_{base}} = \frac{1250\cdot 10^3\,\text{VA}}{\sqrt{3}\cdot 20500\text{V}} = 35.2043\text{A}$$

The base impedance is usually calculated for a star configuration:

$$Z_Y = \frac{U_{ph}}{I_{ph}} = \{\text{for a star connection}\} = \frac{\left(\frac{U_L}{\sqrt{3}}\right)}{I_L} = \frac{\left(\frac{U_L}{\sqrt{3}}\right)}{\frac{S_{rated}}{\sqrt{3}\cdot U_L}} = \frac{(U_L)^2}{S_{rated}}$$

But it could be calculated also regarding a delta connection:

$$Z_\Delta = \frac{U_{ph}}{I_{ph}} = \{\text{for a delta connection}\} = \frac{U_L}{\left(\frac{I_L}{\sqrt{3}}\right)} = \frac{U_L}{\left(\frac{1}{\sqrt{3}}\right)\cdot\frac{S_{rated}}{\sqrt{3}\cdot U_L}} = 3\cdot\frac{(U_L)^2}{S_{rated}}$$

There is a factor of three between the two connection types:

$$Z_\Delta = 3\cdot Z_Y$$

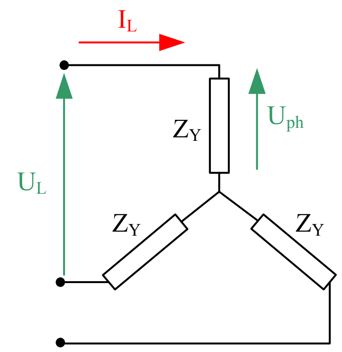

fig. 219. Three phase load in star connection

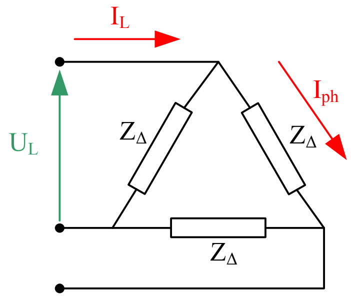

fig. 220. Three phase load in delta connection

The short-circuit impedance of the transformer nameplate is given according to a star connection configuration. This means that the base impedance of the transformer nameplate is:

$$Z_{base\_nameplate\_Y} = \frac{(U_{base})^2}{S_{rated}} = \frac{(20500\text{V})^2}{1250\cdot 10^3} = 336.2\Omega$$
$$Z_k = z_{k(pu\_nameplate)}\cdot Z_{base\_nameplate\_Y} = 0.054\cdot 336.2\Omega = 18.1548\Omega$$

However, the base impedance used to introduce the data of the transformer in PSCAD is referred to a delta connection:

$$Z_{\text{base\_PSCAD\_}\Delta} = 3 \cdot \frac{(U_{\text{base}})^2}{S_{\text{rated}}} = 3 \cdot \frac{(20500\text{V})^2}{1250 \cdot 10^3} = 1008.6\Omega$$

$$z_{\text{k(pu\_PSCAD)}} = \frac{Z_{\text{k}}}{Z_{\text{base\_PSCAD\_}\Delta}} = \frac{18.1548\Omega}{1008.6\Omega} = 0.018 \text{ p.u (in PSCAD base)}$$

The short-circuit reactance is obtained from the short-circuit resistance, which is found from the short-circuit power. The short-circuit power is measured short-circuiting the secondary at the rated current.

$$P_{\text{k}} = 3 \cdot R_{\text{k}} \cdot (I_{\text{ph\_rated}})^2 = 3 \cdot R_{\text{k}} \cdot \left(\frac{I_{\text{L\_rated}}}{\sqrt{3}}\right)^2 = R_{\text{k}} \cdot (I_{\text{L\_rated}})^2$$

$$R_{\text{k}} = \frac{P_{\text{k}}}{(I_{\text{L\_rated}})^2} = \frac{11971\text{W}}{(35.2043\text{A})^2} = 9.65916\Omega$$

$$r_{\text{k(pu\_PSCAD)}} = \frac{R_{\text{k}}}{Z_{\text{base\_PSCAD\_}\Delta}} = \frac{9.65916\Omega}{1008.6\Omega} = 0.009577\text{pu (in PSCAD base)}$$

$$x_{\text{k(pu\_PSCAD)}} = \sqrt{\left(z_{\text{k(pu\_PSCAD)}}{}^2 - r_{\text{k(pu\_PSCAD)}}{}^2\right)} = \sqrt{\left(0.018^2 - 0.009577^2\right)} = 0.015241\text{p.u (in PSCAD base)}$$

$$X_{\text{k}} = x_{\text{k(pu\_PSCAD)}} \cdot Z_{\text{base\_PSCAD\_}\Delta} = 0.015241 \cdot 1008.6\Omega = 15.372\Omega$$

$$L_{\text{k}} = \frac{X_{\text{k}}}{2\pi f} = \frac{15.372\Omega}{2\pi \cdot 50\text{Hz}} = 48.93\text{mH}$$

3.2. TRANSFORMER TX2

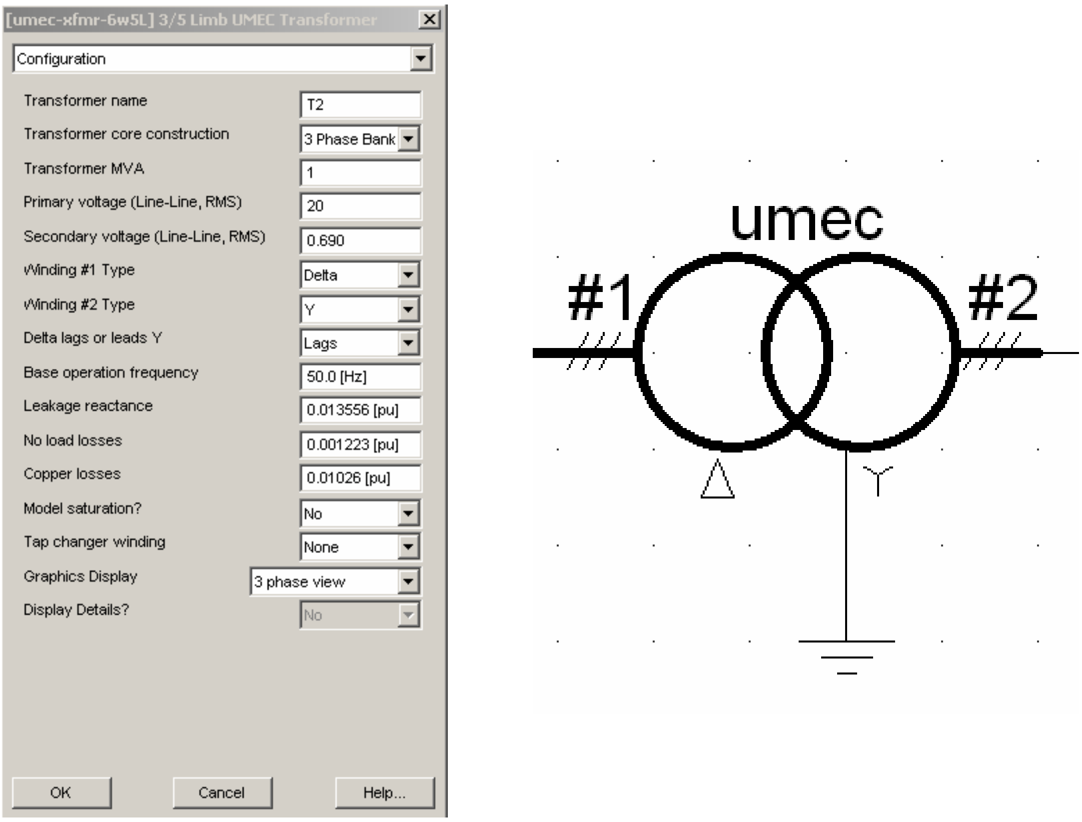

fig. 221. PSCAD transformer 2 configuration table

Most of the parameters are inserted straightforward from the nameplate data. In this case, if saturation is not modelled, the only parameters that need to be modified are the leakage reactance, the no-load losses and the copper losses.

The total no-load losses and the copper losses are given in the nameplate but must be scaled to to per unit values. The base power is the rated transformer power, 1000 kVA.

$$S_{\mathrm{base}} = 1000kVA$$

$$P_{\mathrm{o}}(p.u) = \frac{P_{\mathrm{o}}}{S_{\mathrm{base}}} = \frac{1123\mathrm{W}}{1000\mathrm{kVA}} = 0.001223\mathrm{p.u}$$

$$P_{\mathrm{k}}(\mathrm{p.u}) = \frac{P_{\mathrm{k}}}{S_{\mathrm{base}}} = \frac{10260\ \mathrm{W}}{1000\mathrm{kVA}} = 0.01026\mathrm{pu}$$

The leakage reactance can be calculated using the short-circuit power (P_k) and per-unit short-circuit impedance (z_k (pu)).

Attention must be paid here to the used base system. In three phase systems the base systems is often calculated as follows:

$$S_{\mathrm{base}} = S_{\mathrm{rated}} = 1000\mathrm{kVA}$$

$$U_{\mathrm{base}} = U_{\mathrm{L-rated}} = 20000\mathrm{V}$$

where,

$$I_{\mathrm{base}} = \frac{S_{\mathrm{base}}}{\sqrt{3}\cdot U_{\mathrm{base}}} = \frac{1000\cdot 10^{3}\,\mathrm{VA}}{\sqrt{3}\cdot 20000\mathrm{V}} = 28.86\mathrm{A}$$

The base impedance is usually calculated for a star configuration:

$$Z_{\mathrm{Y}} = \frac{U_{\mathrm{ph}}}{I_{\mathrm{ph}}} = \{\text{for a star connection}\} = \frac{\left(U_{\mathrm{L}}/\sqrt{3}\right)}{I_{\mathrm{L}}} = \frac{\left(U_{\mathrm{L}}/\sqrt{3}\right)}{\left(\dfrac{S_{\mathrm{rated}}}{\sqrt{3}\cdot U_{\mathrm{L}}}\right)} = \frac{(U_{\mathrm{L}})^{2}}{S_{\mathrm{rated}}}$$

But it could be calculated also regarding a delta connection:

$$Z_{\Delta} = \frac{U_{\mathrm{ph}}}{I_{\mathrm{ph}}} = \{\text{for a delta connection}\} = \frac{U_{\mathrm{L}}}{\left(\dfrac{I_{\mathrm{L}}}{\sqrt{3}}\right)} = \frac{U_{\mathrm{L}}}{\dfrac{1}{\sqrt{3}}\cdot\left(\dfrac{S_{\mathrm{rated}}}{\sqrt{3}\cdot U_{\mathrm{L}}}\right)} = 3\cdot\frac{(U_{\mathrm{L}})^{2}}{S_{\mathrm{rated}}}$$

There is a factor of three between the two connection types:

$$Z_{\Delta} = 3\cdot Z_{\mathrm{Y}}$$

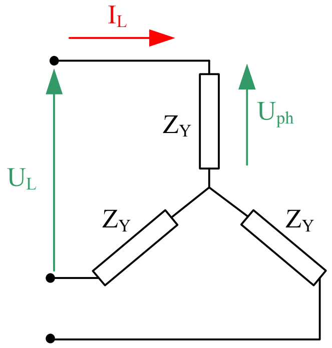

fig. 222. Three phase load in star connection

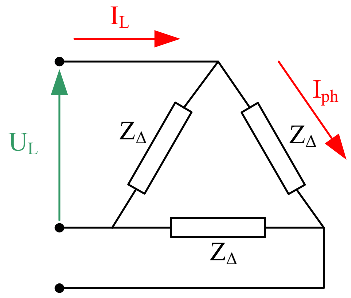

fig. 223. Three phase load in delta connection

The short-circuit impedance of the transformer nameplate is given according to a star connection configuration. This means that the base impedance of the transformer nameplate is:

$$Z_{\text{base\_nameplate\_Y}} = \frac{(U_{\text{base}})^2}{S_{\text{base}}} = \frac{(20000\text{V})^2}{1000 \cdot 10^3} = 400\Omega$$

$$Z_{\text{k}} = z_{\text{k(pu\_nameplate)}} \cdot Z_{\text{base\_nameplate\_Y}} = 0.051 \cdot 400\Omega = 20.4\Omega$$

However, the base impedance used to introduce the data of the transformer in PSCAD is referred to a delta connection:

$$Z_{\text{base\_PSCAD\_}\Delta} = 3 \cdot \frac{(U_{\text{base}})^2}{S_{\text{base}}} = 3 \cdot \frac{(20000\text{V})^2}{1000 \cdot 10^3} = 1200\Omega$$

$$z_{\text{k(pu\_PSCAD)}} = \frac{Z_{\text{k}}}{Z_{\text{base\_PSCAD\_}\Delta}} = \frac{10.4\Omega}{1200\Omega} = 0.017\ \text{p.u (in PSCAD base)}$$

The short-circuit reactance is obtained from the short-circuit resistance, which is found from the short-circuit power. The short-circuit power is measured short-circuiting the secondary at the rated current.

$$P_{\text{k}} = 3 \cdot R_{\text{k}} \cdot (I_{\text{ph\_rated}})^2 = 3 \cdot R_{\text{k}} \cdot \left(\frac{I_{\text{L\_rated}}}{\sqrt{3}}\right)^2 = R_{\text{k}} \cdot (I_{\text{L\_rated}})^2$$

$$R_{\text{k}} = \frac{P_{\text{k}}}{(I_{\text{L\_rated}})^2} = \frac{10260\text{W}}{(28.8675\text{A})^2} = 12.312\Omega$$

$$r_{\text{k(pu\_PSCAD)}} = \frac{R_{\text{k}}}{Z_{\text{base\_PSCAD\_}\Delta}} = \frac{12.312\Omega}{1200\Omega} = 0.01026\ \text{p.u (in PSCAD base)}$$

$$x_{\text{k(pu\_PSCAD)}} = \sqrt{\left(z_{\text{k(pu\_PSCAD)}}{}^2 - r_{\text{k(pu\_PSCAD)}}{}^2\right)} = \sqrt{\left(0.017^2 - 0.01026^2\right)} = 0.013556\ \text{p.u (in PSCAD base)}$$

$$X_{\text{k}} = x_{\text{k(pu\_PSCAD)}} \cdot Z_{\text{base\_PSCAD\_}\Delta} = 0.013555 \cdot 1200\Omega = 16.2658\Omega$$

$$L_{\text{k}} = \frac{X_{\text{k}}}{2\pi f} = \frac{16.2658\Omega}{2\pi \cdot 50\text{Hz}} = 51.775\text{mH}$$

4. EQUIVALENT PHASE MODEL OF THE PSCAD TRANSFORMER

In order to verify that the preceding equations are correct an equivalent model has been built and validated in PSCAD.

This equivalent model is only valid for power frequencies.

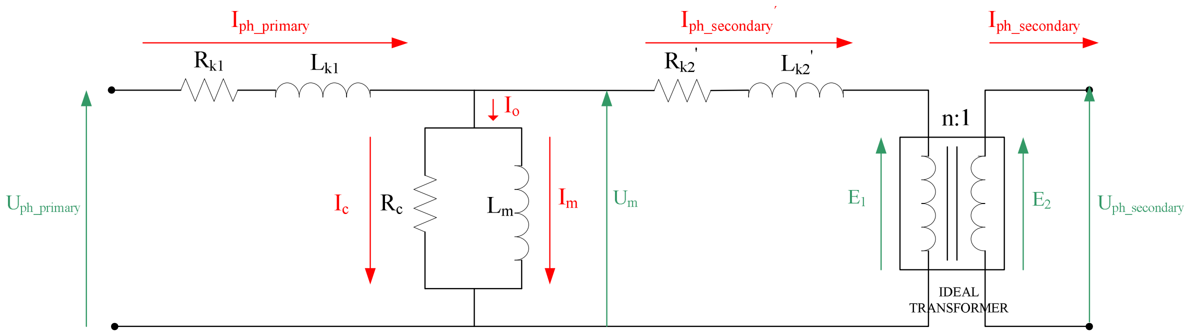

fig. 224. Equivalent transformer model for power frequencies (per phase)

4.1. TRANSFORMER TX1

The short-circuit impedance has been split in to equal parts corresponding to the primary and secondary impedances:

$$R_{k1} = R_{k2}' = \frac{R_k}{2} = \frac{9.65916}{2} = 4.82958\Omega$$

$$L_{k1} = L_{k2}' = \frac{L_k}{2} = \frac{48.93\text{mH}}{2} = 24.465\text{mH}$$

The core resistance and magnetizing inductance are calculated from the no-load power losses. The no-load test is performed at rated voltage with the secondary terminals opened. This means that at no load all the current, the no-load current, is flowing trough the core branch:

$$P_o = 3 \cdot \frac{(U_{\text{ph\_rated}})^2}{(R_{k1} + R_c)}$$

$$R_c = \frac{3 \cdot (U_{\text{ph\_rated}})^2}{P_o} - R_{k1} = \frac{3 \cdot (U_{\text{ph\_rated}})^2}{P_o} - R_{k1} = \frac{3 \cdot 20500\text{V}^2}{1455\text{W}} - 4.82958\Omega = 866.490\text{k}\Omega$$

Assuming that the no-load current is 1% of the rated current:

$$S_o = \sqrt{3} \cdot U_{\text{L\_rated}} \cdot I_o = \sqrt{3} \cdot U_{\text{L\_rated}} \cdot (0.01 \cdot I_{\text{L\_rated}}) = \sqrt{3} \cdot U_{\text{L\_rated}} \cdot \left(0.01 \cdot \frac{S_{\text{rated}}}{\sqrt{3} \cdot U_{\text{L\_rated}}}\right) = 0.01 \cdot S_{\text{rated}}$$

$$Q_o = \sqrt{(S_o^2 - P_o^2)} = \sqrt{([0.01 \cdot 1250 \cdot 10^3]^2 - 1455^2)} = 12415\text{VAr}$$

$$Q_o = 3 \cdot \frac{(U_{\text{ph\_rated}})^2}{(X_{k1} + X_m)}$$

$$X_m = \frac{3\cdot(U_{ph\_rated})^2}{Q_o} - X_{k1} = \frac{3\cdot(U_{ph\_rated})^2}{Q_o} - X_{k1} = \frac{3\cdot 20500\text{V}^2}{12415\text{VAr}} - 7.68591\Omega = 101543\Omega$$

$$L_m = \frac{X_m}{2\pi f} = \frac{101543\Omega}{2\pi\cdot 50\text{Hz}} = 323.221\text{H}$$

4.2. TRANSFORMER TX2

The short-circuit impedance has been split in to equal parts corresponding to the primary and secondary impedances:

$$R_{k1} = R_{k2}' = \frac{R_k}{2} = \frac{12.312}{2} = 6.156\Omega$$

$$L_{k1} = L_{k2}' = \frac{L_k}{2} = \frac{51.775\text{mH}}{2} = 25.8875\text{mH}$$

The core resistance and magnetizing inductance are calculated from the no-load power losses. The no-load test is performed at rated voltage with the secondary terminals opened. This means that at no load all the current, the no-load current, is flowing trough the core branch:

$$P_o = 3\cdot\frac{(U_{ph\_rated})^2}{(R_{k1}+R_c)}$$

$$R_c = \frac{3\cdot(U_{ph\_rated})^2}{P_o} - R_{k1} = \frac{3\cdot(U_{ph\_rated})^2}{P_o} - R_{k1} = \frac{3\cdot 20000\text{V}^2}{1223\text{W}} - 6.156\Omega = 981188\text{k}\Omega$$

Assuming that the no-load current is 1% of the rated current:

$$S_o = \sqrt{3}\cdot U_{L\_rated}\cdot I_o = \sqrt{3}\cdot U_{L\_rated}\cdot(0.01\cdot I_{L\_rated}) = \sqrt{3}\cdot U_{L\_rated}\cdot\left(0.01\cdot\frac{S_{rated}}{\sqrt{3}\cdot U_{L\_rated}}\right) = 0.01\cdot S_{rated}$$

$$Q_o = \sqrt{(S_o^2 - P_o^2)} = \sqrt{([0.01\cdot 1000\cdot 10^3]^2 - 1223^2)} = 9924.93\text{VAr}$$

$$Q_o = 3\cdot\frac{(U_{ph\_rated})^2}{(X_{k1}+X_m)}$$

$$X_m = \frac{3\cdot(U_{ph\_rated})^2}{Q_o} - X_{k1} = \frac{3\cdot(U_{ph\_rated})^2}{Q_o} - X_{k1} = \frac{3\cdot 20000\text{V}^2}{9924.93\text{VAr}} - 8.1329\Omega = 120900\Omega$$

$$L_m = \frac{X_m}{2\pi f} = \frac{120900\Omega}{2\pi\cdot 50\text{Hz}} = 384.835\text{H}$$

5. *VALIDATION IN PSCAD*

The model has been proven to be right by simulations in PSCAD. The actual PSCAD three phase transformer model (UMEC) has been compared with the custom made model. The custom made model has some little limitations since there is no real ideal PSCAD transformer model (observe fig. 227) but it will not affect the overall performance of the model because its leakage reactance has chosen to be very small. The resistors in the primary are due to PSCAD internal requirements.

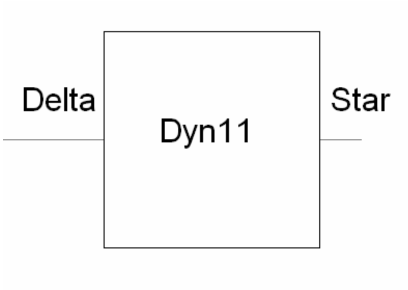

fig. 225. PSCAD custom made model

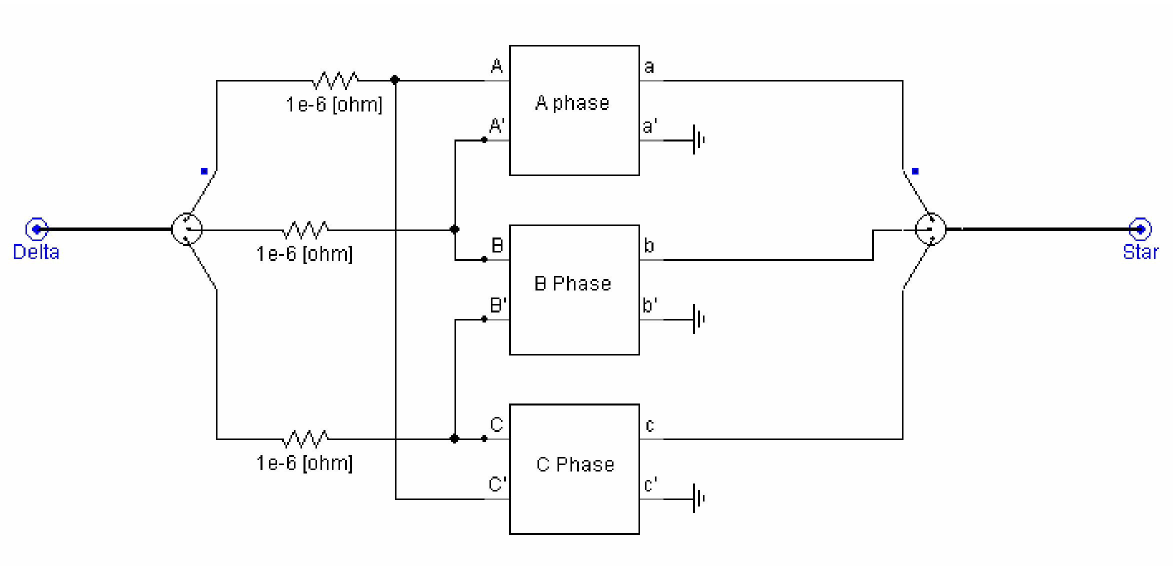

fig. 226. Equivalent transformer model for power frequencies in PSCAD

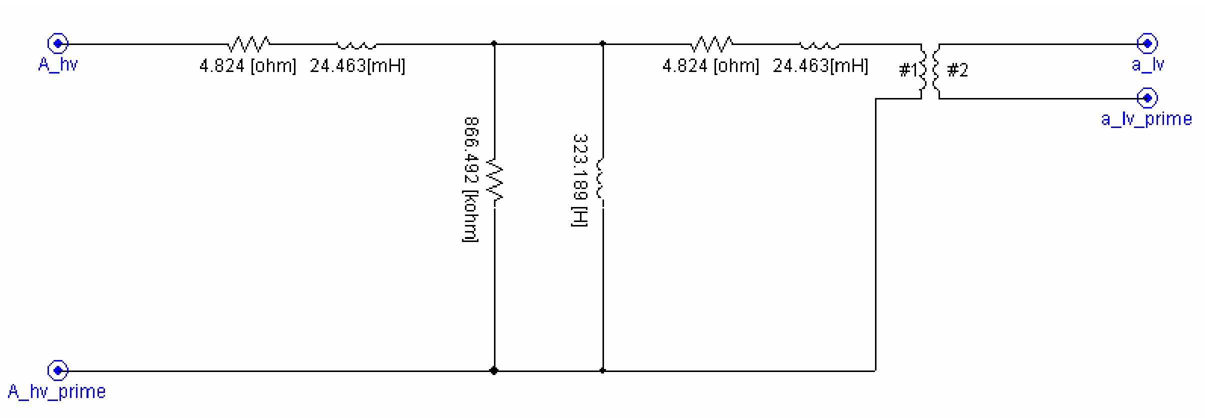

fig. 227. Equivalent transformer phase model for power frequencies in PSCAD

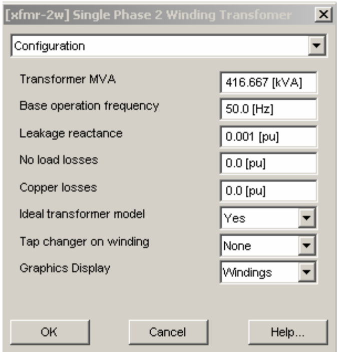

fig. 228. Configation of the ideal transformer of the PSCAD transformer phase

The following simulations have been performed:

a) No-load test with the rated voltage as input.

b) Short-circuit test with the rated current flowing through the primary.

c) Resistive load (100 Ω) at V_{in}=10 kV rms line to line.

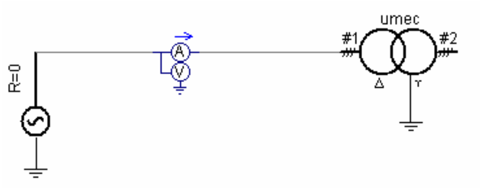

$V_{prim\_ph\_peak}$=16.49 kV
I_{prim_peak}=0.5 A
P_{prim_pu}=0.001163 pu
Q_{prim_pu}=0.009998 pu
$\theta(Q_{prim},P_{prim})$=83.361°

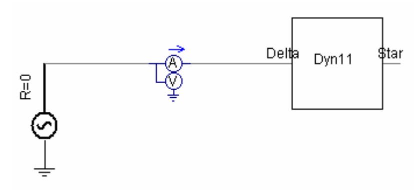

$V_{prim\_ph\_peak}$=16.7381 kV
I_{prim_peak}= 0.49 A
P_{prim_pu}=0.001164 pu
Q_{prim_pu}=0.009932 pu
$\theta(Q_{prim},P_{prim})$=83.31°

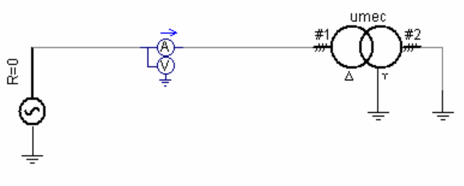

$V_{prim\_ph\_peak}$=0.3011 kV
I_{prim_peak}=0.04978 kA
P_{prim_pu}=0.009577 pu
Q_{prim_pu}=0.01524 pu
$\theta(Q_{prim},P_{prim})$=57.85 °

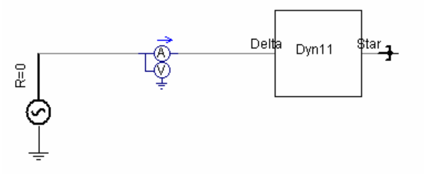

$V_{prim\_ph\_peak}$=0.3012 kV
I_{prim_peak}=0.048 kA
P_{prim_pu}=0.00899 pu
Q_{prim_pu}=0.01494 pu
$\theta(Q_{prim},P_{prim})$=58.96°

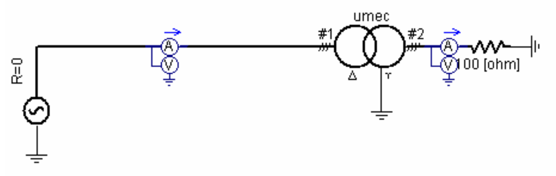

$V_{prim\_ph\_peak}$=8.1648 kV
I_{prim_peak}=0.25 A
P_{prim_pu}=0.5968m pu
Q_{prim_pu}=0.002379 pu
$\theta(Q_{prim},P_{prim})$=75.91°
$V_{sec\_ph\_peak}$=0.1632 kV
I_{sec_peak}=0.001632 kA
P_{sec_pu}=0.3198m pu
Q_{sec-pu}=0
$\theta(Q_{sec},P_{sec})$= 0°

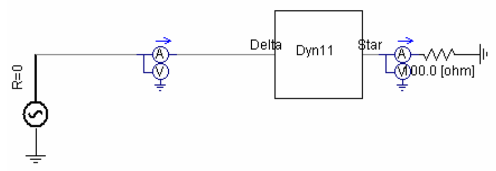

$V_{prim\_ph\_peak}$=8.165 kV
I_{prim_peak}=0.24875 A
P_{prim_pu}=0.597m pu
Q_{prim_pu}=0.0023635 pu
$\theta(Q_{prim},P_{prim})$= 75.82°
$V_{sec\_ph\_peak}$=0.16321 kV
I_{sec_peak}=0.001632 kA
P_{sec_pu}=0.3198 pu
Q_{sec_pu}=0
$\theta(Q_{sec},P_{sec})$=0 °

6. MODELLING OF NO-LOAD LOSSES IN PSCAD

While simulating a single phase circuit which was supplied by a three phase step-up transformer some not logical results were obtained. A very simple circuit was used to analyse the phase and line currents given by PSCAD.

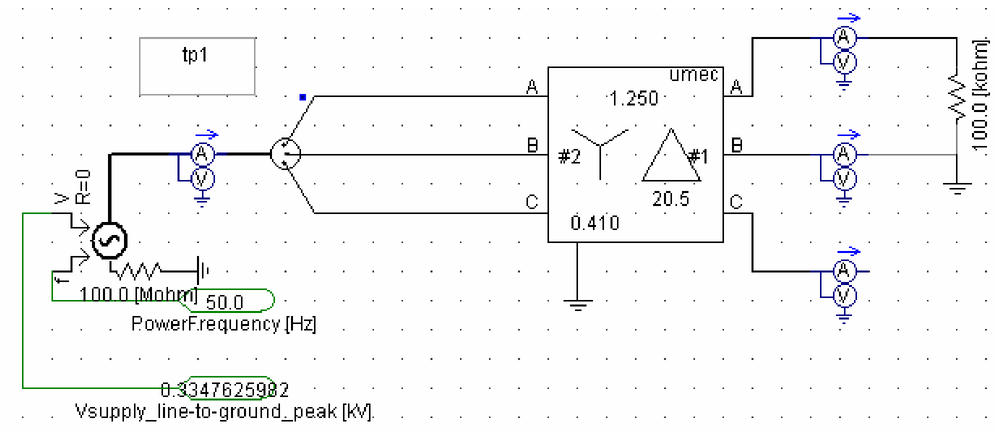

fig. 229. Circuit used to analyse the phase currents given by PSCAD

PSCAD three phase transformers give the option to view the phase and line currents at each winding. However, when no-load losses are present, these values seem not to be correct. In this particular case, for instance, the phase currents

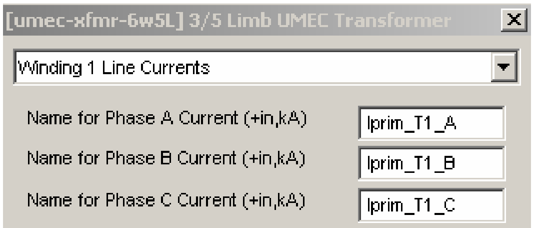

fig. 230. Line currents of the delta side given by PSCAD

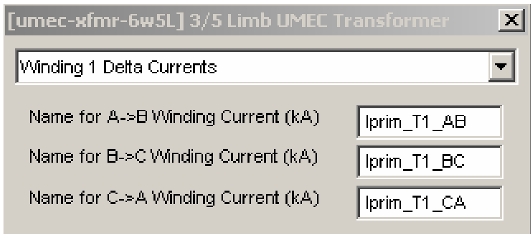

fig. 231. Phase currents of the delta side given by PSCAD

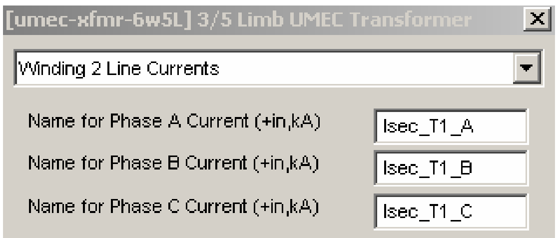

fig. 232. Line currents of the star side given by PSCAD

The transformer under study is a Dyn11 transformer used as a step-up transformer. Therefore, the load side is chosen as high voltage side:

$$a = \frac{U_{\text{ph\_left\_side}}}{U_{\text{ph\_right\_side}}}$$

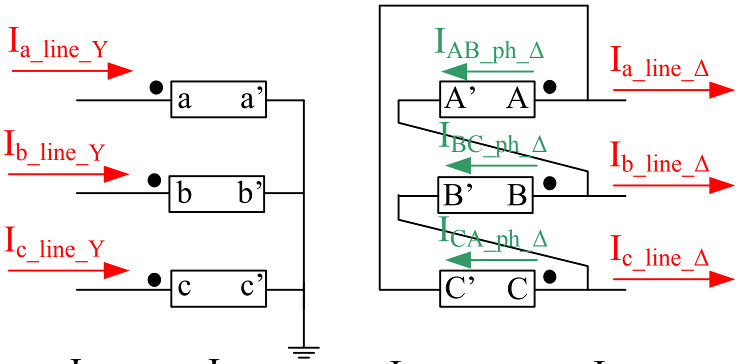

$$I_{a\_line\_\Delta} = I_{AB\_ph\_\Delta} - I_{AB\_ph\_\Delta} \qquad I_{AB\_ph\_\Delta} = -\,a \cdot I_{a\_line\_Y}$$

$$I_{b\_line\_\Delta} = I_{AB\_ph\_\Delta} - I_{BC\_ph\_\Delta} \qquad I_{BC\_ph\_\Delta} = -\,a \cdot I_{b\_line\_Y}$$

$$I_{c\_line\_\Delta} = I_{BC\_ph\_\Delta} - I_{CA\_ph\_\Delta} \qquad I_{CA\_ph\_\Delta} = -\,a \cdot I_{c\_line\_Y}$$

fig. 233. Relationship between phase and line currents in the transformer

If the C phase (in the delta side) is not connected it would be reasonable to think that:

$I_{C\_line\_\Delta} = 0$ and,

$I_{BC\_ph\_\Delta} = I_{CA\_ph\_\Delta}$

After simulation it could be observed that both currents were not only no equal (see fig. 234) but were not either in phase.

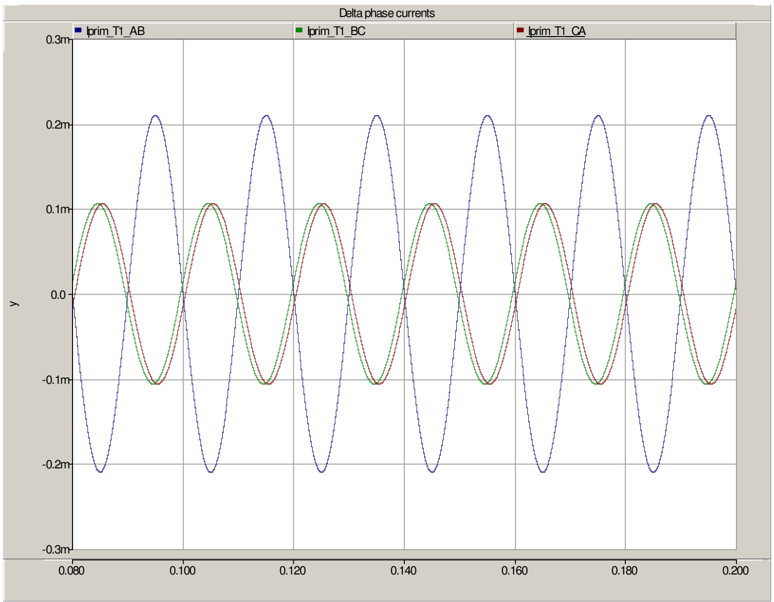

fig. 234. Delta side phase currents given by PSCAD

It was also observed that the difference between the delta side phase currents changed with the load. If a low impedance load was used, a higher current was absorbed by the load and both currents (BC and CA) where the same. This experience indicated that there the problem must be related to the model used by PSCAD to represent no-load losses and also the point where the current measurement is done. There is a strong evidence to believe that when the no-load losses option is enabled a parallel resistance is added at the input of the primary phase.

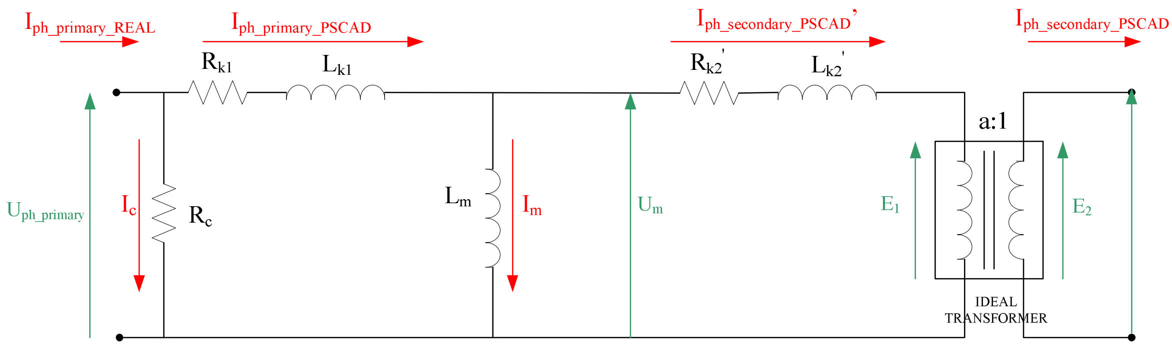

fig. 235. Single phase transformer model used by PSCAD (not sure)

This problem is also translated in the secondary line currents provided by PSCAD. They are not the real ones as it has been proved in fig. 236.

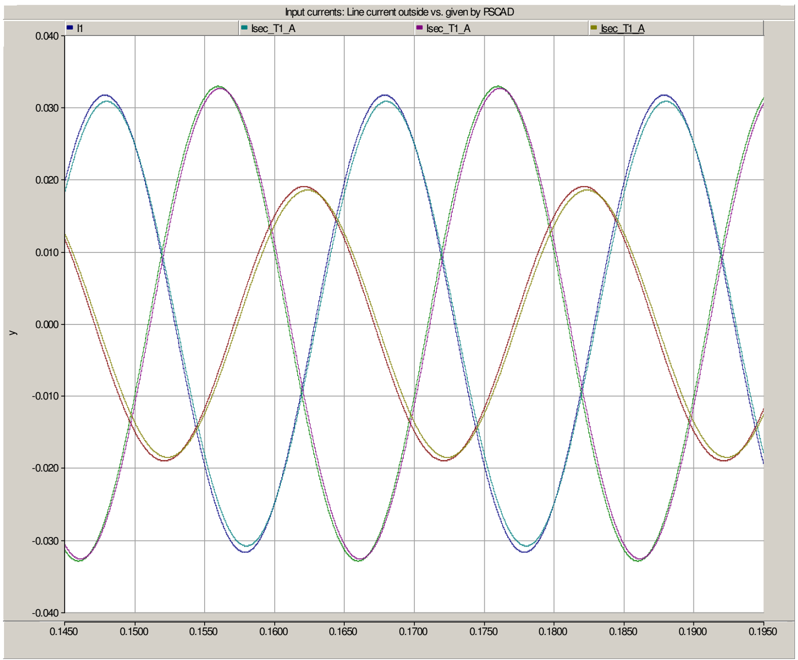

fig. 236. Star side phase currents given by PSCAD and measured

PSCAD will give the following data:

$I_{ph\_primary\_PSCAD}$

$I_{ph\_secondary\_PSCAD}=a*I_{ph\_secondary\_PSCAD}'$

The data given by PSCAD does not represent the real phase currents.